The Stability and Control of Power Grids with High Renewable Energy Share

Dissertation
zur Erlangung des akademischen Grades

doctor rerum naturalium

(Dr. rer. nat.)

im Fach: Physik

Spezialisierung: Theoretische Physik

eingereicht an der

Mathematisch-Naturwissenschaftlichen Fakultät

der Humboldt-Universität zu Berlin

von

MSc. Sabine Auer

Präsidentin der Humboldt-Universität zu Berlin:
Prof. Dr.-Ing. Dr. Sabine Kunst

Dekan der Mathematisch-Naturwissenschaftlichen Fakultät:
Prof. Dr. Elmar Kulke

Gutachter: 1. Prof. Dr. Dr. h.c. mult. Jürgen Kurths

2. Prof. Dr. rer. nat. Philipp Maass

3. Prof. Dr. Ing. Florian Dörfler

Tag der mündlichen Prüfung: 30. Januar 2018

Abstract

This PhD thesis is centered around the "Stability and Control of Power Grids with high Renewable Energy Share". With a conceptual modelers approach, I tackle three overarching questions related to the novel challenges the energy transition poses for the stability of future power grids.

The first question focuses on how to measure and subsequently improve the resilience of a power grid. Here, I contribute important insights to conceptual modelers by providing information on the necessary model detail for transient stability assessments.

The second question concerns how to ensure static voltage stability and avoid capacity overloading when the deployment of Renewable Energy Sources (RES) in the distribution grid layers is massively increasing. As a possible solution to this problem I analyze the future technical potential of reactive power provision from decentral resources in Germany.

The third question, and main focus of this thesis, is on how to integrate renewable energies in a dynamically stable way. Specifically, I investigate the influence of intermittent RES and measurement delays from power electronic resources on frequency stability and how the latter can be restored by concepts of demand control. First, for local intermittent fluctuations in lossy distribution grids I find a remarkable and subtle but robust interplay of dynamical and topological properties, which is largely absent for lossless grids. Second, I show how delays may induce resonance catastrophes and how the existence of critical delays sets an upper limit for measurement times. Further, I investigate whether centralized vs. decentralized power production, for different grid topologies, changes this behavior. Third and last, I present how the right parameterization of decentral electric vehicle control can completely overcome issues of short-term dynamic instability related to RES fluctuations. This control avoids demand synchronization and high battery stress.

Altogether, this thesis investigates the stability of future power grids moving towards integrating more aspects of renewable energy dynamics. Finally, I point out open questions to encourage further research.

Zusammenfassung

Die vorliegende Dissertation untersucht die Stabilität und Regelung von Stromnetzen mit hohem Anteil Erneuerbarer Energien (EE). Dabei stehen drei Forschungsfragen, zu den neuartigen Herausforderungen für die zukünftige Stromnetzstabilität im Zuge der Energiewende, im Vordergrund.

Erstens soll untersucht werden wie die Resilienz von Stromnetzen gemessen und im zweiten Schritt auch verbessert werden kann. Dabei zeige ich den, für den konzeptionellen Modellierer wichtigen, notwendigen Detailgrad für transiente Stabilitätsuntersuchungen auf.

Die zweite Frage lautet wie, trotz des zunehmenden Ausbaus von EE in Verteilnetzen, die statische Spannungsstabilität garantiert und Leitungsüberlastungen verhindert werden können. Als eine mögliche Lösung für dieses Problem analysiere ich mit einem konzeptionellen hierarchischen Verteilnetzmodell das zukünftige Potential für die Erzeugung von Blindleistung aus dezentralen Ressourcen am Beispiel Deutschlands.

Die dritte Frage, wie eine dynamisch-stabile Integration von EE möglich ist, bildet den Hauptfokus meiner Dissertation. Dabei untersuche ich wie neuartige dynamische Aspekte EE, wie intermittente Fluktuationen oder auch Mess- und Reaktionszeiten von Leistungselektronik, die dynamische Netzstabilität beeinflussen und wie mögliche Instabilitäten durch Konzepte der Nachfragesteuerung behoben werden können. Dabei stoße ich bei der Analyse lokaler intermittenter Fluktuationen in ohmschen Verteilnetzen auf ein bemerkenswertes Wechselspiel zwischen Eigenschaften der Netzdynamik und -topologie, welches für Netze ohne Verluste nicht in Erscheinung tritt. Als Zweites zeige ich wie mit der Einführung von Leistungselektronik und den damit verbundenen Mess- und Reaktionszeiten Resonanzkatastrophen hervorrufen werden können. Zudem existiert ein oberes, kritisches Limit für solche Verzögerungen, das nicht überschritten werden sollte. Weiterer Bestandteil dieser Untersuchungen ist der Einfluss dezentraler gegenüber zentraler Erzeugung für verschiedene Netztopologien. Schließlich präsentiere ich wie die dezentrale Nachfragesteuerung von Elektroautos dynamische Instabilitäten, hervorgerufen durch Fluktuationen von EE, bereinigen kann. Dabei achte ich explizit auf die Vermeidung von Nachfragesynchronisation und Batteriedegradierung.

Zusammenfassend behandelt diese Arbeit verschiedene Aspekt zur Stabilität zukünftiger Stromnetze und integriert dabei sukzessive neuartige dynamische Aspekte von EE. Letztendlich werden offenen Fragen, zur Anregung weiterführender Forschungen, dargelegt.

Danksagung

Für ihre Unterstützung, ihren Rat und Beistand will ich mich bei meinem Doktorvater, meiner Familie, Dominik, meinen Kollegen und Freunden bedanken.
Die besondere Atmosphäre der Stromnetzgruppe des Potsdam-Instituts für Klimafolgenforschung (PIK) hat diese Arbeit gefördert und inspiriert. Als mein Doktorvater hat Jürgen Kurths mich auf meinen Weg geleitet und dabei Raum für meine eigene Kreativität gelassen. Frank Hellmann hat mit seinem Wissen meinen Ideen stets analytische Tiefe verliehen und mich meine Stärken erkennen lassen. Während Jobst Heitzig in meiner Promotionszeit die Rolle des Ideengebers, kritischen Mathematikers und Systemtheoretikers innehatte.
Wichtig für den Erfolg meiner Arbeit war der beständige Diskurs mit Paul Schultz, Benjamin Schäfer, Mehrnaz Anvari, Katrin Schmietendorf, Dirk Witthaut, Marc Timme und anderen Projekt-Partnern. Außerdem will ich unseren Studenten Kirsten Kleis, Casper Roos, Marie Krause, Anton Plietzsch und Maria Jarolin für ihre Arbeit danken.
Unsere PIK-Bandmitglieder Jobst, Jonathan, Paul und Liubov haben meine Dissertationszeit musikalisch bereichert.
Als wichtige Strategieberater für Lebensfragen will ich außerdem explizit Thomas Pichl, Silvana Tiedemann, Leonie Wismeth, Tim Kittel, Marie Gerber, Thomas Bruhn und Christoph Minz nennen.
Das exzellente IT-Team des PIK, mit Sandro Waldschmidt, Benjamin Kriemann und Dietmar Gibietz, hat IT-Notfälle stets schnell behoben. Marcel Meistring ist die gute Seele der PIK-Bibliothek.
Zudem will ich Philipp Maaß und Florian Dörfler für ihre Bereitschaft danken diese Arbeit zu begutachten.

Contents

List of Frequently Used Symbols

α	Damping term of synchronous machine (Eq. (2.3))
$B = \mathrm{Im}(Y)$	Susceptance or imaginary part of the admittance Y (see Sect. 2.1.1)
cc	closeness centrality (see Sect. 2.1.1)
$f = \omega/(2\pi)$	Frequency in co-rotating frame, $[f]$ =Hz (see Sect. 4.1)
$G = \mathrm{Re}(Y)$	Conductance or real part of the admittance Y (see Sect. 2.1.1)
k	Network degree (see Sect. 2.1.1)
H	Inertia of the synchronous machine (Eq. (2.3))
μ_B	Basin stability (Eq. (3.2))
μ_S	Survivability (Eq. (3.3))
ω_R	Reference frequency (Eq. 2.22)
$\tilde{\omega}$	Angle velocity of generator, $[\tilde{\omega}] = s^{-1}$ (Eq. 2.22)
$\omega = \tilde{\omega} - \omega_R$	Angle velocity in co-rotating frame (Eq. (2.3))
ϕ	Voltage angle of alternating current (Eq. (2.3))
$P = \mathrm{Re}(S)$	Active power or real part of the apparent power S (see Sect. 2.1.2)
$Q = \mathrm{Im}(S)$	Reactive power or imaginary part of the apparent power S (see Sect. 2.1.2)
$R = \mathrm{Re}(Z)$	Resistance or real part of the impedance Z (see Sect. 2.1.1)
$S = P + \mathrm{i}Q$	Apparent complex power (see Sect. 2.1.2)
TI	Troublemaker index (see (3.5))
$V = Ue^{\mathrm{i}\phi}$	Complex voltage
$X = \mathrm{Im}(Z)$	Reactance or imaginary part of the impedance Z (see Sect. 2.1.1)
$Y = G + \mathrm{i}B$	Line admittance (see Sect. 2.1.1)
$Z = R + \mathrm{i}X$	Line impedance (see Sect. 2.1.1)

List of Abbrevations

AC	Alternating Current (see Sect. 2.2)
BS	Basin Stability (see Sect. 3.3.1)
DC	Direct Current (see Sect. 2.2)
DG	Distribution Grid (see Sect. 1.1)
DSGC	Decentral Smart Grid Control (see Sect. 2.3)
EAC	Equal Area Criterion (see Sect. 3.3)
ENTSO-E	European Network of Transmission System Operators for Electricity (see Sect. 3.1)
EV	Electric Vehicle (see Sect. 8)
HV	High-Voltage (see Sect. 2.1.2)
LV	Low-Voltage (see Sect. 2.1.2)
MV	Medium-Voltage (see Sect. 2.1.2)
PDF	Probability Distribution Function (see Sect. 2.2.3.2)
pu	per unit (see Sect. 2.1.2)
PV	Photovoltaic (see Sect. 2.2.3.1)
ROCOF	Rate of Change of Frequency (see Sect. 3.1)
RES	Renewable Energy Sources (see Sect. 1.1)
SIME	Single-Machine Equivalent (see Sect. 3.3)
SM	Synchronous Machine (see Sect. 2.2)
TAFD	Time Average of Frequency Dispersion (see Sect. 3.4)
TD	Time Domain (see Sect. 3.3)
TG	Transmission Grid (see Sect. 1.1)
TI	Troublemaker Index (see Sect. 3.4)
TSI	Total System Inertia (see Sect. 3.1)
UHV	Ultra-High-Voltage (see Sect. 2.1.2)

List of Figures

List of Tables

Chapter 1

Introduction

The full decarbonization of the energy sector by 2050 is non-negotiable to meet the emission targets of the Paris agreement (Rogelj et al. 2016). This requires the deployment of Renewable Energy Sources (RES) in the electricity, transport and heat sector. While the production from large, conventional power sources was centralized, RES units are usually smaller in size, more decentralized, and numerous. Hence, the power system will undergo a regime shift from central to distributed power production. Today, in Germany 90% of all RES capacity is installed in distribution grids (BMWi 2014). The increasing share of RES poses a wide range of challenges for static and dynamic power grid stability[1] but also creates opportunities for innovations in power supply and distribution. At the same time, increased rates of extreme weather events[2] and the possibility of attacks on power grid infrastructure ask for an improvement in the resilience of power grids[3].

[1]The stability of a power system is its ability to remain in the state of equilibrium under normal operating conditions and after being subject to perturbations (Kundur et al. 1994). There are many possibilities to classify power grid stability. I use the term dynamic stability for angle- and frequency stability. With static stability I refer to the absence of over-or undervoltages and grid congestions, also called long-term voltage stability (see Sect. 3 for a detailed explanation).

[2]Extreme weather events are exceeding a predefined threshold in time series of meteorological variables. Examples are heatwaves or precipitation extremes (Coumou et al. 2012).

[3]The resilience of a power grid is defined as its ability to resist failures induced by external hazards, to reduce their impacts and to rapidly restore grid services after disruptions (Brown 2008)

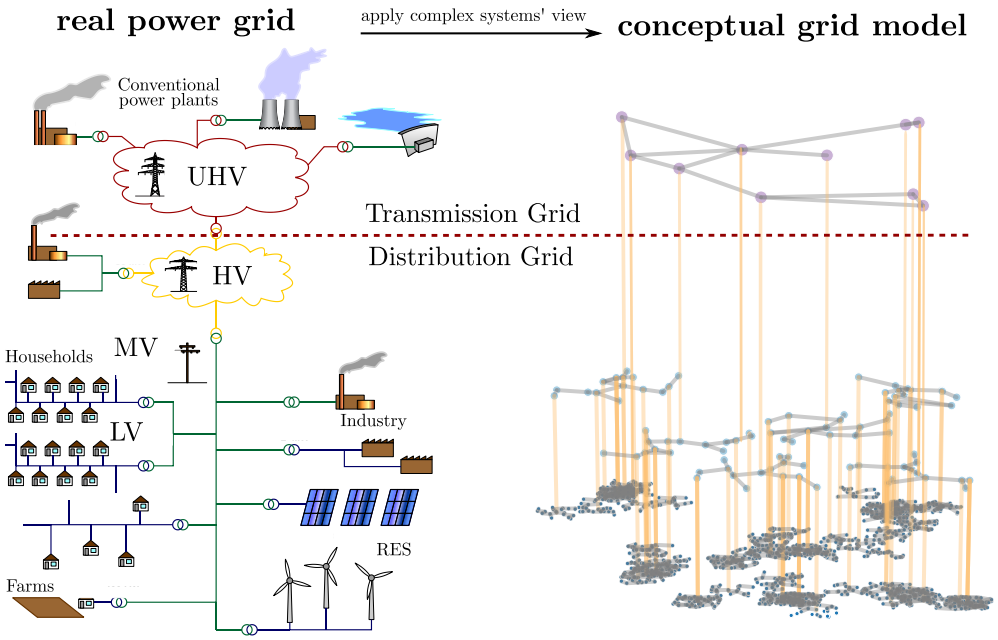

Figure 1.1: **Complex systems' view on the power grid.** The real power grid consists of transmission (Ultra-High-Voltage, UHV) and distribution grid layers (High-Voltage, HV, Medium-Voltage, MV, and Low-Voltage, LV) that are connected via transformers (marked as overlapping double-circles). With the complex systems' view a conceptual grid model is built. The complex network's nodes are producer or consumer nodes, the links correspond to the power lines and the different network hierarchies stand for the different grid layers. The figures are taken from Wikipedia 2010 and Schultz, Hellmann, et al. 2016, respectively.

1.1 Conceptual Power Grid Modeling

"Make things as simple as possible, but not simpler"
A. Einstein

The power system can be understood as a complex system, since it is composed of many interacting components. With the transmission grid (TG) and the distribution grid (DG) it has several system layers (see the illustration of Fig. 1.1). Historically, the TG, mainly the Ultra-High-Voltage (UHV) level, with its large conventional generators was the main scene of power system dynamics since the DG layers, covering the High-Voltage (HV), Medium-Voltage (MV) and Low-Voltage (LV) levels, mainly accommodated passive loads from households and industry. Thus, for power grid modeling in the past it was sufficient to mainly analyze this grid level. The energy transition is increasing the complexity of the power system. It leads to the addition of a large number of heterogeneous production units, smart

consumers, electric vehicles, as well as new battery storage and control devices that may interact in a swarm-type manner.

Here, the theoretical physicist in close cooperation with the electrical engineering community may contribute to the analysis of such systems by integrating the systems view and new stability methods. This thesis applies the complex systems' view and conceptually approaches the research questions, presented in the following section, according to the principle "as simple as possible, as complex as necessary".

1.2 Overarching Research Questions

This PhD thesis is centered on the "Stability and Control of Power Grids with high Renewable Energy Share". I identify three overarching questions concerning the novel challenges the energy transition poses for the stability of future power grids. With a conceptual modelers approach, I tackle three overarching questions and derive subsequent research questions.

1. *How can the resilience of power grids towards extreme events be measured and improved?*

2. *How can static voltage stability be ensured and grid congestions be avoided?*

3. *How can renewable energies be integrated in a dynamically stable way?*

The last question constitutes the main part of this thesis.

1.3 Power Grids and Extreme Events

How can the resilience of power grids towards extreme events be measured and improved?

Extreme weather events or human-made attacks may lead to a complete break-down of the power system. Densely populated urban areas and their power-driven public infrastructure would be inoperable or even permanently damaged with unknown consequences for urban life. Climate change increases the frequency of extreme weather events (Coumou et al. 2012). For example, the island of Zanzibar had a disastrous three-months-blackout in 2009 damaging the island's main industry, tourism, endangering food and water security and even threatening life and health of the island's citizens (Elisabeth Ilskog 2011). South Australia had a major black-out in September 2016 due to a line fault from a storm in combination with bad wind

power control setups causing around $367 million damage (Nick Harmsen 2016).

This creates a need for comprehensive studies on grid resilience. An improved sensitivity analysis is the basis to strengthen the resilience of power grids against such large and local perturbations. To build grid models that approach the question of how to measure and subsequently improve the resilience of a power grid, I derived the following research question:

What is the necessary level of detail to model and assess the response of power grid networks to large generic disturbances? (see Chapter 4)[4]

1.4 Static Voltage Stability of Power Grids with High Renewable Energy Share

How can static voltage stability be ensured and grid congestions be avoided?

For power grid operators the distributed character of RES implies: instead of centrally controlling and distributing large amounts of power from a few power plants to the lower grid levels, the new challenge is to control lots of small generation units in a swarm-type manner. Thus, the decentral placement of power plants shifts the focus of power stability analysis from exclusively considering transmission grid layers towards the distribution grid and it causes the interaction of several network layers. The distributed character of RES also leads to a bidirectional flow of power. At sunny and windy times of the day, surplus power from distributed resources in the lower grid levels may flow upstream, from the lower to the upper grid levels, to be redistributed from there on. If this is not the case, power is mainly flowing downstream to satisfy consumers' demand in the distribution grids. The latter case is the old-fashioned way of power systems operation. The grid infrastructure and grid stability control is optimized to purely serve the scenario of unidirectional downstream power flows. The bidirectional case requires an improved voltage control scheme and reactive power management. A possible solution to this problem is the provision of reactive power from decentral resources. This leads to the question:

What is the potential of reactive power provision from decentralized sources? (see Chapter 5)

[4]Such measures also feature in Chapter 7.

1.5 Dynamic Stability of Power Grids with High Renewable Energy Share

How can renewable energies be integrated in a dynamically stable way?

Not only the placement but also the dynamics of power generators is changing. With a growing number of wind and solar power plants, new dynamic features are introduced into the lower grid layers which need to be understood. Here, power electronic devices, so-called inverters, that connect RES to the power grid, and the fluctuating input of intermittent solar and wind power production play a central role. Synchronous machines and their large rotating masses possess inertia and thus store kinetic energy that is able to instantly balance fluctuations in power. Inverters do not have inertia. Instead, programmed frequency and voltage control schemes determine their characteristics of operation. Since there are many possibilities of such programming, it is important to model the dynamics and stability of power grids that connect a large number of interacting inverters.

Isolated island systems are the first to be affected by the low-inertia problem. E.g. Ireland poses a limit of currently 55% (ENTSO-E 2017) for RES penetration fearing that system security to be threatened above this threshold. The issue of how intermittent renewable power generation is impacting static and dynamic stability is highly debated (50Hertz et al. 2012; Boyle 2004; Turner 1999). Intermittent power time series are correlated in time and space and are spiky with large jumps in the generation (Anvari, Lohmann, et al. 2016; Anvari, Werther, et al. 2017; K. Schmietendorf et al. 2016). Such fluctuations occur on different time scales, including seasonal, inter-day (Heide et al. 2010) and intra-second fluctuations (Milan et al. 2013). Whether the specifics of intermittency play a central role in grid stability analysis and whether the network position of fluctuating power sources is affecting dynamic grid stability is to a large extent unknown. This leads to my third research question:

What is the influence of local intermittent fluctuations from RES on distribution grid stability? (see Chapter 6)

The volatile nature of RES raises the need for more flexibility options for power market supply and balancing energy (BMWi) 2014) arises. In this regard, it is essential to identify options that are both cost efficient and system stabilizing. Smart grid technologies may balance fluctuations from production on different timescales (of minutes, hours and above). Since the market does not incentivize such flexibility options in a cost-effective manner yet (Jansen et al. 2015), policy makers have determined benchmarks for the

deployment of smart metering devices in the grid (Vasconcelos 2008). However, both inverters and smart grid control need measurement and reaction times before triggering their control (ENTSO-E 2017; Schäfer, Matthiae, Timme, et al. 2015; Schiffer, Dörfler, et al. 2017). I am interested in the question:

How do delays impact dynamic stability? (see Chapter 7)

Most of the demand related discussions are circling around the subject of smart grids. An often underestimated effect is the structural change in demand. Since consumer devices are increasingly connected to the grid via inverters as well, the contribution of consumption units such as motors to the overall system's inertia is decreasing just as the one from production units. This again affects the ability of the grid to balance short-term fluctuations. Electromobility could fill this gap by providing balancing reserves with their battery storage systems. In this context, I ask the question:

Can dynamic stability be restored by concepts of electric vehicle demand control? (see Chapter 8)

1.6 How to read this Thesis

In this PhD thesis I investigate several aspects of future power grids. Starting from static stability assessment this work moves towards integrating more aspects of future power grid dynamics. The results of this thesis are related to the three overarching questions and subsequently derived research problems.

Chapter 2 introduces to power grid modeling. This includes transmission and distribution grid representations, synchronous machine models of different order, inverter models, Decentral Smart Grid Control (DSGC), and the nature of intermittent noise.

Chapter 3 presents the stability measures used to analyze power grids with respect to their static and dynamic stability. This includes the concepts of power flow, linear stability, basin stability, survivability, and stochastic stability analysis.

First results of this thesis are shown in Chapter 4. It gives important insights to conceptual modelers on the necessary model detail for assessing the dynamic stability of power grids that are subject to large perturbations. This relates to the question of how resilient power grids are in the case of natural or human-made extreme events.

To assess the challenges for static voltage stability, Chapter 5 starts with a case study of the German power grid. This involves the question

whether decentral reactive power management is able to solve over- and undervoltage problems. Here, RES may not only be part of the problem but also of the solution. With their potential to provide decentral active and reactive power, RES are able to contribute to voltage stability.

The remaining three chapters build the main part of this thesis and all relate to the question of how to enable a dynamically stable integration of RES. The research topic of Chapter 6 is the robustness of distribution networks towards local intermittent power fluctuations and investigates the grid's ability to dampen such fluctuations within safety bounds. To shed light on the influence of smart grid and inverter control on the stability of power grids, Chapter 7 investigates the impact of delays related to measurement and reaction times. Chapter 8 closes this field of research with the design of an decentral electric vehicle control scheme that is able to efficiently balance fluctuations from RES while avoiding demand synchronization.

Chapter 9 summarizes the main insights and contributions of the thesis, relates them to each other, and presents open questions for future research.

1.7 List of Publications

List of published papers:

S. Auer, K. Kleis, P. Schultz, J. Kurths, and F. Hellmann. "The impact of model detail on power grid resilience measures". In: The European Physical Journal Special Topics 225.3 225.3 (2016), pp. 609–625. doi: 10.1140/epjst/e2015-50265-9.

B. Schäfer, C. Grabow, **S. Auer**, J. Kurths, D. Witthaut, and M. Timme. "Taming instabilities in power grid networks by decentralized control". In: The European Physical Journal Special Topics 225.3 (2016), pp. 569–582.

S. Auer, F. Hellmann, M. Krause, and J. Kurths. "Stability of Synchrony against Local Intermittent Fluctuations in Tree-like Power Grids". In: Chaos 27 (12 2017). doi: 10.1063/1.5001818.

S. Auer, F. Steinke, W. Chunsen, A. Szabo, and R. Sollacher. "Can distribution grids significantly contribute to transmission grids' voltage management?" In: PES Innovative Smart Grid Technologies Conference Europe (ISGT-Europe), 2016 IEEE. IEEE. 2016, pp. 1-6.

List of papers in preprint:

S. Auer, C. Roos, J. Heitzig, F. Hellmann, and J. Kurths. "The Contribution of Different Electric Vehicle Control Strategies to Dynamical Grid Stability". In: arXiv preprint arXiv:1708.03531 (2017).

The listed publications were published in the runtime of the CoNDyNet project[5]. Hereby, I want to acknowledge the funding of my PhD through this project by the Federal Ministry of Education and Research (FK. 03SF0472A).

[5] **Co**llective **N**onlinear **Dy**namics of complex **Net**works

Chapter 2

Power Grid Modeling

I identified three necessary main pillars for building conceptual models of the future power grid that are able to grasp the major changes the power grid is undergoing (see Fig. 2.1). These are the network structure (Schultz20142.1), the generator dynamics (Schultz20142.2) and the agents or consumers (Schultz20142.3). Originally, models of power systems dynamics needed to cover only TGs where large conventional power plants were driving the relevant dynamics. With the production of RES in distribution grids (DGs) conceptual power grid models need to include DG layers. The node dynamics are built by systems of differential equations describing synchronous machines or inverter control in combination with fluctuating power input. The consumers with demand response ability may

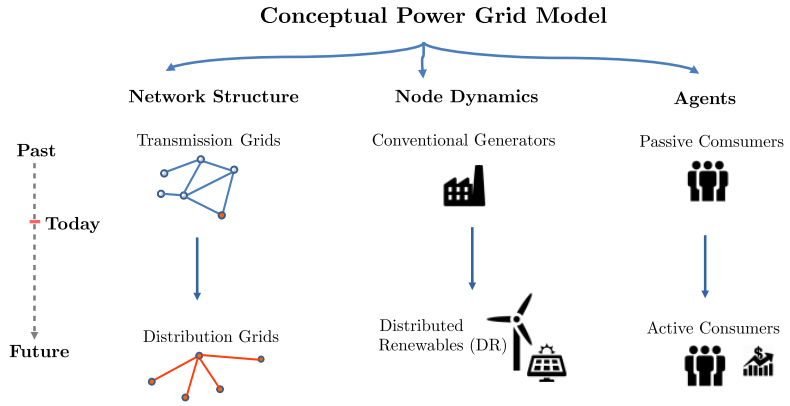

Figure 2.1: **Ingredients of conceptual power grid models**. Each building block is transforming during the energy transition. In the past, grid modeling focused on transmission grids with their conventional generators and passive consumers. With the energy transition future power grid models need to contain distribution grids with their distributed resources and potentially active consumers.

behave in a non-trivial way that needs to be modeled with an agent-based approach.

Which degree of detail and granularity a model needs depends on the type of question to be answered. It is then crucial to construct a model according to the principle "as simple as possible and as complex as necessary". Thus, the objective is to find the lowest complexity model to answer the initial questions.

2.1 Network Structure

For the purpose of country or European scale studies the transmission grid models are usually exhausting computational limits, already. Whereas distribution grid models are of great use in studying grid dynamics and control on a micro- and meso-scale. In a later stage both types of grid layer modeling may serve as components in order to build networks of networks. Here, the understanding of the subsystems eases to investigate the components of the complex power system. Despite the necessity of modeling hierarchical grids, stand-alone transmission and distribution grid models still give important answers to specific research questions.

As a starting point, Section 2.1.1 introduces power grids as complex networks. In order to computationally handle the model complexity of multilayer power grids, Section 2.1.2 illustrates a conceptual approach with a symmetric, tree-like representation for all grid levels. Section 2.1.3 presents typical properties of transmission grids (TGs) whereas Section 2.1.4 points out the novelties of distribution grid models with respect to the model's network structure.

2.1.1 Power Grids as Complex Networks

A power grid can be understood as an *undirected, weighted graph* with the effective consumers and generators as network nodes or vertices, i, and the power lines as links or edges between nodes i an $i \neq j$. Hence, the corresponding adjacency matrix has non-zero entries between nodes that are connected by a power line. The weighted adjacency matrix forms the admittance matrix, $Y_{ij} = G_{ij} + \mathrm{i}B_{ij} \in \mathbb{C}$ with conductance, $G_{ij} \in \mathbb{R}$, and susceptance, $B_{ij} \in \mathbb{R}$. Important network measure is the degree, k_i, of a vertex which is equal to the number of edges connected to a vertex or to the number of nodes j in the set of i's neighbors $j \in \mathcal{N}$. The betweenness is a centrality measure of a vertex i and refers to the relative number of shortest paths that run through i. The closeness centrality of node i corresponds to

the inverse sum of the shortest path distances between node i and all other nodes $j \neq i$ of the graph. For an introduction to complex networks and further network measures, I refer the interested reader the review articles by Newman 2003 or Boccaletti et al. 2006.

Power grids can have different topological structures. In a fully meshed network nodes would connect to as many other nodes as possible whereas in contrast a minimum-spanning tree does not show any cycles or loops. The *random growth model* of Schultz, Heitzig, et al. 2014b may be used to generate synthetic grid topologies of such different kind by tuning the network's meshing. These synthetic grids exhibit realistic power grid characteristics such as the network degree or the betweenness. The growth process is controlled by a heuristic redundancy/cost optimization function. It considers not only the length of transmission lines but also additionally created redundancy in the form of alternative routes. For a detailed discussion of the algorithm, I refer to Schultz, Heitzig, et al. 2014b. Note that the resulting power grid topologies come with a spatial embedding of the network and hence information about the link lengths. This allows to estimate appropriate admittances from textbook parameter values (see the Appendix A).

2.1.2 Multi-layer Power Grids

In the future, multi-layer power grid modeling becomes indispensable to capture the interaction of transmission and distribution grids. The analysis of such hierarchical network topologies presents a challenge due to its high dimensionality and complexity. Schultz, Hellmann, et al. 2016 present approaches to construct such grid models as interconnected networks of networks, however, static and dynamic stability analysis of such models remain to be done. Here, I present the most simple representation of a multi-layer power grid by assuming a fully symmetric tree-like structure. This allows to reduce the dimensionality of the grid model to a simple chain structure. Later, in Section 5, I will apply this method to the case of Germany. This approach was introduced in **Auer, Steinke, et al. 2016**.

Starting point is the assumption that at every connection of the TG (the ultra-high voltage (UHV) level) to the DG (the high-voltage level and below), a specific number of identical copies of an average distribution grid is connected. This DG has a fully symmetric topology. Since the generation capacity and the loads are assumed to be fully symmetric as well, the complex voltage state at each node on the same level of the grid will be identical in each load situation. Thus, I have to consider only one represen-

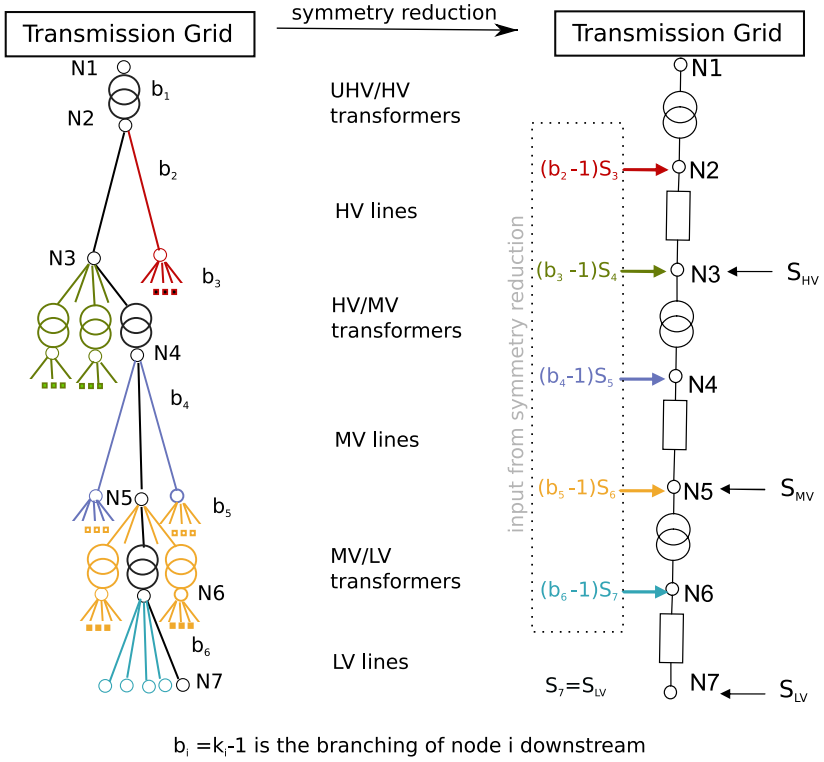

Figure 2.2: **Schematic illustration of grid topology reduction** to a simplified chain-like structure with the model assumption of full tree symmetry. The black line illustrates the reduction of the network tree to a simple chain structure. E.g. the partial red tree is reduced to a single input at node N2. The green subtree surrounded is the input at node N3 and so on. The input at the nodes is according to the branching, $b_i = k_i - 1$, of the tree at each node i that are reduced into inputs with number of branches minus one. k_i is the degree of each node.

tative path from the UHV connection point down to the LV level for the power flow calculations (see Fig. 2.2 for a schematic illustration). For such a representative path, I introduce nodes at all branching points, which sit between transformers and line impedances. In the left scheme of Fig. 2.2 the black line illustrates the reduction of the network tree to a simple chain structure. E.g. the partial tree colored in red is reduced to a single input at node N2. The subtree in green is the input at node N4 and so on. The power input at the nodes is according to the branching of the tree at each level. Besides, the actual power infeed from each grid level (S_{LV}, S_{MV} and S_{HV}) the input from the reduced branches needs to be added. The complex apparent power $S_i = P_i + jQ_i$ at node i (with active power P_i and reactive power Q_i) is then the total power infeed from one of the N_i nodes at each node level in the simplified power chain network. The injections at

transformer level comes from the symmetric generation accumulation.

The power flow calculations along this chain across different voltage levels is simplified via per unit (pu) calculations. The per unit system is used in electrical engineering to express system quantities such as voltage, power and impedance as a fraction of base quantities (Elgerd 1982). E.g. for the case of Germany the base voltages for the the LV, MV and HV levels are 0.4kV, 20KV and 110kV. Voltage values are expressed relative to the base voltage of the corresponding grid level.

In this model consumer loads are placed at the end of the lines. However, in real MV and LV grids loads are rather distributed homogeneously along the power lines. Thus, I take only half of the lines' typical length in order to get the same voltage drops (as for homogeneous load placement) along the lines (Dierkes et al. 2014).

Altogether, the above assumptions allow the reduction of the multi-layer power grid to a simple chain structure. For the approximate tree branching and parameterization for the case of Germany see Section A.

2.1.3 Transmission Grid Models

Transmission grid (TG) models are usually built with test cases as bus systems with their according line parameterization. However, *Monte Carlo* type studies, that rely on repeated random sampling (Hammersley 2013), would require the availability of large ensembles of test cases. This kind of data which the data is usually not available. The random growth model of Schultz, Heitzig, et al. 2014b can be used to create synthetic grid topologies. For TGs I choose rather meshed grid topologies since the average degree of TGs is usually higher than that of DGs. The resistance and thus losses of the TG lines are usually very low (Auer, Steinke, et al. 2016) and thus assumed to be zero.

2.1.4 Distribution Grid Models

Models of one distribution grid layer or models of small islanded grids, so-called *microgrids*, are a starting point for the creation of multi-layer power grids. A basic understanding of such distribution grid models is a necessary prerequisite before it is possible to construct of large interconnected and interacting multiple layers in a holistic power grid model.

A microgrid is internally balanced and not connected to a higher grid level, it does not belong to a hierarchical grid topology. Islanded microgrids play a role for the decentral provision of energy, but also as part of a

safety and stability strategy to localize faults by partitioning the grid into autonomous units.

Distribution grid layers in contrast are part of the larger grid hierarchy. They are not self-balanced and have a connection point to the next higher grid level, called the slack bus or heavy node. Such a slack bus carries all inertia and other dynamic properties of the upper grid levels. Generally, the LV, MV and HV grid layers are attributed to the distribution grid.

Throughout this thesis, tree-shaped networks represent the underlying distribution grid topology (generated with the previously in Section 2.1.1 mentioned random growth model of Schultz, Heitzig, et al. 2014b). For modeling distribution grids it is necessary to take lossy lines into account. The common assumption of non-lossy lines for TGs does not hold for distribution grids since the resistance, R, of DG lines is non-zero, $R = \mathrm{Re}(Z) > 0$. The lossy lines will show to have significant impact on power grid stability.

2.2 Generator Dynamics

I start this section with a short introduction of power grids as nonlinear dynamical systems. In Section 2.2.2, I explain the Synchronous Machine (SM) model that describes conventional generator dynamics. With Sections 2.2.3 and 2.3, I show the necessity to model renewable generators and demand response in the lower grid levels.

2.2.1 Power Grids – Nonlinear Dynamical Systems

A *continuous dynamical system* refers to any physical or abstract entity whose configuration at any given time can be specified by some set of numbers, called system variables, $x(t)$, (Hilborn 2000; Watts et al. 1998), and whose time evolution is given by an ordinary differential equation (ODE):

$$\frac{\mathrm{d}x}{\mathrm{d}t} = \mathrm{rhs}(x) \tag{2.1}$$

where rhs is the right-hand side function.

There are linear and nonlinear dynamical systems. The first involves only polynomial functions of degree one in the system variables, the latter contains at least one term of higher degree, a product of system variables or more complicated functions. For any linear system there is one special solution where the variables are time-independent, the *fixed point*. This can be either stable or unstable, meaning that all trajectories either approach or diverge from this solution eventually. In the former case the fixed point is an attractor of the dynamical system.

However, a power system is a nonlinear system. Hence, it may contain multiple attractors, each with its own *basin of attraction*. Further attractors might not simply be fixed points but can be limit cycles or even chaotic. Limit cycles in nonlinear systems may be quite complicated. In chaotic systems two trajectories may be arbitrarily close to each other in state space, yet rapidly diverge from each other afterwards. Bistability, the existence of multiple attractors, is a generic feature of nonlinear dynamics and raises the question which points in state space approach which attractor. Those trajectories that run towards a particular attractor are said to lie in its basin of attraction.

For a detailed review of the theory of dynamical systems, I refer the interested reader to the books from Hilborn 2000 and Watts et al. 1998.

2.2.2 Conventional Generator Dynamics

For the node dynamics in a transmission grid I assume mainly conventional generators which are described by the well-known Synchronous Machine (SM) model. Under steady-state condition, synchronous machines rotate with the same speed as the induced voltage that drives the alternating current (AC) of an AC power grid. For this SM model various degrees of accuracy have been developed (Sauer et al. 2006; Schmietendorf et al. 2014; Weckesser et al. 2013).

In the next two subsections I will describe two power grid models of different detail or order. The *second-order model or swing equation* is the model used overwhelmingly in the theoretical physics literature. The *fourth-order model* is a more detailed model separating the electric and mechanical aspects of the power grid to some degree. This was found to give a better picture of the long term dynamics of power generators (see Section 4 and Auer, Kleis, et al. 2016).

2.2.2.1 Second-Order Model

The swing equation describes the power grid dynamics of N synchronous machines with two equations per node $i \in \{1, \dots, N\}$: one for phases ϕ_i and one for frequency deviations ω_i. Hence, it is also called second-order model. Further names are the classical model or Kuramoto model with inertia (Filatrella et al. 2008; Rodrigues et al. 2016). In this second-order model, generators are represented as constant power, constant voltage sources (Anderson et al. 2003; Nishikawa et al. 2015) with voltage magnitude U_i and rotating complex voltage $V_i = e^{\mathrm{i}\phi_i} U_i$. Besides the constant voltage magnitude the machines are parametrized by the constant mechanical input

power P_i, the moment of inertia H_i and an effective damping term α_i. The frequency and phase are the instantaneous speed and position of both the electric field voltage and the rotating mass. Note that the power infeed P_i represents the net generation at a node which is a mix of consumption and generation from the underlying distribution grid connected to the node in the transmission network. I assume that the net generation P_i is not affected by the dynamics I study. All nodes are represented as synchronous machines where positive and negative P_i distinguish net producers from net consumers and the sum over all input powers P_i is zero. The admittance matrix of the transmission network, with components $Y_{ij} = G_{ij} + \mathrm{i}B_{ij}$, is symmetric and the diagonal elements are defined as $Y_{ii} = -\sum_j Y_{ij}$. These assumptions allow a fairly accurate description of the system's transient behavior after a disturbance in the time period of the first swing which is usually one second or less (Anderson et al. 2003). The swing equation describes the dynamics of such a deviation, ω_i, from the grid frequency ω_R. That is, the instantaneous speed of rotation is $\tilde{\omega}_i = \omega_i + \omega_R$, normal operations are characterized by $\omega_i = 0$. Equation (2.3) represents the system's energy conservation:

$$\frac{\mathrm{d}\phi_i}{\mathrm{d}t} = \omega_i \ , \tag{2.2}$$

$$\frac{2H_i}{\omega_R}\frac{\mathrm{d}\omega_i}{\mathrm{d}t} = P_i - \mathrm{Re}\sum_{j\neq i}(V_i I_{ij}^*) - \alpha_i\omega_i \ . \tag{2.3}$$

where $\mathrm{Re}(V_i I_{ij}^*)$ is the real part of the power flow between node i and node j, P_i the input power from node i and $\alpha_i\omega_i$ a friction term. The complex current I_{ij} from node i to node j is given by:

$$I_{ij} = Y_{ij}(U_i e^{\mathrm{i}\phi_i} - U_j e^{\mathrm{i}\phi_j}) \ . \tag{2.4}$$

It is convenient to introduce the current $I_i^c = e^{-\mathrm{i}\phi_i}\sum_j I_{ij}$ in the co-rotating frame. The total co-rotating current at a node is given by:

$$I_i^c = e^{-i\phi_i}\sum_{j=1}^{N} Y_{ij}V_j = e^{-\mathrm{i}\phi_i}\sum_{j=1}^{N} Y_{ij}U_j e^{\mathrm{i}\phi_j} = \sum_{j=1}^{N} Y_{ij}U_j e^{\mathrm{i}(\phi_j-\phi_i)} \tag{2.5}$$

As I have $Y_{ii} = -\sum_j Y_{ij}$ I can combine these equations into the swing equation:

$$\begin{aligned}\frac{\mathrm{d}\phi_i}{\mathrm{d}t} &= \omega_i \ , \\ \frac{2H_i}{\omega_R}\frac{\mathrm{d}\omega_i}{\mathrm{d}t} &= P_i - \mathrm{Re}(U_i(I^c)^*) - \alpha_i\omega_i \\ &= P_i - \mathrm{Re}\sum_j U_i Y_{ij}^* U_j e^{\mathrm{i}(\phi_i-\phi_j)} - \alpha_i\omega_i .\end{aligned}$$

In the special case of zero ohmic resistances of the power lines, $G_{ij} = 0$, which is reasonable assumption for transmission grids, the swing equation reduces to the familiar form:

$$\begin{aligned}\frac{\mathrm{d}\phi_i}{\mathrm{d}t} &= \omega_i \ , \\ \frac{2H_i}{\omega_R}\frac{\mathrm{d}\omega_i}{\mathrm{d}t} &= P_i - \mathrm{Re}\sum_j U_i B_{ij} U_j (\mathrm{i}e^{\mathrm{i}(\phi_j-\phi_i)})^* - \alpha_i\omega_i \\ &= P_i - \sum_j U_i B_{ij} U_j \sin(\phi_i-\phi_j) - \alpha_i\omega_i .\end{aligned} \tag{2.6}$$

The above equations have a fixed point. It corresponds to the synchronous state of the frequency dynamics. There are other attractors where one or more nodes oscillate in a limit cycle while others remain in a stationary state. Asymptotically, the frequency of a limit cycle is given by the uncoupled rotation $\omega_i^l = P_i/\alpha_i$. To determine the stationary state, solve

$$\frac{\mathrm{d}\phi_i}{\mathrm{d}t} = 0, \ \frac{\mathrm{d}\omega_i}{\mathrm{d}t} = 0 \ \forall i. \tag{2.7}$$

The fixed point equations of the dynamics simplify to the power flow equations:

$$\begin{aligned}\omega_i^\star &= 0 \ , \\ P_i &= \sum_j U_i B_{ij} U_j \sin(\phi_i^\star - \phi_j^\star) \ .\end{aligned} \tag{2.8}$$

where the star marks the frequency and phase at the fixed point.

2.2.2.2 Fourth-Order Model

Usually the swing equation is used for short time periods to analyze the transient behavior of generators in a power grid, the so-called first swing.

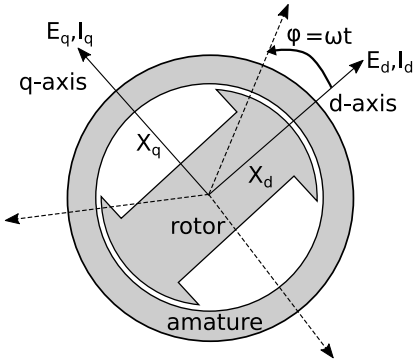

Figure 2.3: **Scheme of a synchronous machine** in the co-rotating frame. Typical generators have three-rotor windings with three axis (dotted arrows), one for each phase. The transformation in the co-rotating (d-q)-frame reduces the dimensions of state space. Here, the d-q coordinates rotate at a reference frequency ω and are phase shifted compared to the three original axis by $\phi = \omega t$.

The fourth-order model (Eqns. (2.10) – (2.15)) also takes the back reaction of the power flow onto the voltage into account. This has the effect that the voltage, as seen by the power grid, and the rotating mass are no longer the same but become dynamically coupled. The voltage is described in a co-rotating frame with axes labeled d and q (see Fig. 2.3). Thus I have the voltages $E_{q,i}$ and $E_{d,i}$ (see Eqn. (2.14) and Eqn. (2.15) respectively), and the complex voltage $U_i = E_{q,i} + \mathrm{i}E_{d,i} = e^{-\mathrm{i}\phi_i}V_i$ and in the co-rotating frame is now dynamical. For convenience I again use the notation

$$I_i^c = I_{q,i} + \mathrm{i}I_{d,i} \tag{2.9}$$

for the co-rotating current $I_i^c = e^{-\mathrm{i}\phi_i}\sum_j I_{ij}$.

Now the equations for the swing mass are unchanged, being merely energy conservation with phase shifts through the power flow across the lines:

$$\frac{\mathrm{d}\phi_i}{\mathrm{d}t} = \omega_i \tag{2.10}$$

$$\frac{2H_i}{\omega_R}\frac{\mathrm{d}\omega_i}{\mathrm{d}t} = P_i - \mathrm{Re}\sum_{j\neq i}(V_j I_{ij}^*) - \alpha_i\omega_i \tag{2.11}$$

$$= P_i - \mathrm{Re}(U_i(I_i^c)^*) - \alpha_i\omega_i \tag{2.12}$$

$$= P_i - E_{d,i}I_{d,i} - E_{q,i}I_{q,i} - \alpha_i\omega_i \tag{2.13}$$

but they are now complemented by two equations for the complex voltage,

$$T_{d,i}\frac{\mathrm{d}E_{q,i}}{\mathrm{d}t} = -E_{q,i} + X_{d,i}I_{d,i} + E_{f,i}\ , \tag{2.14}$$

$$T_{q,i}\frac{\mathrm{d}E_{d,i}}{\mathrm{d}t} = -E_{d,i} + X_{q,i}I_{q,i}\ . \tag{2.15}$$

The new parameters have the following physical interpretation: $E_{f,i}$ is the reference voltage at which the generator is run. The time constants $T_{d,i}$, $T_{q,i}$

parametrize the speed of the voltage dynamics in the d- and q-axis. Finally the reactances $X_{d,i}$, $X_{q,i}$ parametrize the influence of the currents in the generator on the voltage.

The limit towards the swing equation is provided by setting $E_{q,i} = E_{f,i}$ and $E_{d,i} = 0$, and ensuring that $\frac{\mathrm{d}E_{q,i}}{\mathrm{d}t} = \frac{\mathrm{d}E_{q,i}}{\mathrm{d}t} = 0$. This occurs in the limit

$$\frac{X_{d/q,i}}{T_{d/q,i}} \to 0 \; . \tag{2.16}$$

For the fixed point of the 4th-order model it requires more than just the power flow balancing:

$$\omega_i^\star = 0 \; , \tag{2.17}$$
$$P_i = E_{d,i}^\star I_{d,i}(E_d^\star, E_q^\star, \phi^\star) - E_{q,i}^\star I_{q,i}(E_d^\star, E_q^\star, \phi^\star) \; , \tag{2.18}$$
$$E_{q,i}^\star = X_{d,i} I_{d,i}(E_d^\star, E_q^\star, \phi^\star) + E_{f,i} \; , \tag{2.19}$$
$$E_{d,i}^\star = X_{q,i} I_{q,i}(E_d^\star, E_q^\star, \phi^\star) \; . \tag{2.20}$$

In Appendix B I provide a derivation of the form of the equation used here, from the form in the engineering literature, which allows to use reference numerical values for the various parameters introduced.

2.2.3 Renewable Generator Dynamics

Besides certain specifics of the distribution grid architecture it is important to analyze the novelties of the node dynamics induced by RES. First, distribution grids are increasingly dominated by inverters since 90% of RES, which are grid-connected via inverters, are installed in distribution grids. In the past, distribution grids held hardly any dynamic components. In Section 2.2.3.1 a brief review of different inverter types and their corresponding dynamics shall give an idea of the broad application ranges for inverters with their chances and risks. Second, previously passive electricity consumers are equipped with smart metering technology and become active power balancers. A simple approach to incorporate demand response is the the concept of Decentral Smart Grid Control, explained in Section 2.3. Third, the fluctuating generation from RES, its intermittent nature and its influence of grid stability is an important topic. To raise awareness for this issue, in Section 2.2.3.2 the wind and solar model (Anvari, Lohmann, et al. 2016; Anvari, Werther, et al. 2017; K. Schmietendorf et al. 2016) will be discussed briefly.

2.2.3.1 Inverter Types and Control

Control theory deals with the control of continuously operating dynamical systems where power system control is one potential application. Power system control operates on many levels and time scales. Usually, transmission system operators are in charge of balancing the power system and for that they introduced the concepts of primary, secondary and tertiary control for which reserves are traded on different markets. Primary control needs to balance second-fast fluctuations with automatic so-called *droop control*. Droop control is solely based on local measurements with a "proportional controller" that regulates the power output from conventional generators' rotating masses or inverters' fast storage systems (De Brabandere et al. 2007). The lack of central communication infrastructure comes at the price of small error or small offset in power grid frequency. Hence, these methods are called droop control methods. The frequency is again reset to the normal frequency of 50Hz with secondary control mechanisms. Finally, tertiary control takes over by balancing the power mismatch where it appeared locally. Fast primary and secondary control are then available again to globally balance frequency fluctuations (Dörfler, Simpson-Porco, et al. 2016).

Future power system control will be the task of inverters that connect most RES to the grid. Inverters do not have an inherent physical relation between frequency and active power generation as synchronous machines do. However, inverters can be programmed in many different ways of control to artificially establish such a relationship. Generally, two main operation modes for inverters can be distinguished – *grid-forming* and *grid-feeding*

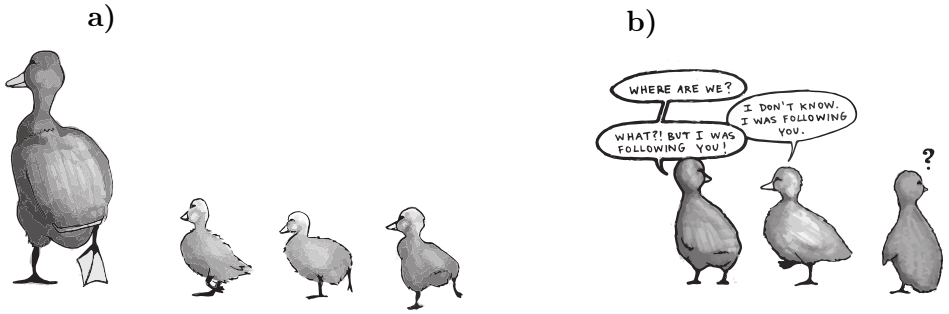

Figure 2.4: **Illustration of power systems a) with and b) without grid-forming inverters** that shows the problem that power systems with b) only grid-following inverters create in the absence of grid-forming inverters of frequency-setters. The small ducks represent grid-following inverters. At the absence of grid-forming inverters, represented by the adult duck in a), frequency setters are missing and thus the remaining inverters have no frequency to follow. The figures are designed and kindly provided by Outi Supponen.

mode. This section closely follows the classification of (Schiffer, Zonetti, et al. 2016). The latter type may also be called grid-following mode. Such inverters adjust their power output according to the measured frequency signal. With more conventional generators being replaced by such frequency following devices a lack of frequency setting or forming elements appears. In simple words, with all devices following the grid frequency, there is no leading element. This issue is illustrated in Fig. 2.4. At the same moment, grid-feeding inverters do not contribute to the power system's inertia. For this reason, grid-forming inverters are of great importance to give a frequency set point to the remaining following elements and to provide virtual inertia (Groß et al. 2017).

In grid-feeding mode the inverter operates as a power source which means active and reactive power, P and Q respectively, are specified. Typically, these values are set by higher control scheme such as tertiary control. Most photovoltaic (PV) and wind power plant units are connected to the grid via inverters operating in grid-feeding mode. Here, the grid frequency serves as input signal for the control loop that adjusts the active power, $P_i(t)$, linearly anti-proportional with droop constant $\tilde{k}_p$ to deviations, ω, from the desired reference frequency, ω_R. Note: here and in the following $\omega =: \tilde{\omega} - \omega_R$ is always the frequency in the co-rotating frame relative to the absolute frequency $\tilde{\omega}$:

$$P_i(t) = P_{d,i} - \frac{1}{\tilde{k}_p}\omega_i(t) \tag{2.21}$$

$P_{d,i}$ is the desired or possible power output from the generation unit. This control scheme does not support virtual inertia provision. On top, the measurement of the frequency input signal leads to a delayed control reaction (ENTSO-E 2017). This transforms the power grid dynamics into a system of delayed differential equations.

In grid-forming mode the output voltage can be specified by the control designer. Grid-forming inverters are an important element for frequency and voltage regulation in a power grid. E.g. a microgrid with large RES shares connected in grid-feeding mode, need a certain percentage of grid-forming inverters. This is the case because grid-forming inverters may act as Virtual Synchronous Machines and are able to replace conventional generators inertia with virtual inertia to maintain grid stability after sudden power changes. For this, they use a smooth droop control that sets frequency according to a desired power infeed, $P_{d,i}$:

$$\omega_i(t) = \tilde{\omega}_i(t) - \omega_R = k_p(P_{m,i}(t) - P_{d,i}). \tag{2.22}$$

$P_{m,i}(t)$ is a low-pass measurement of the actual power, P_i, at node i:

$$\tau_P \frac{\mathrm{d}P_{m,i}}{\mathrm{d}t}(t) = P_{m,i}(t) - P_i(t). \tag{2.23}$$

This then leads to the same equations for the voltage angle ϕ and frequency ω in terms of the (virtual) inertia H, power infeed $P_{d,i}$, (virtual) damping α and the power flowing in and out at node i, P_i, (Schiffer, Goldin, et al. 2013):

$$\begin{aligned} \frac{\phi_i}{\mathrm{d}t} =& \omega_i, \\ \frac{\mathrm{d}\omega_i}{\mathrm{d}t} =& \frac{1}{H}(P_{d,i} - \alpha\omega_i - P_i(t)). \end{aligned} \tag{2.24}$$

The virtual inertia and damping for the network model is given by the low-pass filter exponent τ_p and the droop control parameter k_p from grid-forming inverters: $H = \tau_p/k_p$, $\alpha = 1/k_p$, $\forall i$ with $i = 1, .., N$.

The grid-supporting mode is provided by grid-forming inverters with an additional outer control-loop that is able to determine the reference output voltage.

2.2.3.2 Intermittent Characteristics of Renewable Power Fluctuations

Wind and solar power production exhibit intermittent characteristics, which are defined through the presence of large and correlated high frequency fluctuations (Anvari, Lohmann, et al. 2016; Anvari, Werther, et al. 2017). The stochastic nature of such processes was identified in Anvari, Lohmann, et al. 2016 with the help of time series analysis. Important characteristics are the probability distribution function (PDF), the increment distribution and the power spectrum. The increment X_τ defines the change of a variable, $X(t)$, within a time lag, τ:

$$X_\tau = X(t + \tau) - X(t). \tag{2.25}$$

The increment analysis can be done with considering the τ- dependence of the probability density functions (PDFs). If both PDFs, of the power time series and its increments, are heavy tailed, with high probabilities of extreme events, this is defined as intermittency (the tails are not exponentially bounded (Asmussen 2008)).

The power spectrum is the discrete Fourier transform of the fluctuations time series. According to the Wiener–Khinchin theorem, autocorrelation and power spectrum are Fourier pairs (Chatfield 2016). Considering the power spectrum of the wind and solar power time series in the frequency domain, $0.001 < f < 0.1$ Hz, indicates that they are turbulent-like sources. The power generation from wind and solar power plants has a power spectrum that is power-lawed with $-5/3$, the Kolmogorov exponent of turbulence (Anvari, Lohmann, et al. 2016; Milan et al. 2013). Consequently, the RES time series shows long-term temporal correlations. The Hurst exponent, $0 < h < 1$, is a measure for such long-time memory in a time series (Alessio et al. 2002; Carbone et al. 2004; Hurst 1956; Preis et al. 2009). It quantifies the rate at which the autocorrelations of the time series decreases with increasing time lag. Due to their turbulent nature, wind and solar time series have a long-term positive autocorrelation, i.e. h is close to unity.

Both intermittency and spectrum with power-law behavior remain in the cumulative wind farms and solar fields (Anvari, Lohmann, et al. 2016; Anvari, Werther, et al. 2017; Milan et al. 2013).

In K. Schmietendorf et al. 2016, the authors have compared the grid stability influence of white Gaussian noise, Gaussian noise with a turbulent power spectrum and intermittent noise. Their results show how the time-correlated noise leads to the stronger network destabilization. Whereas

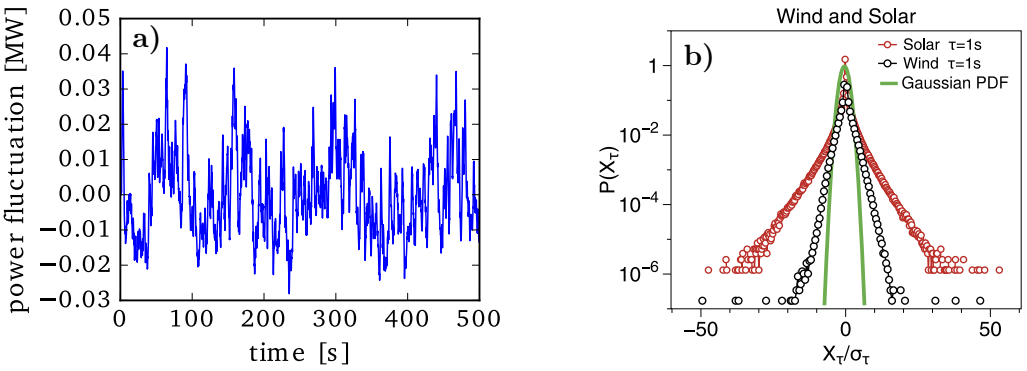

Figure 2.5: **a) Time series and b) increment distribution of intermittent power fluctuations.** The intermittent power time series $\Delta P(t)$ in a) is jointly generated by the solar and wind models of (Anvari, Lohmann, et al. 2016; K. Schmietendorf et al. 2016). b) Comparison of the increment probability distribution functions (PDFs), $P(X_\tau)$, for solar and wind power fluctuations. The PDFs are plotted in log-linear scale with a time lag of 1s. X_τ values (see (2.25)) are measured in units of their standard deviation σ_τ. A Gaussian PDF with unit variance is plotted for comparison. Figure b) is taken and adapted from (Anvari, Lohmann, et al. 2016).

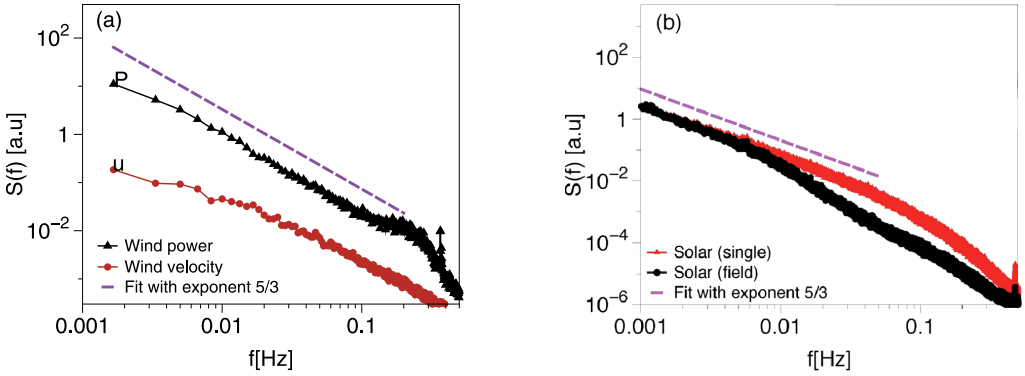

Figure 2.6: **Power Spectra for a) wind and b) solar power fluctuations.** The figures are taken from (Anvari, Lohmann, et al. 2016). (a) Power spectra of wind velocity, wind power fluctuations in log–log scale, for a data set with a resolution of 1 Hz. The Kolmogorov exponent of 5/3 is represented by dashed lines. (b) Power spectra of irradiance fluctuation for a single site (red) and averaged over 16 sensors (black) in log–log scale measured in Hawaii (S2) with a sample rate of 1 Hz.

noise with the same power spectrum but without intermittency induces smaller frequency deviations. Consequently, it is most important to include the intermittent nature of RES power fluctuations in future grid stability analysis.

Wind and Solar Models. Recently, models for the reproduction of wind and solar power fluctuations were introduced (Anvari, Lohmann, et al. 2016; Anvari, Werther, et al. 2017; K. Schmietendorf et al. 2016; Milan et al. 2013). A sample time series, $\Delta P(t)$, of equally weighted wind and solar power fluctuations, $\Delta P_W(t)$ and $\Delta P_S(t)$ respectively, is shown in Fig. 2.5.

$$\Delta P(t) = 0.5\Delta P_W(t) + 0.5\Delta P_S(t). \tag{2.26}$$

In order to raise an awareness for the special stochastic properties of wind and solar power fluctuations in the following both models are explained in more details.

The wind model is based on a *Non-Markovian Langevin* type model, developed in (K. Schmietendorf et al. 2016). A Langevin equation is a stochastic differential equation describing the time evolution of a subset of the degrees of freedom (Chandler 1987). These degrees of freedom typically are collective, slow (macroscopic) variables and fast (microscopic) variables of the system. The latter are responsible for the stochastic nature of the Langevin equation.

The model introduces the correlation in time and hence memory by coupling two Langevin-type processes, $\dot{x}$ and $\dot{y}$. This way the wind power dynamics become Non-Markovian. The correlation conceptually depicts the strongly non-Gaussian intermittent increment statistics. All model parameters are fitted to the time series data to reproduce the $-5/3$-power-lawed power spectrum:

$$\dot{y}(t) = -\gamma y(t) + \Gamma(t), \tag{2.27}$$

$$\dot{x}(y,t) = x(t)\left(g - \frac{x(t)}{x_0}\right) + \sqrt{Dx^2(t)}y(t). \tag{2.28}$$

The parameter D controls the strength of the intermittency. Choosing $D = 0.1$ and $D = 2.0$, and generates Gaussian and strongly intermittent data sets, respectively. Thus, for high values of D the time series become jumpier with more heavy-tailed increment PDFs.

The solar model generates time series of the solar clear sky index, the irradiance on earth with cloud-free atmosphere (Anvari, Lohmann, et al. 2016; Anvari, Werther, et al. 2017), which again can be related to solar power generation with geographic and power plant data. The model is a generalization of Langevin-type modeling which includes a jump process. The model reproduced properties that can also be determined from measured time series. Since it has been shown that the dynamics of wind power output can be modeled by an estimation of the Langevin equation (K. Schmietendorf et al. 2016; Milan et al. 2013) and wind turbulence influences solar irradiance and cloud formation, it is natural to base the model for solar fluctuations on Langevin equations as well. Only, the solar fluctuations can be even spikier since clouds moving over 2D solar panels can create shades within an instance. Although, the sunny and cloudy states could be modeled by the Langevin equation, flickering states (when there are lots of rapid cloud movements in the sky) do not belong to the class of continues diffusion processes. Accordingly, it requires a modified Langevin equation, i.e. jump-diffusion equation to model the clear-sky index for flickering states. The clear-sky index $x(t)$ is then given by

$$\mathrm{d}x(t) = \underbrace{D^{(1)}(x,t)\mathrm{d}t + \sqrt{D^{(2)}(x,t)}\mathrm{d}w(t)}_{\text{Langevin process}} + \underbrace{\xi \mathrm{d}J(t)}_{\text{jump process}} . \tag{2.29}$$

$\{w(t),\ t \geq 0\}$ is the scalar Brownian motion, and $D^{(1)}(x,t)$ and $D^{(2)}(x,t)$ are the deterministic drift and the diffusion functions, respectively, also known as the first and second Kramers-Moyal (KM) coefficients. All of the

functions and parameters in the modeling can be extracted directly from measured time series.

To model the fat tails of the increment distribution, the jump process $J(t)$ is introduced. It is a time-homogeneous Poisson zero-one jump process with jump rate λ which means in an infinitesimal time interval $\mathrm{d}t$, jumps may occur with the probability $\lambda \mathrm{d}t$. The waiting times between two successive jumps are characterized by an exponential (Poissonian) distribution (Anvari, Werther, et al. 2017).

2.3 Consumers and Smart Grid Control

Different *smart grid* approaches have been proposed to present ways to match supply and demand in such a fluctuating power grid. However, economic and political feasibility and market integration are often missed out. A key idea of various smart grid concepts is to regulate the consumers' demand (Butler 2007), a massive paradigm shift compared to the current power grid operation schemes (Albadi et al. 2008; Palensky et al. 2011). Many proposals for smart grids are based on sufficient information and communication technology infrastructure (Hofmann et al. 2015; Kok et al. 2005). However, such a centralized system would raise questions of cyber security and privacy protection (Ericsson 2010; Fang et al. 2012) and several studies highlight the cost burden these proposals implicate (EY GmbH 2013). In contrast, an alternative approach without massive communication between consumers and producers directly utilizes the grid frequency to adjust production and consumption. The frequency increases in times of power excess while it decreases in times of underproduction (Schweppe 1982; Short et al. 2007).

A novel smart grid concept, *Decentral Smart Grid Control* (DSGC), was introduced in (Walter 2014), based on earlier ideas by (Schweppe 1982), and its mathematical model proposed and analyzed in (Schäfer, Matthiae, Timme, et al. 2015). Using DSGC prosumers control their momentary demand on the basis of the grid frequency which can easily be measured everywhere with cheap equipment. This concept works very similar to inverter control. DSGC aims to stabilize the power system by encouraging consumers to lower their consumption in times of high load and low production and increase consumption in times of low load but high production. Instead of paying a constant price for electric power, consumers are offered a linear price-frequency relation $p_i(\frac{\mathrm{d}\phi_i}{\mathrm{d}t})$ (see Fig. 2.7)

$$p_i\left(\frac{\mathrm{d}\phi_i}{\mathrm{d}t}\right) = p_\omega - c_1 \cdot \frac{\mathrm{d}\phi_i}{\mathrm{d}t} \tag{2.30}$$

to motivate grid-stabilizing behavior. Although consumer reaction might be very complex, I assume a linearized power-price relation $\hat{P}_i(p_i)$

$$\hat{P}_i(p_i) \approx P_i + c_2 \cdot (p_i - p_\omega) \tag{2.31}$$

by the consumers close to the stable operational state. Plugging (2.30) into (2.31) and defining $\gamma = c_1 \cdot c_2$ leads to a linear response of consumed and produced mechanical power $\hat{P}_i(t)$ as a function of frequency deviation $\mathrm{d}\phi_i/\mathrm{d}t$:

$$\hat{P}_i(t) = P_i - \gamma_i \frac{\mathrm{d}\phi_i}{\mathrm{d}t}(t) \quad \forall i \in \{1, ..., N\}, \tag{2.32}$$

where γ_i is proportional to the price elasticity of each node i, i.e., measures how much a producer or consumer is willing to adapt their consumption or production, see also Schäfer, Matthiae, Timme, et al. 2015. In general, such an adaptation will not be instantaneous but with a certain delay τ that is due to measurement and reaction times and hence:

$$\hat{P}_i(t - \tau) = P_i - \gamma_i \frac{\mathrm{d}\phi_i}{\mathrm{d}t}(t - \tau) \quad \forall i \in \{1, ..., N\}. \tag{2.33}$$

I can now substitute the function $\hat{P}_i(t - \tau)$ from (2.33) for the fixed value P_i in the system without DSCG (2.6) and obtain the equation of motion

$$\begin{aligned} &\frac{\mathrm{d}^2\phi_i}{\mathrm{d}t^2} = P_i - \alpha_i \frac{\mathrm{d}\phi_i}{\mathrm{d}t} + \sum_{j=1}^{N} K_{ij} \sin(\phi_j - \phi_i) - \gamma_i \frac{\mathrm{d}\phi_i}{\mathrm{d}t}(t - \tau) \\ &\forall i \in \{1, ..., N\}, \end{aligned} \tag{2.34}$$

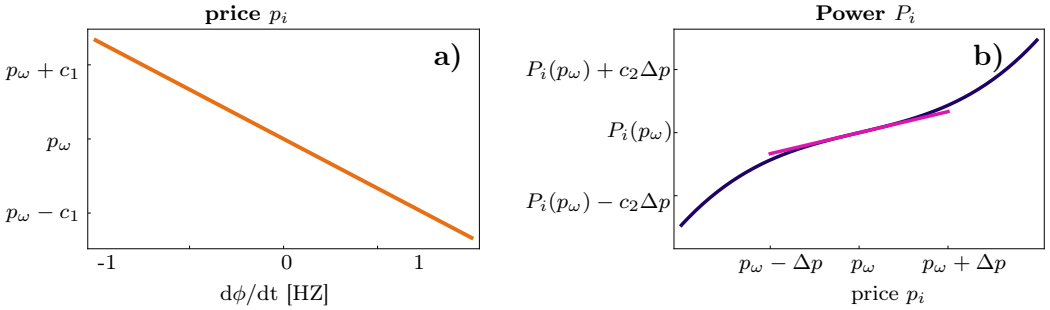

Figure 2.7: **a) Price-frequency function and b) demand elasticity for Decentral Smart Grid Control.** The linear price-frequency relation of DSGC in a) shall motivate consumers to stabilize the grid. For example, if the production is larger than the consumption, the power grid frequency increases. Hence, decreasing prices should motivate additional consumption. b) Although consumers might react nonlinearly towards price-changes (dark blue), I assume a linear relationship (purple) close to the operational frequency in the co-rotating frame, which corresponds to $\omega = \mathrm{d}\phi_i/\mathrm{d}t = 0$.

with DSGC including a delayed power adaptation.

Chapter 3

Power Grid Analysis

3.1 Future Stability Challenges

The European Network of Transmission System Operators (ENTSO-E) recently published a guidance document for national grid codes providing information about "operational stability challenges" for power systems with a "High Penetration of Power Electronic Interfaced Power Sources" (ENTSO-E 2017). Since most RES are connected to the grid via power electronics, this document gives an overview of grid stability issues with high shares of RES. In the broad spectrum of stability analysis, this work gives a central role to the maintenance of the synchronizing state.

With respect to frequency and voltage angle stability (for an explanation see Sect. 3.2), ENTSO-E points out how a low total system inertia (TSI) leads to an excessive rate of change of frequency (ROCOF). At the same time, the heterogeneous distribution of TSI poses the risk that the synchronous European grid may split into subnetworks. The low synchronizing torque decreases the system's ability to synchronize the voltage angle and power between generation units and to overcome sudden voltage angle disturbances (see Section 3.3). Finally, the interaction between conventional generators and power electronics may lead to unwanted resonance effects.

In terms of voltage stability (see Sect. 3.2) the adverse interaction between closely connected inverter controllers was pointed out that may lead to "SubSynchronous Resonances (SSR) or Super Synchronous Instability (SSI)". It is also imaginable that the system voltage collapses after a frequency instability induced a system splitting into power imbalanced subareas.

The power quality or quality of supply is expected to decrease due to a lack of "sinks" to correct low order system harmonics including "inter-

harmonics" and "to correct phase unbalance".

Thus, according to ENTSO-E the holistic dynamic modeling and analysis of future power grids with high shares of RES is an important prerequisite for pushing the RES share in Europe's power system. In the following, with this recommendation in mind, the methods for analyzing future power systems and their stability are presented. Specific focus are the transient stability of non-stochastic systems and the stability and power quality of systems with intermittent power generation.

3.2 Introduction to Power Grid Analysis

Generally, power grid analysis evaluates the power system's performance with respect to its *reliability, security, power quality and power system stability* (Von Meier 2006). To give an overview, all four aspects of power system analysis are presented in short, however, the main focus will be power system stability and how it relates to the issue of power quality.

The power system's reliability describes the continuity of electric supply to the customer. It is measured by the ability of the power system to meet load demand, with reserve margins, loss of load probability, outage frequency, outage durations and the derived total outage time. The aspect of reliability is rather diagnostic giving policy makers, regulators and grid operators comparative numbers for their strategic planning.

System security is directly affecting grid maintenance and operation. A secure system can sustain one or more contingencies where the $(N-1)$-criterion is a widely used standard, which states that after one line fault event the system must remain functional. A further system security standard involves power flow analysis with line constraints, limiting the degree of line capacity utilization. These steady-state analysis methods do not consider system states during a fault event and the transition into the new state.

Power quality refers to whether voltage and frequency stay within a prescribed range and whether the waveform or shape of the voltage time evolution resembles a sine wave or has harmonic distortions. Such distortions appear from grid-connected devices inducing oscillations higher than 50Hz. The subject of power quality is strongly connected with power system stability since certain stability measures may be derived from whether a system crosses certain frequency or voltage bounds (see 3.3.2 and 3.4). E.g. the frequency threshold of 0.01Hz corresponds to the so-called dead band from the German transmission code which defines at which frequency primary control actions kick in to balance deviations from the desired 50Hz

set point (Verband der Netzbetreiber e.V. 2007). This precaution is supposed to guarantee power quality with the grid frequency not exceeding ±0.2Hz. Similarly, over- and undervoltage have to stay in the limits of ±10% deviation from their nominal value (Verband der Netzbetreiber e.V. 2007).

Power system stability is the system's ability to maintain synchrony, hold a balanced operating state and thus remain in its operating equilibrium (Kundur et al. 1994; Pavella et al. 2000; Sauer et al. 2006).

Synchronization defines the matching of frequency between the dynamic grid units in an alternating current (AC) power system. It is established by an "adjustment of rhythms of oscillating objects due to their weak interaction" (Pikovsky et al. 2003). In a power grid such weak interaction is the coupling of oscillators through the power flow on the lines. The synchronization in power grids is different from the notion of complete or phase synchronization. In the synchronized state, generators are rotating at the same frequency, ω, the phases, ϕ, however remain different but constant since the transmission of power between two generators is proportional to the sine of the phase difference. Formally, it is defined as:

$$\lim_{t\to\infty} |\omega_i - \omega_j| = 0 \text{ and } \lim_{t\to\infty} |\phi_i - \phi_j| \geq 0 \tag{3.1}$$

where the phase difference is constant and eq. (3.1) holds for all N grid nodes: $i, j \in \{1, ..., N\}$.

Power system stability can be classified into angle, frequency and voltage stability (see Fig. 3.1). The first defines the power system's ability to maintain synchrony which divides into small-signal stability and transient stability. Here, the differentiation is according to the disturbance

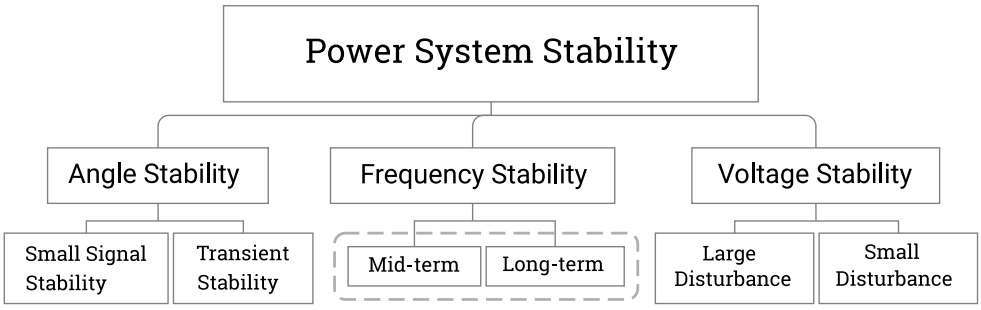

Figure 3.1: **Classification of power system stability** into angle, frequency and voltage stability according to (Kundur et al. 1994; Pavella et al. 2000; Sauer et al. 2006).

strength. Small-signal stability concerns the system's ability to synchronize after small perturbations that can be approached with linear stability analysis. Poor small-signal stability can lead to non-oscillatory and oscillatory instability due to a lack of inertia or synchronizing torque or damping, respectively. In contrast, transient stability denotes the system's ability to restore synchrony after large disturbances. Power system transient stability is a strongly nonlinear and high-dimensional problem. The time window for this type of stability analysis does not exceed 10s.

Frequency stability refers to the system's ability to keep the frequency in an acceptable range and relates to the system's generation and load imbalance. Here, the corresponding time scale is in the mid- and long-term ranging from minutes up to several tens of minutes.

Voltage stability relates to the system's ability to maintain acceptable steady voltages. After large disturbances, such as system faults and loss of generation, long time-domain simulations from seconds to minutes are necessary to check whether the voltage can be securely controlled. The reaction of voltage to small disturbances at a given instant in time defines small-disturbance voltage stability.

3.3 Transient Stability of Deterministic Systems

This section is mostly based on parts of the publication Auer, Kleis, et al. 2016. It starts with the introduction of conventional tools for transient stability analysis in order to motivate the necessity of novel measures for analyzing a system's stability with respect to large perturbations.

Transient stability can be either assessed through time-domain (T-D) analysis or by non-conventional approaches as direct stability assessments and automatic learning ones. T-D approaches assess stability by solving the system's dynamic equations in the during-fault (around 100ms) and post-fault configurations (3-15s). The definition of criteria for the loss of synchronism is usually left to system operator's experience. T-D methods are able to accurately asses stability information and relevant parameter ranges for any power system design. However, due to the computational costs, they are not suitable for real time stability screening or power system control. Further, they are no quantitative measures of the system's instability (Pavella et al. 2000).

Another method for the assessment of transient stability is the Equal Area Criterion (EAC) that was used to compare different model details

(Weckesser et al. 2013). The EAC allows to assess information about grid stability in real time to prevent a system break-down. It determines the system's capability to absorb the kinetic energy change induced by a disturbance in electric power (Pavella et al. 2000). In order to be usable as a real-time preventive measure, the EAC avoids full time-domain simulations. The EAC is a long-known method for a single machine connected to an infinite bus. An infinite bus describes how most small households "see" the grid: a bus whose voltage and frequency remains constant even with load variations since it has infinite power capacity (Sauer et al. 2006). For larger systems, the SIME (Single-Machine Equivalent) separates the network into critical and non-critical machines by T-D simulations and aggregates them into groups to determine the parameters of the one-machine infinite bus system (Weckesser et al. 2013). Here, a possible source of errors is to correctly determine the critical and non-critical groups where the initial conditions in the T-D analysis are pivotal.

A direct method to assess small-signal stability is the study of Lyapunov exponents. The largest non-zero eigenvalue of the system's Jacobian, and thus the linearized dynamics around the fixed point, determines the local stability in a nonlinear dynamical system after small perturbations. The fixed points are given by the steady-state solution of the dynamical system equations (Pikovsky et al. 2003).

A convenient way to use this method on a network is the master stability function approach (Nishikawa et al. 2015; Pecora et al. 1998). This approach separates out the local dynamics and the network structure. As the general shape of the master stability function is independent of the actual network, it is possible to quickly evaluate the asymptotic stability of a given dynamical system for various topologies. However, problems arise if the Laplacian is not symmetric (Acharyya et al. 2012), e.g. in the case of ohmic transmission lines.

A direct method to evaluate the response to large perturbations in order to assess the domain of attraction of a certain fixed point is the Lyapunov direct method, also called Lyapunov's second method. It constructs a set of suitable Lyapunov functions for the dynamic equations of motion and investigates the sign the function and its derivatives have on the boundary of the stability domain (Bergen et al. 1981; Kundur et al. 1994; Pai et al. 1981; Willems et al. 1970). In this method, the difficulty is the right choice of Lyapunov functions and unfortunately there is no effective method to build such functions for general dynamical systems. Hence, Lyapunov exponents only give information about small-signal stability, and Lyapunov's second method is hard to realize in practice.

The measures I will discuss in the following assess the basin of stabil-

ity and so-called survivability (Hellmann et al. 2016) of the system against large, random perturbations at single nodes of the network. They are applicable to general dynamical systems and thus outside the scope of the other methods. Still, in my description I focus on *deterministic systems*[1]. Further, basin stability and survivability give information about the high-dimensional basin of attraction or desirable region, respectively, with a sampling-based approach. This way the stability analysis becomes numerically tractable since the random sampling of initial conditions, analogously to a repeated Bernoulli experiment, has an estimated standard error proportional to $1/\sqrt{N}$ (Menck, Heitzig, Marwan, et al. 2013).

3.3.1 Basin Stability

The Basin Stability (BS) of a multi-stable dynamical system with trajectories $x(t)$ corresponds to the fraction of random initial conditions whose trajectories approach a desired attractor $X^\star$ (Menck, Heitzig, Marwan, et al. 2013), which in the following I take to be a fixed point of the system. Unstable paths will lead the system to a different, undesirable attractor. Key feature of basin stability is that, by studying just the volume rather than the shape of the basin of attraction, it becomes numerically tractable to analyze even very high-dimensional systems (Hellmann et al. 2016). More formally, given a region in phase space X^0 that contains the initial conditions, the basin of attraction within X^0 is then $X^{BS} = \{x(0) \in X^0 | \lim_{t\to\infty} x(t) \in X^\star\}$. Assuming a uniform distribution of perturbations, the basin stability is the ratio of the volumes

$$\mu_B = \frac{\mathrm{Vol}(X^{BS})}{\mathrm{Vol}(X^0)} \,. \tag{3.2}$$

For a detailed discussion of BS, including the case of non-homogeneous distributions of perturbations, see Hellmann et al. 2016.

In the case of power grids I define the desirable attractor to be exactly the stationary state: $\omega^\star = 0$. For single-node basin stability only one node at a time is perturbed. The generic perturbations I study depend on the initial operating state of the system, $(\phi^\star, \omega^\star)$ for the second-order SM model or $(\phi^\star, \omega^\star, E^\star)$ for the fourth-order model (see Sect. 2.2.2). They are constructed by taking an arbitrary phase space perturbation $\delta\phi \in [-\pi, \pi]$ and $\delta\omega \in [-\omega_{\max}, \omega_{\max}]$ and adding them to a single entry in the vectors $\phi^\star$

[1] A deterministic systems does not involve randomness in the development of future states of the system. For a given initial condition it produces the same output (Hilborn 2000; Watts et al. 1998).

and $\omega^\star$, respectively. That is: $\phi_i(0) = \phi_i^\star + \delta_{ij}\delta\phi$, $\omega_i(0) = \omega_i^\star + \delta_{ij}\delta\omega$, and $E(0) = E^\star$.

3.3.2 Survivability

Survivability measures the ability of a system to stay within some predefined operating regime when experiencing large perturbations. For the power grid, this generally means I want to keep the frequency deviation below $\omega_{\text{crit}} = 0.2$Hz before controls kick in (according to ENTSO-E 2016). In Chapter 4 I investigate a number of different frequency and voltage thresholds that are more forgiving than the ones used in practice. The surviving region X^S of the system is defined as the set of those initial conditions whose trajectories never violate these bounds. Thus, the frequency maximum, $\max_t |\omega(t)|$, over the whole time series trajectory must be smaller than the critical frequency ω_{crit}: $X^S = \{(\phi(0), \omega(0)) \in X^0 | \max_t |\omega(t)| < \omega_{crit}\}$.

I construct the initial conditions through perturbing a single node again, choosing $\omega_{\max} = \omega_{\text{crit}}$. Assuming a uniform distribution of perturbations, the survivability is then given by the ratio of volumes

$$\mu_S = \frac{\text{Vol}(X^S)}{\text{Vol}(X^0)} \,. \tag{3.3}$$

In contrast to basin stability, which does not depend on the transient behavior of the system, the survivability is concerned with the entire trajectory. This can be considered a more adequate measure for power grids where large transient deviations could damage the power grids and require manual intervention to bring it back to an acceptable operating regime.

3.4 Stability of Stochastic Systems and Power Quality

The stability measures typically used in power grid synchronization analysis (Auer, Kleis, et al. 2016; Belykh et al. 2004; Hellmann et al. 2016; Menck, Heitzig, Marwan, et al. 2013; Nishikawa et al. 2006; Pecora et al. 1998), described in Section 3.3, are mostly studied for deterministic systems. First generalizations of basin stability to stochastic systems have been suggested (Serdukova et al. 2016; Zheng et al. 2016), but still remain to bee translated to high-dimensional systems. Instead, this thesis uses stability measures closely related to power quality guidelines since it is straightforward to evaluate whether power fluctuations lead to exceedances of frequency and voltage safety ranges.

The *exceedance* quantifies the instability of the synchronous state. It is the cumulated time an observable stays outside a defined "safe" region (Feller 1967). For this case I define a frequency threshold of 0.01Hz. This threshold corresponds to the so-called dead band from the German transmission code which defines at what frequency primary control actions kick in to balance deviations from the desired 50Hz set point (Verband der Netzbetreiber e.V. 2007). In Chapter 6, single-node fluctuations are applied

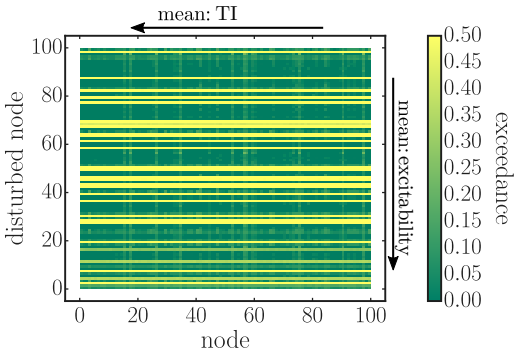

Figure 3.2: **Emergence of troublemaker and excitability from single-node exceedance.** Exemplary colorplot of single-node exceedances (see (3.4)) for each simulation run or disturbed node (y-axis) and each node in the network (x-axis) lossy lines: $Z = Y^{-1} = (0.4 + 0.3j)\Omega/km$.

to an example system with one run for each node, $i = \{1, .., N\}$, and the frequency response for each node $j = \{1, .., N\}$ is recorded. Thus, at this point I want to introduce derived exceedance measures. There are $N \times N$ frequency time series from which stability measures are obtained. Fig. 3.2 shows the $N \times N$ single-node exceedances, E_{ij}, for an example network. One grid value represents the probability of a network node j to be outside the given frequency band when node i is perturbed:

$$E_{ij} = P_i(|f_j| > 0.01\text{Hz}). \tag{3.4}$$

where $f = \omega/(2\pi)$ is the frequency in the co-rotating frame. This can be further aggregated into the following nodal measures:

- The average exceedance over all N nodes given a perturbation at i, which I call *Troublemaker Index* (TI):

$$\text{TI} = \bar{E}_i = \frac{1}{N} \sum_{j=1}^{N} E_{ij}. \tag{3.5}$$

  Power fluctuations at a node with a high TI causes large frequency deviations, often at many nodes.

- *Excitability* quantifies how much a single node is exceeding the frequency threshold on average when a random node in the network is

perturbed:

$$\bar{E}_j = \frac{1}{N} \sum_{i=1}^{N} E_j. \tag{3.6}$$

Nodes with high excitability react strongly for many origins of the perturbation within the network. I call such nodes highly sensitive.

Further, I study the *time average of frequency dispersion* (TAFD), the spread in frequency values between the network nodes averaged over the simulation time:

$$\text{TAFD} = \frac{1}{T} \int_0^T \left[\frac{1}{N} \sum_{i}^{N} (f_i(t) - \mu(t))^2 \right] \text{dt}, \tag{3.7}$$

where $f_i(t)$ is the ith node's frequency deviation and $\mu(t)$ is the mean frequency deviation, averaged over all nodes, at time t. This is a direct measure of the inhomogeneity introduced by the localized fluctuations.

And as a measure for temporal correlations I recorded the Hurst exponent h_{ij} (the Hurst exponent for the frequency time series of node j with fluctuation power input at node i). The single-node influence of node i on the mean Hurst exponent of the whole grid is calculated with:

$$h_i = \frac{1}{N} \sum_{j=1}^{N} h_{ij}. \tag{3.8}$$

Chapter 4

The Impact of Model Detail on Grid Stability Assessment

This chapter treats the question of how detailed a dynamical model of the power grid needs to be to accurately assess the impact of extreme events. Therefore, it refers to the overarching question: *How is it possible to measure and improve the resilience of power grids towards extreme events?* (see Sect. 1.3). The results from this work can be interpreted as a usability check of the novel methods – basin stability and survivability – that were just recently introduced to the power system's community (Hellmann et al. 2016; Menck, Heitzig, Marwan, et al. 2013). In Section 3.3.1, basin stability (BS) has been defined as the fraction of random, non-small initial conditions whose trajectories approach the fixed point. Section 3.3.2 has introduced survivability as the ability of a system to stay within some predefined operating regime when experiencing large perturbations. This chapter is to a great extent adopted from the related publication: **Auer, Kleis, et al. 2016**[1].

To keep the dimensionality of power grid modeling as low as possible, it is important to identify the necessary model detail for a specific research question. So far, it has not been studied which level of model detail is actually required to assess the response of large networks to large generic disturbances. This work starts to fill this gap by comparing the 4th-order synchronous machine (SM) model to the classic swing equation or 2nd-order model (see Section 2.2.2 for a detailed explanation of the SM model). Weckesser et al. 2013 have found the 4th-order model to be necessary for the post-fault analysis of power systems, however so far, the 2nd-order model is used in most of the theoretical work on power system analysis.

[1]

This chapter starts with analyzing representative time series of both model orders and highlights the differences in the grid model dynamics (see Sect. 4.1). Then, Section 4.2 compares the impact of model detail on the basin stability and survivability measure for different grid topologies. As the fourth-order model increases the model detail by the inclusion of voltage dynamics, Section 4.3 particularly focuses on voltage bounds in the stability paradigm.

The main take-home message is: including the voltage dynamics hardly changes the transient frequency behavior (survivability), but may strongly influence the asymptotic behavior (basin stability) of the model. Sections 4.2 and 4.3 provide a detailed explanation.

4.1 Differences in Model Dynamics

To perturb a system it is necessary to first identify its fixed points. Starting with a random dispatch scenario, that is, a random distribution of generators ($P_i = +1$) and consumers ($P_i = -1$) across the grid, I try to find a stationary solution for the swing equation (see eq. (2.6)). If there is no solution another random distribution of sinks and sources is chosen. Having found such a fixed point I use the state with frequency, $\omega = 2\pi f$, and phase, ϕ, given by the swing equation fixed point (see eq. (2.8)) and $E_d = 0$, $E_q = E_f$ as the starting point of a search for a fixed point of the 4th-order equation (see Eqs. (2.10)-(2.15)). I generally do not choose to perturb voltage to facilitate the comparison between the swing equation and the 4th-order model. There are some dispatch scenarios and networks, for which the fixed point search fails. Hence, there are power configurations, that allow for a dynamically stable power transport in the 2nd-order model, but are dynamically unstable with the inclusion of the voltage dynamics. This indicates that fixed points which are stable in the swing equation can become unstable when the coupling of the voltage is taken into account. In order to proceed with the comparison I choose dispatch scenarios that are dynamically stable for both, the swing equation and the 4th-order equation. I then consider single-node perturbations as described above.

Figures 4.1 and 4.2 contain several example trajectories for the case of the Scandinavian power grid (see Fig. 4.4 for an illustration of the Scandinavian grid). In many cases, the dynamics behave similarly (see Fig. 4.1). Only for the 4th-order model the frequency actually converges faster than for the swing equation while containing a much slower convergence on the voltage side.

In other cases, such as in Fig. 4.2b, the 4th-order model seems to be

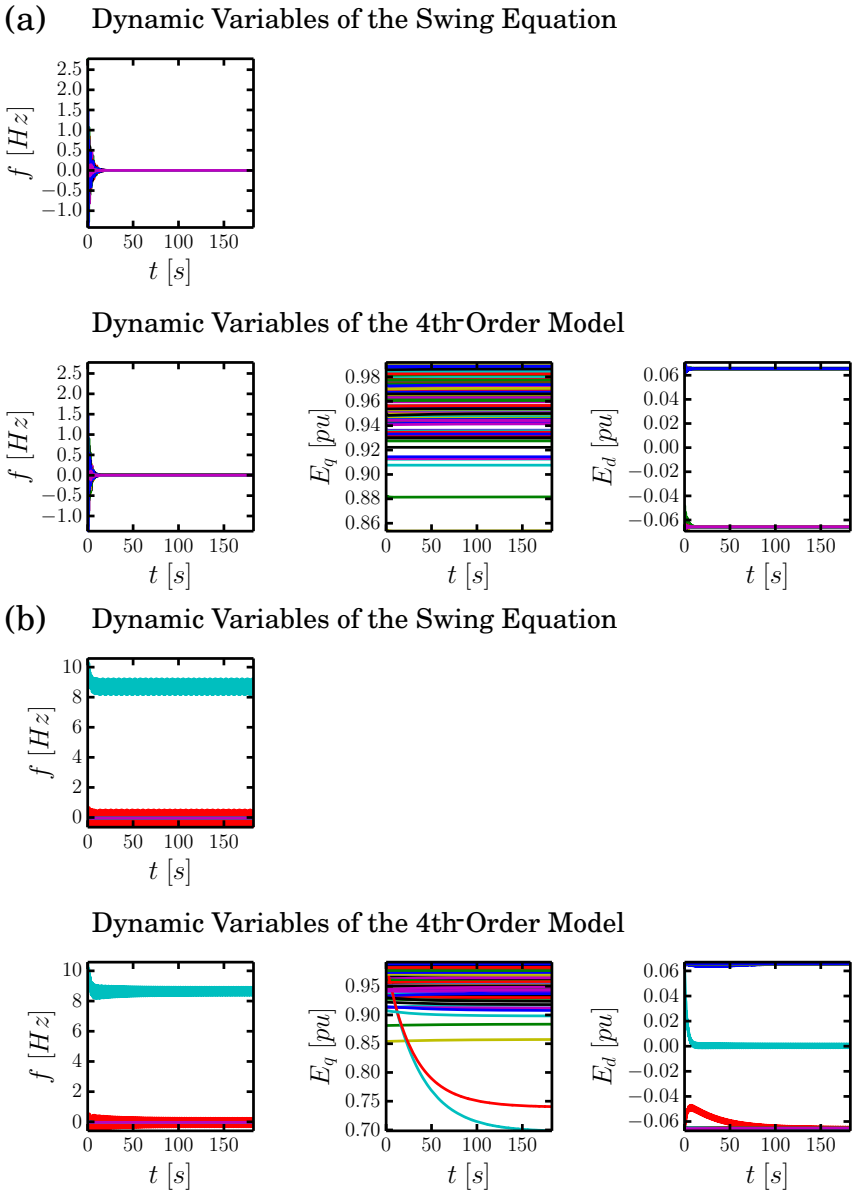

Figure 4.1: **Example trajectories for the Scandinavian power grid and different model detail. (a)** Fixed point convergence and **(b)** the limit cycle for random single-node perturbations with $\phi_{185}(0) = -0.38$ rad, $f_{185}(0) = -10.9$ Hz and $\phi_{199}(0) = -3.00$ rad, $f_{199}(0) = -10.6$ Hz, respectively. The colors of the trajectories represent the different grid nodes. Typically, the 4th-order model follows similar trajectories as the swing equation but converges faster.

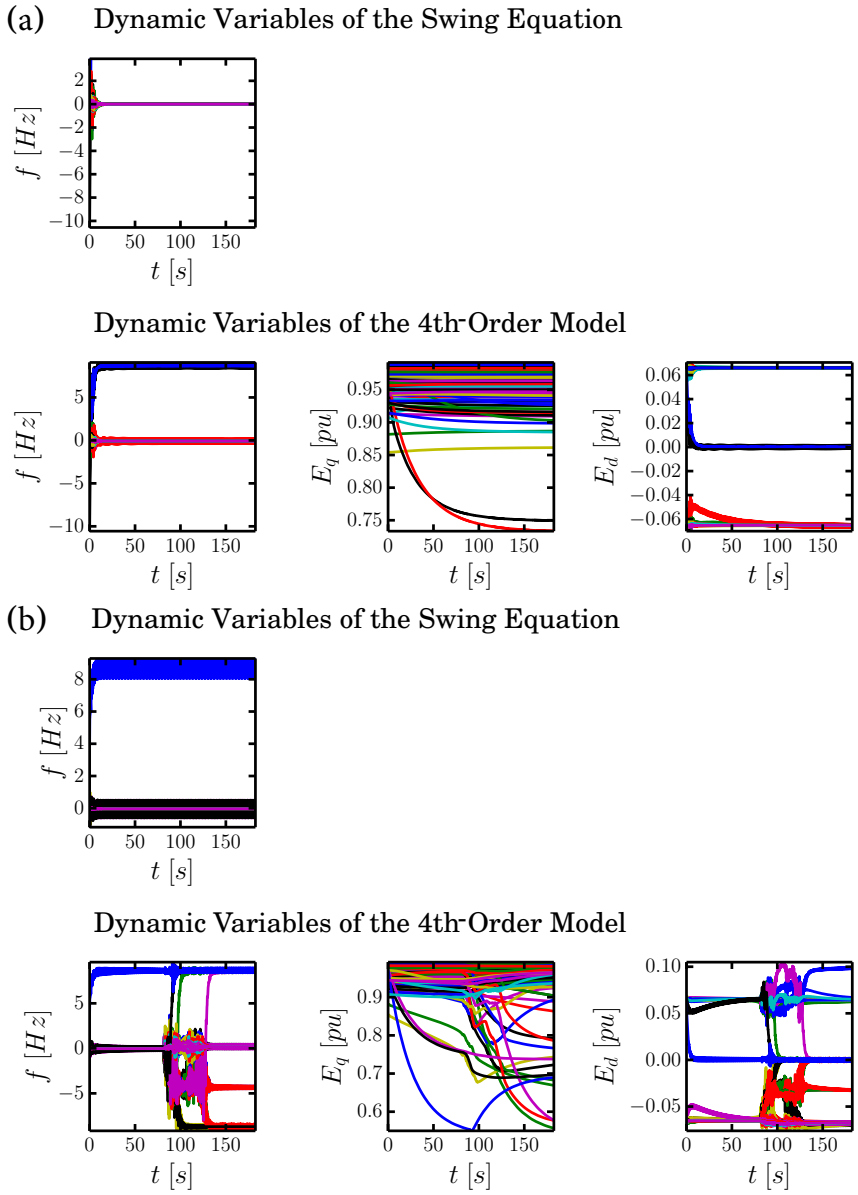

Figure 4.2: **Example trajectories show different attractors for different model detail. (a)** Potentially, the systems ends up in different attractors for 2nd order, fix point convergence, and 4th order, limit cycle ($\phi_{104}(0) = 1.6$ rad, $f_{104}(0) = -10.6$ Hz). **(b)** Occasionally, the slow voltage dynamics will drive the system into a chaotic transient at around 100s ($\phi_{231}(0) = 2.1$ rad, $f_{231}(0) = 4.0$ Hz). The colors of the trajectories represent the different grid nodes.

heading towards the same regime as the swing equation for a considerable amount of time, but then enters a new transient regime before settling into a different fixed point.

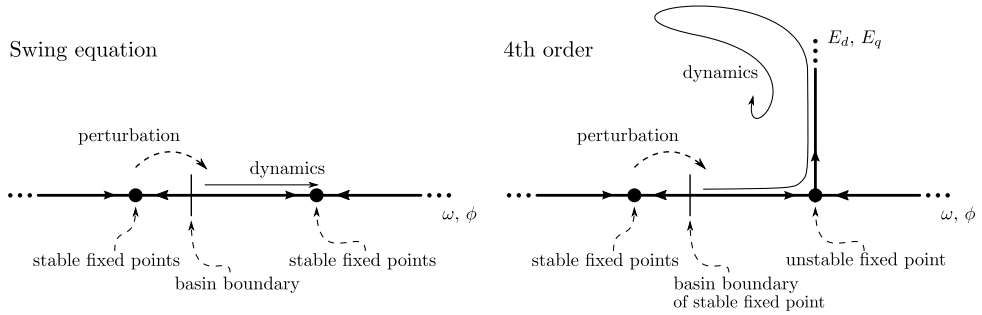

Figure 4.3: **A sketch of the dynamics around the fixed points for different model detail.** The fixed point on the right becomes unstable when adding the voltage directions. The perturbation, being purely in the ϕ, ω directions, leads close to the unstable fixed point, but then diverges in the voltage directions until it enters a nonlinear regime again. Being close to the unstable fixed point means the dynamics are slow on the transient.

This behavior can be understood in terms of the unstable fixed points of the 4th-order equations. In Fig. 4.2b, it appears that the trajectory first converges very fast towards a fixed point of the swing equation that is however unstable in the voltage direction. As the system is perturbed in the dimensions of the swing equation only, the trajectories end up getting very close to the unstable fixed point. This accounts for a long pseudo convergence, before the frequency diverges back into a deeply nonlinear regime and settling on a proper attractor after a transient of variable length (see Fig. 4.3 for illustration). The transient that leads back into the nonlinear regime is voltage driven and leads to large voltage deviations. Thus, in all cases I see a connection between large transient voltage deviations and changes in the asymptotic structure.

As noted above, if the Swing equation and the 4th order approach comparable fixed points, the convergence of the 4th order is faster. In the case of limit cycles, the oscillations tend to be smaller. Indeed, the Lyapunov exponent (see Sect. 3.3) of the 4th-order model, $\lambda^{(4)}$, is always larger than the one of the swing equation, $\lambda^{(2)}$: $\lambda^{(2)} = -0.1$ whereas I have found that in all systems I studied, $\lambda^{(4)} \in [-0.14, -0.2]$.

Generally it is always the case that a limit cycle is associated with a large voltage deviation. Conversely there are cases of large voltage deviations for fixed points, though they are considerably more rare.

4.2 Basin Stability and Survivability for Different Model Detail

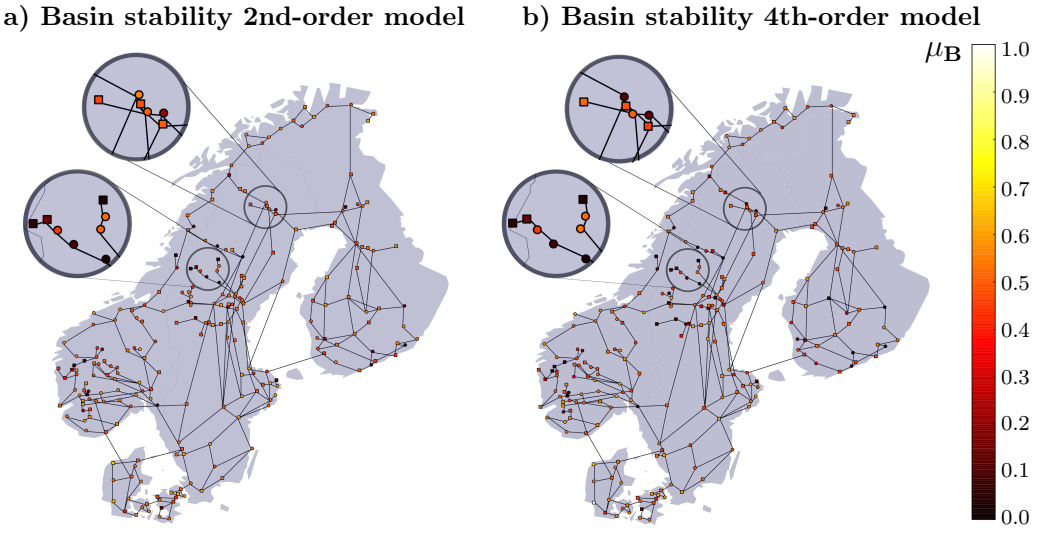

Figure 4.4: **Single node basin stability for (a) 2nd- and (b) 4th-order model** on the Scandinavian network and frequency disturbances in the range $[-100, 100]$. Most nodes do not change much moving from 2nd to 4th order (see inlay I). However, a few (see inlay II and central Finland) become dramatically less stable when including voltage dynamics. The color of the node represents the value of 2nd-order, $\mu_B^{(2)}$ in a), and 4th-order single-node basin stability, $\mu_B^{(4)}$ in b).

In Figure 4.4 compares basin stability for different model detail on a map of the Scandinavian power grid where each node is colored according to its basin stability value (Menck, Heitzig, Kurths, et al. 2014). I show that only few individual nodes have dramatically different frequency convergence. Generally, the geographical distribution of basin stability changes only slightly with increasing model detail.

Figs. 4.5a-4.5c show scatter plots of the single-node basin stability in the 4th-order model versus the Swing equation, for the Scandinavian power grid and two synthetic power grids (see Sect. 2.1.1). They illustrate that the swing equation approximates the stability of power grids well, however, there are some nodes for which it is overestimated. In synthetic grids, with small perturbations, the stability of a small number of already highly stable nodes is boosted by adding voltage dynamics. On the other hand, some nodes of average stability drop precipitously when switching to the 4th order. In the Scandinavian power grid, only the latter effect occurs. I suspect

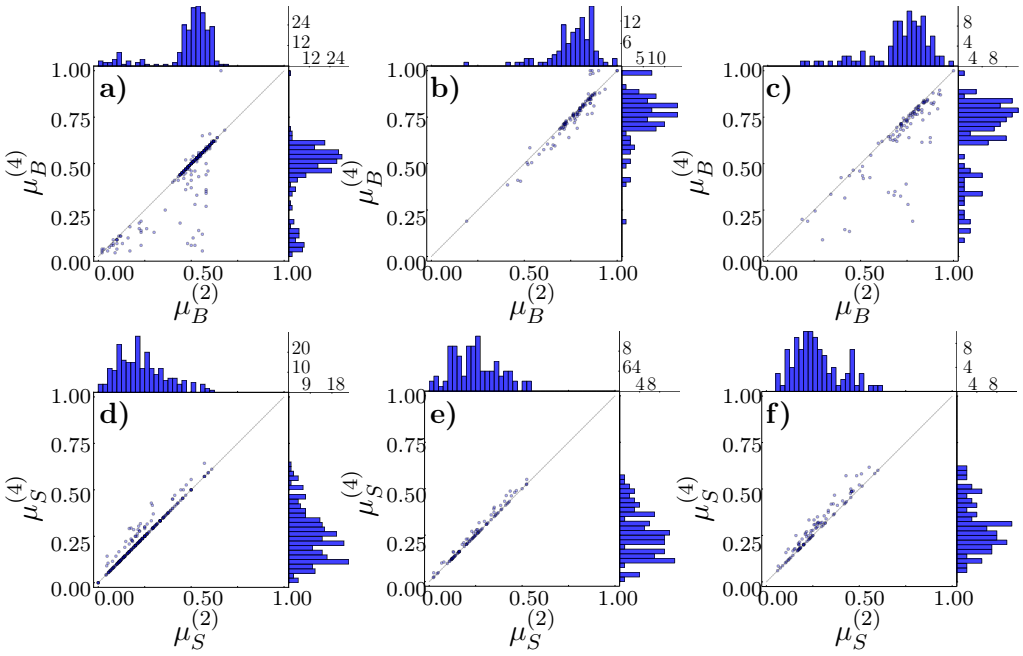

Figure 4.5: **Difference in 2nd and 4th-order single-node basin stability (top) and survivability (bottom)**. Top: Single node basin stability, $\mu_B^{(2)}$, $\mu_B^{(4)}$ and single-node survivability $\mu_S^{(2)}$, $\mu_S^{(4)}$. The left column, **(a)** and **(d)**, shows the Scandinavian grid (maximum frequency perturbation $|f_{\max}| = 87.2$ Hz, critical frequency $|f_{\text{crit}}| = 8.7$ Hz). The other two columns illustrate the results for two synthetic grids ($|f_{\max}| = 11.0$ Hz, $|f_{\text{crit}}| = 2.2$ Hz) with typical, **(b)** and **(e)**, and extremely divergent behavior, **(c)** and **(f)**.

that this is due to a fixed point, that is easily reached by a perturbation at that node, becoming unstable. As the comparison of different synthetic networks shows, the existence of such switching fixed points depends heavily on the network structure. Most networks I investigate behave more like the Scandinavian network, with only a few points changing strongly, some however show almost universal deviation.

Conversely, in the Figs. 4.5d-f the survivability for interesting frequency boundaries shows that the voltage dynamic does not affect the maximum deviations during the transient much. The voltage dynamic is apparently too slow to affect the first swing strongly, and the first swing continues to dominate the transient. Large deviations in the late transients occur mostly when the system is already in a limit cycle, and thus has already violated the frequency bounds.

4.3 Voltage and Asymptotic Dynamics

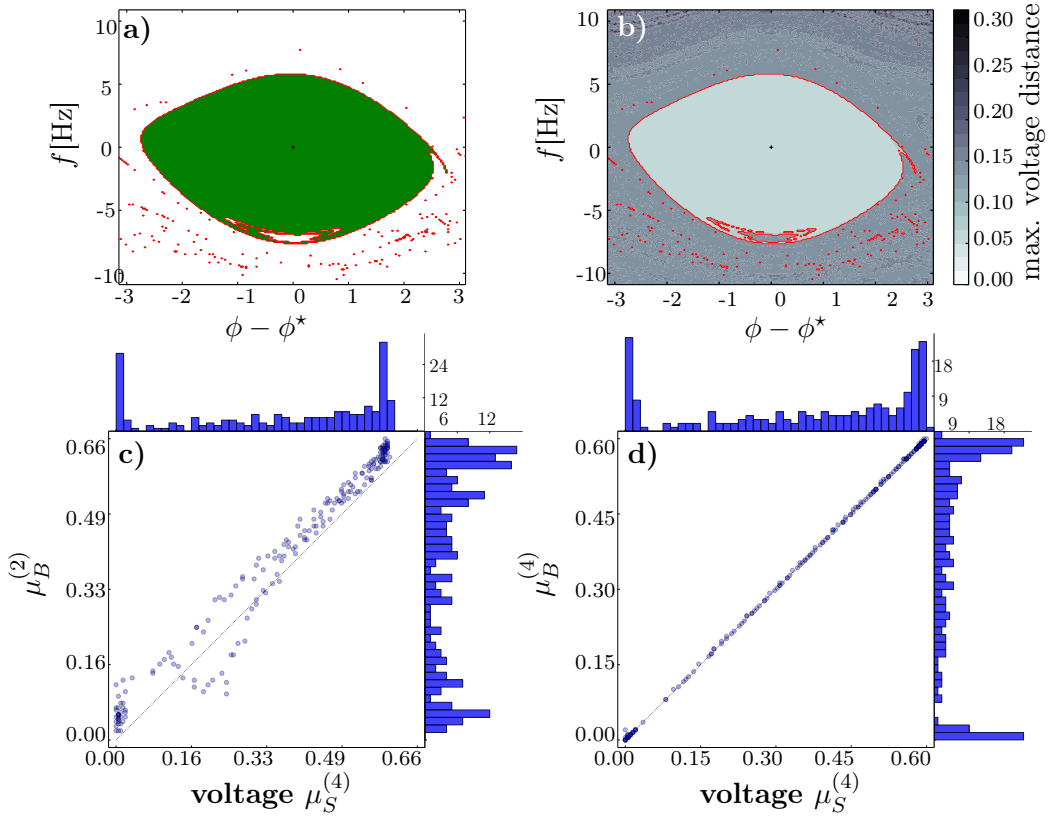

Figure 4.6: **Basin of attraction for different model detail and its relation to the basin of voltage survival.** **(a)** Basin of attraction for the fourth-order model. **(b)** Maximum voltage distance for different initial conditions. The red overlay is boundary of the basin of attraction. Comparison of basin of voltage survival of the 4th-order model with **(c)** basin stability for the swing equation and **(d)** the fourth-order model.

This section looks at the relationship between voltage transients and asymptotic structures in more detail. The plots in Fig. 4.6 are based on single-node perturbations in a synthetic power grid. They show that there is an extremely strong relationship between asymptotic behavior and transient voltages. Fig. 4.6a shows the basin of attraction (in green) of the fixed points after a perturbation in the frequency and phase at a specific node. The red line shows the boundary of the basin of attraction. Fig. 4.6b illustrates that there is a very distinct step in the maximum transient voltage as the basin boundary is crossed. Inside the basin, the maximum voltage disturbance is basically flat, and does not differ noticeably from the one at the fixed point.

After this qualitative reasoning, I also calculated a voltage version of single-node survivability which quantifies the ratio of perturbed trajectories for which the voltage disturbance stays below 0.1pu. For the 4th-order model (see Fig. 4.6d) all nodes of the example synthetic grid have the same ratios of trajectories that stay within voltage bounds and trajectories that show fix point convergence. For the swing equation a the correlation is visible as well (see Fig. 4.6c).

This is remarkable as it links an inherently transient property with an asymptotic one. Transient voltage and asymptotic frequency are interdependent. Hellmann et al. 2016 demonstrated that such a relationship does not exist between transient and asymptotic frequency behavior, $\mu_B^{(2)}$ and $\mu_S^{(2)}$, respectively.

4.4 Summary and Short Discussion

In this chapter I have taken a first step towards applying stability measures from complex systems to more detailed models of the power grid. At the end of this chapter, I want to revisit the initial question of how detailed a dynamical model of the power grid needs to be to accurately assess the impact of extreme events.

In short, I found that realistic voltage bounds play a role for the asymptotic but not for transient frequency structure. From that I can conclude that the survivability assessment for realistic frequency boundaries does not require power grid models with voltage dynamics. For that the 2nd-order model is sufficient.

In this analysis, I searched for distinct features of the different grid models (see Section 4.1). Before perturbation, I identified the system's stable states first. This search already showed that the fixed point structure of the swing equation and the 4th-order model differed more than anticipated. This picture was corroborated by the structure of the late, large transients triggered by slow voltage deviations (see sketch of Fig. 4.3). Most remarkably, the frequency and phase perturbation leads to a long trajectory that comes close to a fixed point which is stable in the swing equation but becomes unstable in the 4th-order model.

This change in the asymptotic structure implies a large change in the asymptotic behavior whenever such a fixed point becomes relevant. This occurred for several nodes in the Scandinavian power grid. Comparisons of several dispatch scenarios for the Scandinavian power grid uncovered a consistent small number of nodes showing these large changes, raising

hope that future work will be able to identify topological origins of such instabilities.

The survivability in contrast barely changes between the swing equation and the 4th-order model. This can be understood as a consequence of two aspects. First, the voltage dynamics is very slow, barely affecting the first swing. The convergence to a fixed point after the first swing are actually faster for the 4th-order model than for the swing equation as the Jacobian's largest non-zero eigenvalue is consistently smaller than that of the swing equation. The large transients that are triggered late in the system, on the other hand, occur mostly when the system is in a limit cycle regime, and thus has already left the acceptable frequency range.

Probably the most surprising result has been that the transient voltage behavior is intimately linked to the asymptotic structure of the system. Figure 4.6 shows the strong connection between voltage transients and asymptotic dynamics in more detail. Astonishingly, the overlay of plots for the basin of attraction and maximum voltage deviation deliver a perfect match (for an example artificial grid). Also, the scatter plot for the survival of voltage for maximum voltage deviations smaller 0.1 pu and basin stability for the 4th-order model has shown nearly perfect correlation.

Conversely this implies that transient voltage bounds are completely dominated by transient frequency bounds. This further removes the need to take voltage dynamics into account for survivability analysis.

Chapter 5

Decentral Reactive Power for Static Voltage Stability

Since Renewable Energy Sources (RES), such as wind and solar power plants, are deployed according to their optimal yield instead of the vicinity to the power consumers the distances of power transmission increase. A higher stress of the power grid infrastructure raises the issue of under- and overvoltages in distribution and transmission grids (DGs and TGs, respectively). Consequently, the demand for reactive power at all grid levels rises. At the same time RES offer a large potential to generate reactive power with their well-controllable DC/AC converters, that transform direct current (DC) to alternating current (AC) (Carrasco et al. 2006). Hence, decentral production units may be able to solve this self-inflicted problem by decentrally providing reactive power.

In this chapter, I estimate the future technical potential of reactive power provision from decentral resources in Germany. This work presents an effort to bridge the gap to research from electrical engineering. As such it uses conceptual models to approach this topic that is close to application. It relates to the overarching question of how to ensure static voltage stability and avoid grid congestion (see Sect. 1.4). To a great extent this chapter is based on the publication **Auer, Steinke, et al. 2016**.

I start this chapter with an introduction to previous work on the subject of reactive power provision from decentral resource (see Sect. 5.1). Section 5.2 describes the methodology and model cases used for this analysis. This includes a short description of the conceptual multi-layer grid model in 5.2.1 and of the reactive power optimization in 5.2.2. For the model cases I construct three prototypical scenarios: a PV-dominated region, a demand- and a wind-oriented one to validate my methodology. The results for the three test cases are shown in Section 5.3. In 5.4, I extend this analysis

to the case of Germany. For this study, I use the future 100% renewable scenario of the Kombikraftwerk 2 (KKW2) study (Fraunhofer IWES et al. 2014), which entails a TG model and values for the future power flows on each line for each hour of a reference simulation year. The KKW2 study also provides information on the reactive power demand for such a scenario. Since this analysis involves the interaction of TG and DG layers, I need to consider a multi-layer power grid model. In Auer, Steinke, et al. 2016, I introduced a simple representation of the remaining voltage levels as a fully symmetric tree-like multi-layer power grid that can be reduced to a simple chain structure (see Section 2.1.2). With optimal power flow computations the minimal and maximal reactive power, that can be provided at the connection point between TG and DG, is determined. This potential is then compared with the TG's demand for reactive power identified in Fraunhofer IWES et al. 2014.

5.1 Related work on Decentral Reactive Power Provision

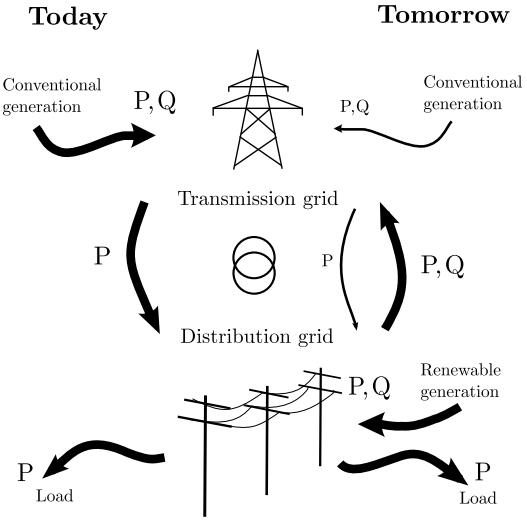

Figure 5.1: **Scheme for today's and future active and reactive power flow** between transmission and distribution grids. The scenario of "today" has conventional power generation at high grid levels whereas "tomorrow" renewable power will be generated in the distribution grid layers. P and Q are active and reactive power, respectively.

Since reactive power is best re-compensated locally, decentral generators are very plausible suppliers of reactive power in the DG. However, several studies (Dierkes et al. 2014; Sowa et al. 2015; Talavera et al. 2015) have shown that reactive power can also be transported to DGs' connection with the TG and have quantified its technical potential for exemplary DGs. Several publications propose local automatic reactive power control approaches and tap changer coordination (Carvalho et al. 2008; Demirok et al. 2011;

Mamandur et al. 1981; Turitsyn et al. 2011; Viawan et al. 2008; H. Wang et al. 2015) to stabilize voltage levels. In Kraiczy et al. 2015, the authors underline the need for a grid code revision for an automated variable RES control. Talavera et al. 2015 and Sowa et al. 2015 analyze the potential of reactive power exchange between MV and HV networks with either fixed or arbitrary *power factor*[1] and remotely controllable HV/MV *tap changers*[2].

In contrast to most previous work, in this analysis I also include the HV grid, allow for arbitrary power factors and controllable tap changers at all voltage levels. A significant technical potential of the decentral (often RES) generators in covering TGs' reactive power demands would be a strong argument in favor of investment in a smart-grid communications infrastructure and additional tap-changeable transformers to enable reactive power optimized DGs. In this chapter I will focus on the technical potential and leave an economic discussion to the future.

5.2 Methodology & Model Cases

5.2.1 Conceptual Multi-layer Grid Model

With the simplifying assumption of a fully symmetric tree-like multi-layer power grid model, it is possible to reduce the hierarchical grid to a simple chain structure. This short Section shall recall the description of the conceptual power grid model from Section 2.1.2.

With the symmetry assumption, I have to consider only one representative path from the UHV down to the LV level for the power flow calculations, see Fig. 2.2 for a schematic illustration. Here, every grid level is represented by one link with an impedance followed by a transformer (with tap changer in the range ± 0.05 p.u.) that connect to the neighboring grid level (see Fig. 2.2).

5.2.2 Optimal Power Flow Calculation

To maximize/minimize the reactive power provision at the connection between HV and UHV, I use a standard interior-point method for non-linear optimization. The independent variables are the reactive power infeeds at

[1] The power factor is defined as the ratio of the real power to the apparent power and is a dimensionless number in the interval $[-1, 1]$ (Sauer et al. 2006).

[2] Tap changers can be integrated in transformers and allow for variable discrete step changes for the ratios of lower and upper voltage (the initial and transformed voltage) (Faiz et al. 2011).

the different voltage levels, namely Q_{HV}, Q_{MV} and Q_{LV}. The objective function is

$$c(Q_{HV}, Q_{MV}, Q_{LV}) = \pm Q_{UHV}. \tag{5.1}$$

The sign of the objective, positive or negative, determines whether capacitive or inductive reactive power is maximized, respectively. Q_{UHV} is calculated using the well-known forward/backward sweep method for solving the power flow equations in tree grids (Eminoglu et al. 2008), in each iteration of the optimization. Constraints to the optimization problem are

- apparent power of the generators $Q^2 < C^2 - P^2$ and
- maximally allowed voltage fluctuations $\Delta U = \pm 10\%$ at each grid node.

The tap changer positions of all transformers were assumed to be adjustable to the discrete values $\{0.95, 1.0, 1.05\}$, and I chose the optimal tap settings from any possible combination of these options. I assume a fixed power factor of 0.95 for loads.

In this study, line capacity constraints were neglected as previous studies have indicated that voltage constraints are typically the first to be violated in distribution grids with massive decentral generation (Lödl et al. 2011). I did, however, check the transformer load limits after the power flow computation and found them to be less crucial than the voltage limits, again similar to (Lödl et al. 2011).

5.2.3 Prototypical Examples Cases

I construct three distribution grids with prototypical mixes of generation capacities and consumption. I investigate their potential for reactive power support from the DG to the TG and the limitations thereof, for demanding load/generation situations. The prototypes are code-named and characterized as follows:

- *Passau*: sunny midday in a rural area with small load and large PV generation in the LV grid
- *Munich*: evening in an urban area with large load and little decentral generation
- *Goerlitz*: windy afternoon in a rural area with small load and large wind generation in the MV and HV grid

5.2.4 Germany-wide Case Study

The Kombikraftwerk 2 study (Fraunhofer IWES et al. 2014) developed a 2050 scenario of the German power system with 100% RES. The study details the installed capacities of renewables, storages and backup power plants to the level of UHV transmission grid nodes in Germany, and develops a dispatch for the full system for each hour of one meteorological weather year. Further, the resulting power flows in the modeled TG, a slightly extended version of the grid proposed in the Netzentwicklungsplan (BNetzA 2013), and a Q(U) droop control law lead to reactive power demands at each node for each point in time.

Note that the reactive power demand of the modeled TG is mostly capacitive. This is because the modeled grid is highly expanded in comparison to today, but the additional lines are only rarely used and thus behave in a capacitive way.

I use the reactive power demand data from Fraunhofer IWES et al. 2014 and match them with the estimate of the possible Q generation from underlying distribution grids. I also use their distributed generation capacities for each TG node and the split it to the different voltage levels mentioned therein. To reduce computational effort I condensed the 8760 given time steps with the known "kmeans" procedure from Matlab (MATLAB 2014) into 30 time clusters that cover a wide range of power flow situations. To account for the local exchange of reactive power between neighboring TG nodes and to reduce the impact of local grid modeling errors (e.g. falsely assigned transformers between the 220kV and 380kV TG levels), I aggregated the possible Q generations over a shortest path radius of $\leq$ 30 km. TG nodes outside Germany and nodes without any consumption load were excluded from this analysis.

5.3 Results for Prototypical Distribution Grids

Passau. The constructed prototype *Passau* shown in Fig. 5.2 has an active power flow of about 100 MW from the DG to the TG, resulting from 160 MW solar generation and 60 MW load (relative to an assumed peak load of 132 MW for the grid). With 80% active power usage of the installed PV capacities there is still a large reactive power potential available. Hence, it is possible to generate both capacitive and inductive reactive power at the connection from the DG to the TG. The full Q potential of the generators in the DG can, however, not be exploited. The limiting factors are the MV

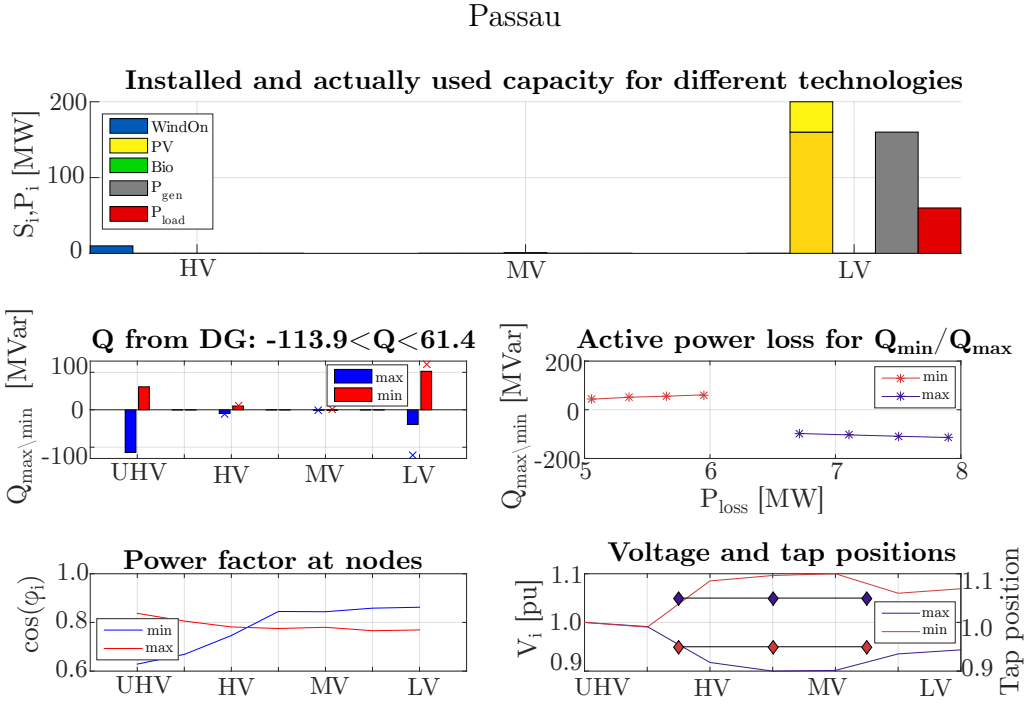

Figure 5.2: **Model results for the Passau case scenario.** Top: Generation capacities and actual generation (light and dark colors respectively) for different technologies and grid levels. Additionally, overall generation and consumer load. Mid-left panel: The bars show the total reactive power generation of the generators per grid level if the reactive power transfer to the TG is maximized (blue) or minimized (red). The UHV values show the generation as seen from a perspective of the TG (inverse sign relative to the DG's view that is used for the other grid levels). Crosses mark the reactive power potential for each grid level as derived from the installed capacities and their current usage. Negative Q corresponds to inductive and positive Q to capacitive reactive power generation. Mid-right panel: The maximally/minimally possible Q transfer to the TG is shown for different constraints on the implied total active power losses in the distribution grid. Lower left panel: The power factor of the injected power (generation minus consumption) is shown. Lower right panel: The right axis encodes the optimal transformer tap positions that minimize and maximize reactive power transfer to the TG. The left axis denotes the voltage magnitude in the different grid levels relative to nominal voltage for Q maximization/minimization.

voltage limits – under the assumption that transformers at all grid levels are switchable. The transformer tap positions are set to extreme values. Despite the restricted usage of the inductive reactive power potential of the PV plants in the LV grid, the possible inductive Q delivery of the DG to the TG grid is large. This is due to the inductive Q generation of loads and the grid itself, shifting the overall Q exchange at the UHV level to negative values. Depending on the desired Q transfer from the DG to the

TG grid, DG's active power losses vary by up to 3MW, which gives a loss to Q generation ratio of 1 to 20.

Munich. The *Munich* prototype represents the classical power flow situation, with active power transferred from the TG (UHV level) to the loads in the HV, MV and LV levels. As shown in Fig. 5.3, few decentral generators lead to a rather small potential for local reactive power generation. Hence,

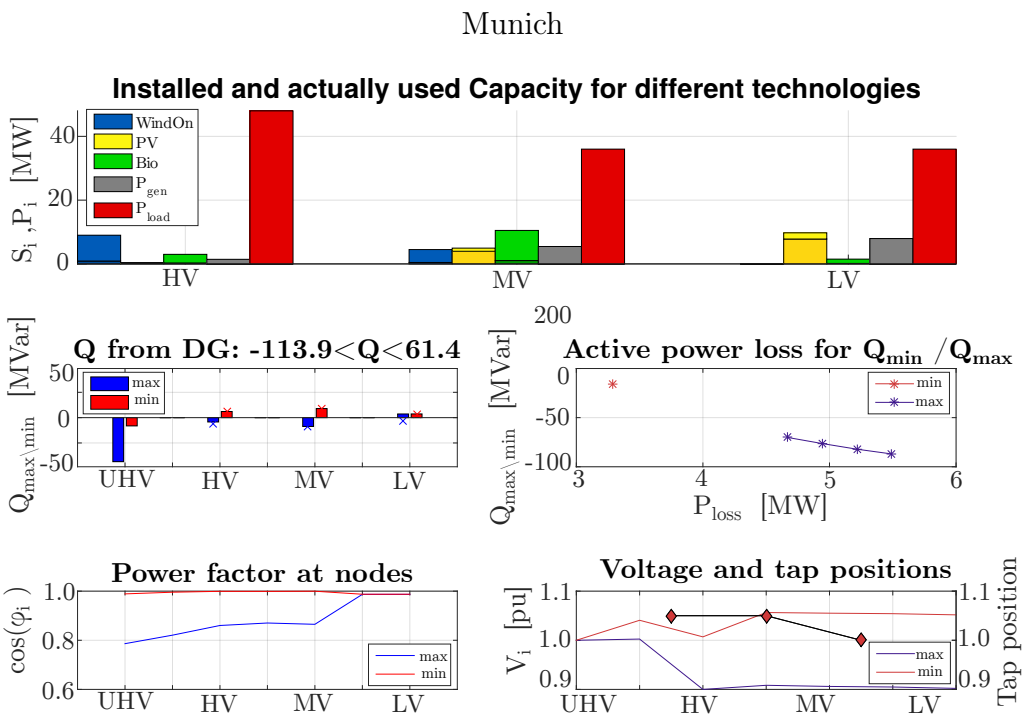

Figure 5.3: **Model results for the Munich case scenario.** Top: Generation capacities and actual generation (light and dark colors respectively) for different technologies and grid levels. Additionally, overall generation and consumer load. Mid-left panel: The bars show the total reactive power generation of the generators per grid level if the reactive power transfer to the TG is maximized (blue) or minimized (red). The UHV values show the generation as seen from a perspective of the TG (inverse sign relative to the DG's view that is used for the other grid levels). Crosses mark the reactive power potential for each grid level as derived from the installed capacities and their current usage. Negative Q corresponds to inductive and positive Q to capacitive reactive power generation. Mid-right panel: The maximally/minimally possible Q transfer to the TG is shown for different constraints on the implied total active power losses in the distribution grid. Lower left panel: The power factor of the injected power (generation minus consumption) is shown. Lower right panel: The right axis encodes the optimal transformer tap positions that minimize and maximize reactive power transfer to the TG. The left axis denotes the voltage magnitude in the different grid levels relative to nominal voltage for Q maximization/minimization.

the total Q potential of the DG as seen from the TG is always inductive, as is typical for load regions today. Aside from the LV inductive Q generation pushing voltage down to its lower limits, the existing Q potential can be fully used. For this prototype, overvoltages are no issue. The main task of the assumed tap changers is that of loss reduction, since high voltages at constant power transmission reduce the electric currents in the power grid and correspondingly the losses.

Goerlitz. The prototype named *Goerlitz* has large power flows from the HV to the UHV level as well as to the LV level. Satisfying 100 MW of electricity demand in the LV grid, the assumed local wind generation still exports an effective active power of 200 MW to the transmission grid. Fig. 5.4 shows how this prototypical DG is mainly able to generate inductive reactive power as seen from the TG perspective. In this model case with lots of HV generators, Q generation is constrained by the HV voltage limits first. Moreover, the existing potential for inductive Q generation cannot be fully used, especially in the MV level, since loss-minimization implies to exploit reactive power capabilities close to the TG first.

5.4 Results for the Germany-Wide Analysis

In order to stay within the voltage limits, the LV reactive power infeed counteracts with the HV one, e.g. to prevent the HV voltage to drop below its limits for an inductive Q exchange at UHV level, it is necessary to feed in capacitive reactive power at LV level. The tap changers are set to their extreme positions. Losses are high since great amounts of power (larger than the 132MW peak load that grid is designed for) flow from the DG to the TG.

Setting the local reactive power potential from the DGs in relation to the reactive power demands of the TG for the Germany-wide 100% RES scenario from the KKW2 study (Fraunhofer IWES et al. 2014) yields the results shown in Fig. 5.5. For almost all TG nodes (98%) the local reactive power demand can be compensated with reactive power generation from the distribution grids in the near neighborhood, i.e. from within 30km, see Fig. 5.5(a).

For the remaining 2% of TG nodes for which the local reactive power demand cannot be balanced with reactive power generation from nearby DGs at most 200MVAr of additional capacitive or inductive reactive power are needed for local compensation, see Fig. 5.5(b). The Q shortage is strongly skewed towards negative values and thus, there is a larger lack in inductive

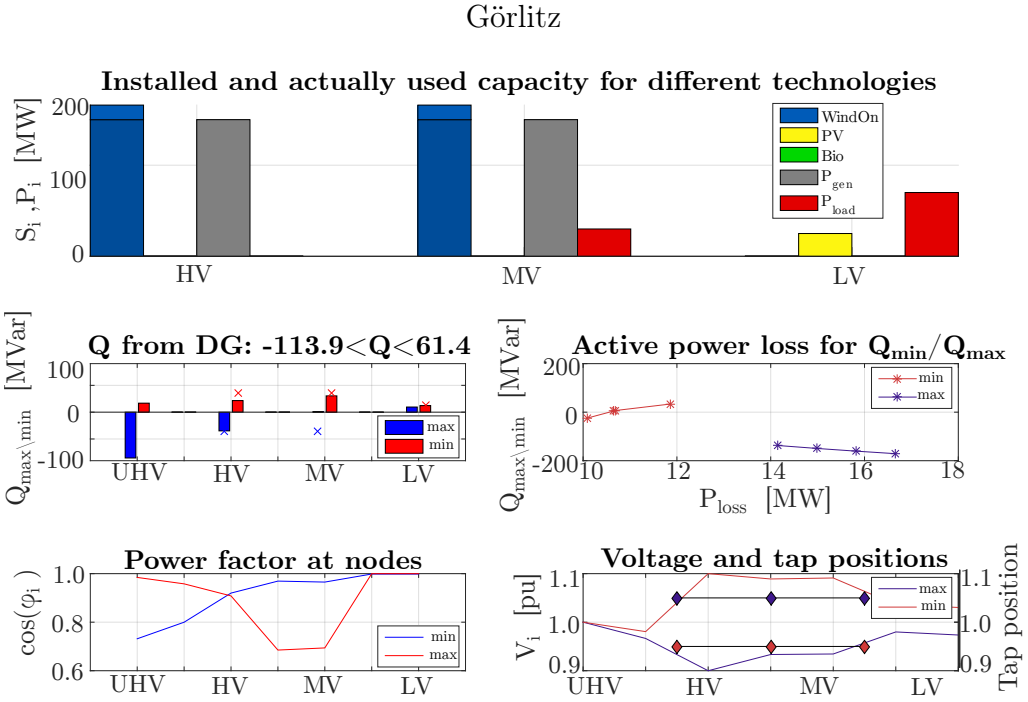

Figure 5.4: **Model results for the Görlitz case scenario.** Top: Generation capacities and actual generation (light and dark colors respectively) for different technologies and grid levels. Additionally, overall generation and consumer load. Mid-left panel: The bars show the total reactive power generation of the generators per grid level if the reactive power transfer to the TG is maximized (blue) or minimized (red). The UHV values show the generation as seen from a perspective of the TG (inverse sign relative to the DG's view that is used for the other grid levels). Crosses mark the reactive power potential for each grid level as derived from the installed capacities and their current usage. Negative Q corresponds to inductive and positive Q to capacitive reactive power generation. Mid-right panel: The maximally/minimally possible Q transfer to the TG is shown for different constraints on the implied total active power losses in the distribution grid. Lower left panel: The power factor of the injected power (generation minus consumption) is shown. Lower right panel: The right axis encodes the optimal transformer tap positions that minimize and maximize reactive power transfer to the TG. The left axis denotes the voltage magnitude in the different grid levels relative to nominal voltage for Q maximization/minimization.

than capacitive reactive power. The unbalanced nodes are geographically isolated (see Fig. 5.6). They also coincide with nodes that have little or no decentral generation capacities and thus very limited local flexibility.

To examine what grid level contributes how much to the reactive power balance, the histograms in Fig. 5.5(c) and (d) show how much Q is injected from each grid level and which share of Q capacity this maximally corresponds to over the year. According to Fig. 5.5(c) all voltage levels of-

ten contribute to some capacitive and inductive reactive power production. Large quantities of inductive reactive power are occasionally provided by LV levels whereas MV and especially HV grid levels succeed at supplying large quantities of capacitive power. The maximal utilization rate of the existing Q capacity, see Fig. 5.5(d), is about 50% for all grid level.

The previous section showed that decentral Q-generation comes at the cost of increased active power in the DGs. The plot of active power loss over optimized reactive power for different average UHV nodes (for normalized grids with scaled loads and power production capacities), see Fig.5.7, shows that active power losses are considerably higher for capacitive Q generation than for inductive one. There is a sharp boundary for capacitive Q generation at $Q = 100$ MVAr (for an average DG designed for 132 MW peak load), close to which the losses shoot up. The ratio of active power losses,P_{loss},to Q generation ratios may rise to the order of 1:3. On the other hand, if

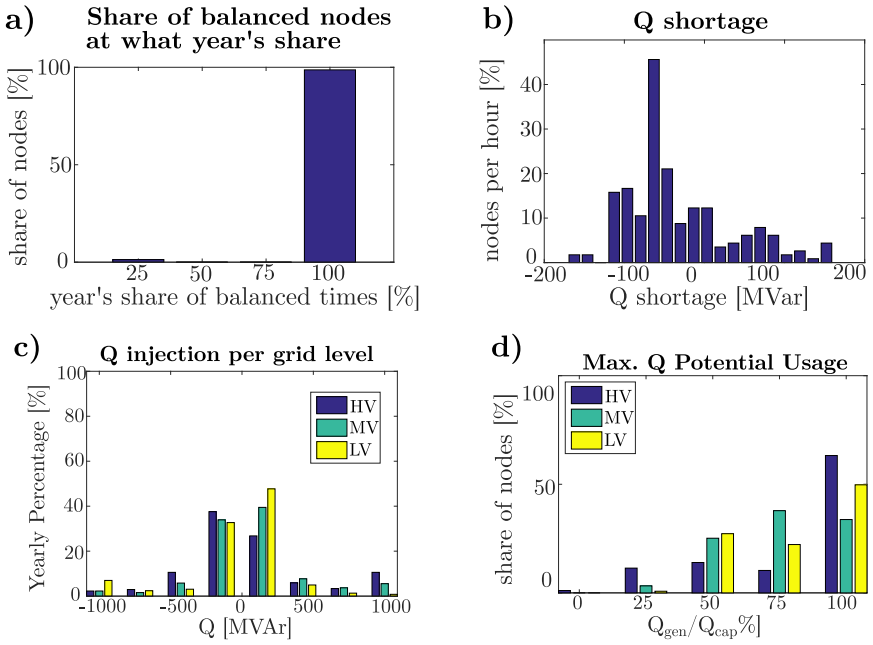

Figure 5.5: **Illustration of potential of decentral reactive power provision for Germany as a case study. a)** Fraction of nodes which can locally be Q-balanced at least a given time-percentage of the year, i.e. the bar at 100% shows the fraction nodes that can always be balanced (98% of the nodes). **b)** Histogram plot of the deviation from Q demand of the transmission grid for what share of nodes per time step. The nodes' Q generation at UHV level was aggregated within a range of shortest path smaller than 30 km. **c)** Histogram of reactive power injection from different grid levels together with **d)** showing how many nodes used what share of their available Q potential per grid level. E.g. 3% of all nodes used their LV reactive power potential on average 100%.

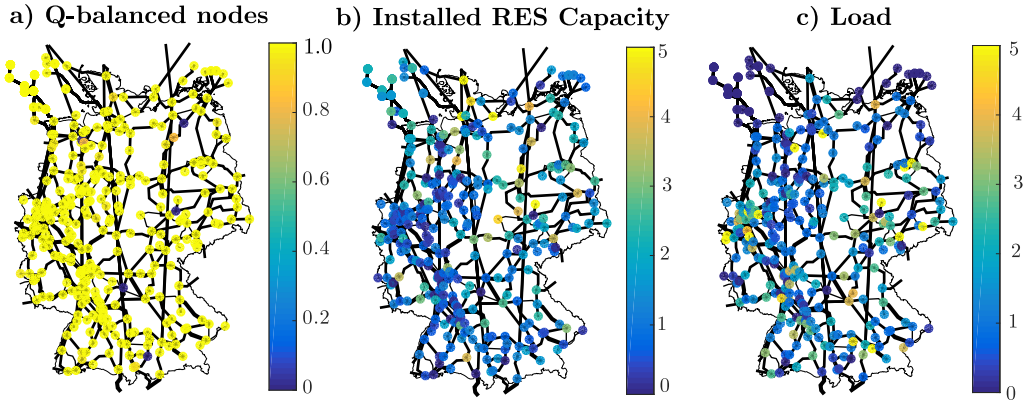

Figure 5.6: **Regional distribution of balanced nodes with decentral reactive power provision as well as installed RES capacity and load distribution.** Results of the Germany-wide demand/supply potential analysis based on the Kombikraftwerk 2 scenario (Fraunhofer IWES et al. 2014). **a)** Colors encode for each TG node the share of time steps where its local reactive power demand can be balanced with local DGs' reactive power generation potential. **b)**, **c)** Heat map of locally installed RES capacity and average consumption load relative to their Germany-wide average values. Values are capped at 5. **d)** Fraction of nodes which can locally be Q-balanced at least a given time-percentage of the year, i.e. the bar at 100% shows the fraction nodes that can always be balanced (98% of the nodes).

one limits oneself to the range $-100 < Q < 70$ MVAr, the additional losses from decentral reactive power generation in the DGs do not seem a pressing issue (see dashed lines of Fig. 5.7).

5.5 Summary

This chapter showed that decentral reactive power from the DG is able to satisfy almost all reactive power demand from the TG, for a 100% RES scenario for Germany. This means that DGs enabled to achieve this technical

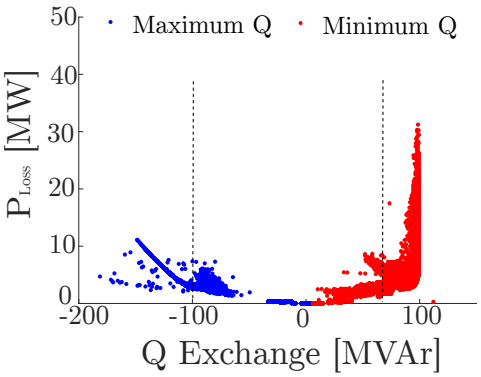

Figure 5.7: **Active power losses for decentral reactive power provision**. Plot of active power losses, P_{loss}, over the exchanged reactive power between the distribution grid and the average UHV nodes (with 132 MW peak load). One data point corresponds to one simulated time cluster of one single node. The dashes vertical lines represent a range of Q with moderate losses.

potential could be *the* major tool for TG operators to manage the voltage in the TGs.

Reactive power demands that cannot be met by underlying DGs are few in this study, and they are locally isolated. Consequently, few additional reactive power compensation devices in the TGs should be able to alleviate the remaining issues. These could be remaining large conventional power plants, HVDC converters, or special purpose compensation.

To enable the proposed exploitation of the Q potential in the existing hardware of decentral RES generators, it would be necessary to activate about half of the decentral power plant potential. This means that their inverters would have to be able to work with arbitrary power factors and their Q generation would have to controllable via online communication. Further research needs to be check whether fixed Q values or fixed droops are feasible as well. Here, I assumed a centrally optimized setting for each situation. Moreover, the DG voltage levels would have to be tightly controlled and thus observability in the DGs would have to be increase significantly. Last, I have assumed tap changeable transformers at all grid levels. Many of these things, however, are already underway for different reasons, e.g. avoiding over-voltages in the DG due to RES infeed – independent of additional Q generation. A dual use for providing reactive power to the TG would thus be very welcome.

An economic counterargument may come from the increased DG losses that result from decentral Q generation. For extreme Q generation values these may be large. On the other hand, additional hardware for special purpose reactive power compensation in the DG grid is saved. The option to provide reactive power from the distribution grid requires new regulation to organize the financial compensation between the TG and the DG operator. First steps in this direction are explored in Switzerland (Scherer 2016).

My technical results on DGs' Q potential may be optimistic for several reasons. I use a symmetric DG grid model, neglecting voltage and corresponding Q limitations due to unsymmetrical branch loadings. The simulations are undertaken for time clusters with load and generation values representing the averages over the clustered hours. Hence, extreme load and generation patterns are not covered. It is also not clear what structure future DG grid extensions, that are required to integrate all the modeled RES, will take. Here, I have assumed them to take the same structure as the existing ones. However, even if all these arguments would in reality reduce the potential of reactive power from the DG by some fraction the lever would still be a large one.

Moreover, while my DG model simplifications (symmetry, full power factor capability, remotely controllable Q set points and tap changers, full

grid observability) are stronger than the one made in earlier work for exemplary networks, my numeric results are comparable (Talavera et al. 2015). The results for the possible ranges of Q generation have a similar span but are shifted towards inductive Q potential. This may be due to the inclusion of load power factors in my calculations whereas in (Talavera et al. 2015) this seems to be excluded from the reactive power exchange. The taken DG model simplifications allow to undertake a full-country study and to thereby compare the computed potential of reactive power from DGs with a plausible future demand in a detailed, consistent future energy scenario for Germany.

In future work, this study should be continued with more realistic DG models, e.g. as done with the random DG grid generator from the project ESDP. Moreover, the economic evaluation also in comparison to the alternatives such as central Q compensation should be extended.

Chapter 6

Local Intermittent Fluctuations and Distribution Grid Stability

This chapter investigates the influence of the placement of variable renewable infeed on stochastic stability measures in distribution grids (DGs). The focus will be the stability of the synchronous state (Arenas et al. 2008; Dörfler and Bullo 2014) and the ability of the system to keep frequency fluctuations small to maintain high power quality within a certain frequency range. Much of this chapter's content has been published in **Auer, Hellmann, et al. 2017**. It relates to the overarching question of how to enable a dynamically stable integration of renewable energies (see Sect. 1.5).

Work on the effect of stochastic fluctuations from RES on grid stability has been started very recently and thus, only few publications on this matter exist. For lossless power grids, the recent work of Zhang et al. 2017 studied analytically the influence of single-node monochromatic oscillations and their spreading throughout the network. There, three frequency regimes were identified: a bulk, a resonant and a local regime. In the bulk regime for low frequencies the network is excited as a whole, whereas in contrast, high frequency perturbations stay localized at the fluctuating node and decay exponentially with the network distance. Most interestingly, for the mid-frequency region the network topology was identified to play a major role in network stability as complex, non-trivial patterns of stability and instability emerge. This analytic work is an important basis for understanding the influence of intermittent noise on power grid stability where fluctuations cover the whole frequency spectrum with a Kolmogorov-like turbulent power spectrum (Anvari, Lohmann, et al. 2016; Milan et al. 2013; Woyte et al. 2007). For a more detailed explanation of intermittency see Section 2.2.3.2.

In K. Schmietendorf et al. 2016, the authors studied the impact that the

stochastic properties of RES infeed have on grid stability. They compared white Gaussian noise, Gaussian noise with a turbulent power spectrum and intermittent noise. The latter noise displays a fat tail in both the power spectrum and the increment time series, which corresponds to a (long-range) correlation in time. The work showed that the time-correlated noise leads to the strongest network destabilization. Noise of the same power spectrum but without intermittency induces smaller frequency deviations. Thus, it is most important to include the intermittent nature of RES power fluctuations in future grid stability analysis. K. Schmietendorf et al. 2016; Zhang et al. 2017 already mentioned the importance of the topology aspect. The work of Schäfer, Matthiae, Zhang, et al. 2017 aimed at better understanding the interplay of the dynamics caused by stochastic power infeed and the network topology. Here, for two nodes (with white-noise power fluctuations) coupled to a bulk grid it was shown how the node with lower coupling strength is the one destabilizing the network. Moreover, with Kramer's escape rate theory the authors demonstrated how in a network with all machines subject to white noise, the weakest links may be identified by the "saddles" of the grid which do not necessarily coincide with most heavily loaded ones.

In contrast to previous studies, this work's focus is the modeling of distribution grids (see Section 2.1.4). The question is how the inclusion of local intermittent fluctuations $\Delta P(t)\delta_{ik}$ at a single node k into the system dynamics (see Sections 2.2.2.1 and 2.2.3.1)

$$\begin{aligned}\dot{\phi}_i =&\omega_i,\\ \dot{\omega}_i =&\frac{1}{H}(P_i + \Delta P(t)\delta_{ik} - \alpha\omega_i - \sum_j U_i|Y_{ij}|U_j \sin(\phi_i - \phi_j + \phi_{ij})).\end{aligned} \tag{6.1}$$

influences the frequency stability and the power quality of distribution grids. And since fluctuations are introduced locally the question arises, whether the position of the perturbed node in the network makes a difference for the grid's stability.

For this purpose, in Section 3.4 I introduced a classification of nodes into troublemakers and fluctuation sensitive nodes. Power fluctuations at troublemaker nodes (for the definition see (3.5)) tend to cause notable frequency fluctuations at all network nodes. They are drivers of instability. The class of nodes with high excitability, see (3.6), describes nodes that react with notable frequency fluctuations irrespective of which node introduces the power fluctuations into the network.

In the following, I consider two model cases: that of a microgrid and of a medium-voltage grid, described in Section 6.1. In Section 3.4 adequate

measures for stability in such a stochastic modeling setup were introduced. Section 6.2 then presents the empiric model observations for both model cases. These observations build the basis for the introduction of predictors for both troublemakers and excitable nodes in 6.3. The results are discussed at the end of this chapter in 6.4.

6.1 Model Cases

In order to understand the ability of a distribution grid to maintain synchrony, I will study two model cases[1]: that of an islanded microgrid and of an medium-voltage grid (MV grid). For both model cases, I choose a network of 100 nodes (Auer, Roos, et al. 2017). It thereby represents an average German MV grid because Germany has 4,500 MV distribution networks that connect 500,000 LV distribution networks (Boßmann et al. 2015).

The goal of observing both model cases is to find one consistent theory that does not depend on the specifics of one model case (see Section 6.3). It is my objective to model both cases in a very conceptual way to study the effect of local fluctuations on dynamic grid stability and isolate the influence of the network structure. These modeling assumptions strive to strike a balance between realistic and conceptual. In the following I describe both model cases and their underlying assumptions.

The medium-voltage grid is part of the larger grid hierarchy. It is not self-balanced in power and has a connection point to the higher grid level (the High-Voltage network) which is called the slack bus or heavy node (labeled as node 0). Downstream each MV grid node may lie a full Low-Voltage (LV) network which effectively every MV grid node represents. The MV grid is a good testing case for modeling power grids with high renewable energy share since most PV power plants are connected to low-voltage- (LV) or MV levels. For this specific MV grid example I assume lots of PV production. Hence, for all MV nodes the effective power input, P_i, the power which is injected into the grid, equals $P_i = 0.1\text{MW}$. All 99 MV nodes are also equal in damping and inertia. The goal of this homogeneity is to isolate the network influence. Since the slack bus is responsible for the power balance its power input equals the negative sum over all MV nodes' power in-feeds and losses on the lines: $P_0 = \sum_{i=1}^{N} P_i + P_{loss}$. As the name "heavy node" tells, the slack bus' inertia highly exceeds the lower level nodes' inertia, here I assume: $H_0 = \sum_{i=1}^{100} H_i$.

[1] See Section 2.1.4 for an introduction to distribution grid modeling.

A microgrid, in contrast, is internally power-balanced and not connected to a higher grid level. Islanded microgrids play a role for the decentral provision of energy, but also as part of a safety and stability strategy to localize faults by partitioning the grid into autonomous units. A microgrid has a non-hierarchical grid topology.

Nevertheless, as in the MV grid case I assume that downstream each microgrid node may lie a full Low-Voltage (LV) network. As it is balanced within itself, in this case there are 50 net producers and 50 net consumers with $P_i = \pm 0.2MW$ power infeed before losses. The power infeeds are chosen homogeneously to isolate topology and network effects in the model. As there is no connection to upper grid levels, losses are compensated locally at each node, and the net power infeed is given by $\tilde{P}_i = (P_i + P_{loss}/N)$. To compensate losses locally, in the fix point search a loss compensator term was added to each node's power input which ensures that the system frequency does not deviate from 50Hz.

The grid parameterization for both distribution grid cases simply relies on the voltage level both microgrids and MV grids are assigned to, which I assume to be in the medium-voltage range.

The line impedance for typical MV grids with 20kV base voltage equals $Z = Y^{-1} = (G + iB)^{-1} = (0.4 + 0.3j)\Omega/km$ (Auer, Steinke, et al. 2016). The coupling strength between a node pair (i, j) then equals

$$K_{ij} = U_i |Y_{ij}| U_j \tag{6.2}$$

where $|U_i| = 20$kV. For simplicity all power, voltage and impedance values are transformed into per unit with a base voltage of 20kV and a base power of 1MW, which are typical values for MV grids (Auer, Steinke, et al. 2016; Sen 2007). The absolute impedance of each line scales with the geographic distance l between linked nodes and is consequently different among the links. The average line length, according to Auer, Steinke, et al. 2016, is 23.7km. The inclusion of resistive lines leads to line losses and at the same time introduces a phase shift of $\phi_{ij} \approx \arctan(\frac{G_{ij}}{B_{ij}})$ which was shown to have significant consequences for stability (Auer, Hellmann, et al. 2017).

Further, I assume distribution grid cases which are dominated by inverters because I want to analyze a scenario with high RES penetration where wind and solar power plants are connected to the grid via inverters. Network nodes are to be considered as effective nodes with a mix of at least one grid-forming inverter, a number of grid-feeding inverters and demand (Schiffer, Zonetti, et al. 2016). I assume, that for reasons of grid stability, grid-forming inverters will be widely deployed but smaller in number

compared to grid-feeding inverters. Because grid-feeding inverters do not contribute any inertia, the effective nodes have inertia much lower than nodes fully consisting of grid-forming inverters would have. I model grid forming inverters following Schiffer, Zonetti, et al. 2016 as having droop controlled frequency based on a low pass filtered power measurement. The virtual inertia and damping for the network model is then given by the low-pass filter exponent τ_p and the droop control parameter k_p from grid-forming inverters: $H = \tau_p/k_p$, $\alpha = 1/k_p$, $\forall i$ with $i = 1, .., N$. Standard parameters for the droop and time constants of grid-forming inverters are in the range $k_p = [0.1, .., 10]s^{-1}$ and $\tau_p = [0.1, ..., 10]s$ (Coelho et al. 2002; Schiffer, Goldin, et al. 2013). As I am interested in the low inertia case, with few low powered grid forming inverters at each node, I will assume a weakly reacting, strongly smoothed system. This leads me to consider $\alpha = 0.01s$ and $H = 0.1s^2$. Please note that the results are not sensitive to the exact choice of α and H.

6.2 Observations from Model Cases

In this section, I show observations for the influence of local fluctuations on the stability of example MV and microgrids. The designed cases are very

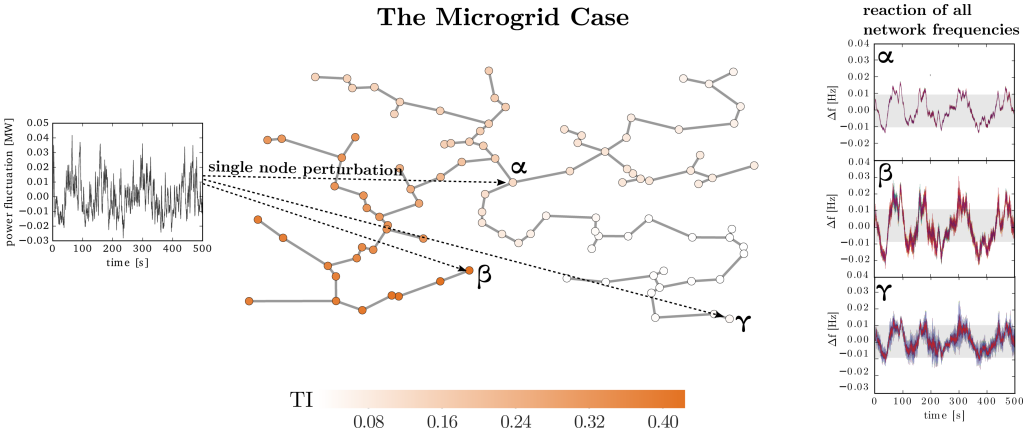

Figure 6.1: **Single-node fluctuations excerted on an example microgrid.** Left: Power fluctuation time series $\Delta P(t)$ jointly generated by solar and wind models that capture their intermittent behavior (Anvari, Lohmann, et al. 2016; K. Schmietendorf et al. 2016). Center: Random microgrid with TI as coloring. One simulation run with single node fluctuations at one specific node produces this node's TI value. Right: Frequency time series for all network nodes $T = 500$s for single-node fluctuations at node α, β and γ. The grey zone is the frequency threshold band of 0.01Hz. All 100 nodes' frequency trajectories are shown with semi-transparent lines.

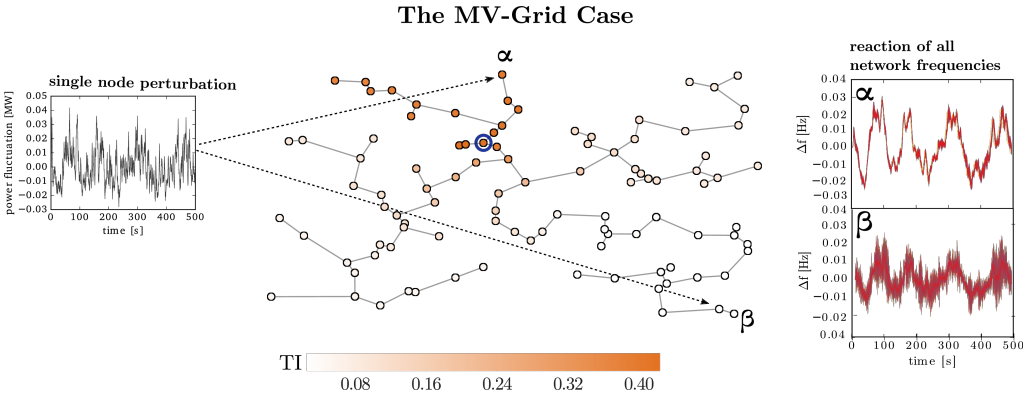

Figure 6.2: **Single-node fluctuations excerted on an example medium-voltage grid.** Power fluctuation time series $\Delta P(t)$ jointly generated by solar and wind models that capture their intermittent behaviour (Anvari, Lohmann, et al. 2016; K. Schmietendorf et al. 2016). Center: Random MV grid with TI as coloring. One simulation run with single node fluctuations at one specific node produces this node's TI value. Right: Frequency time series for all network nodes $T = 500$s for single-node fluctuations at node α and β. The grey zone is the frequency threshold band of 0.01Hz. All 100 nodes' frequency trajectories are shown with semi-transparent red lines. The blue-circled node is the slack bus.

different in their power flow patterns due to their power input configuration. The microgrid case has a homogeneous distribution of consumers and producers of the same absolute size. Whereas the MV grid has one central consumer to which generation from all other nodes is flowing. Also, the distribution of inertia is homogeneous for the microgrid whereas the MV grid, with the connection to the next higher HV-level, has a heavy node. The goal of observing both model cases is to find one consistent common structure for both (see Section 6.3).

In one simulation run single-node fluctuations are introduced for one specific node (see Figs. 6.2 and 6.1 for the micro- and MV grid case, respectively). For better comparability the same fluctuation time series is used for each node. Then, the reaction of the whole network towards such fluctuations at the certain node position in the network is investigated. I find a remarkable interplay of the network structure and the position of the node at which the fluctuations are fed in. The rest of this section will discuss in detail the relationship of various network structures and dynamical properties. For both model cases I find network branches with different stability behavior (see Section 6.2.1).

6.2.1 Network Branches of Different Stability

From the time series plots of the Figs. 6.1 and 6.2 (right) it can be seen that it makes a difference in the evolution of frequency deviation on what node the power fluctuations are exerted. The distribution of troublemaker index, TI (see eq. (3.5)), over the network (Fig. 6.1 center) shows how nodes of the same branch behave coherently, they have similar capabilities to be drivers of instability. The frequency time series $\Delta f(t)$ of all network nodes further illustrates the different reaction of the network towards power fluctuations, $\Delta P(t)$ (see eq. (8.1)), at single nodes.

For the microgrid case of Fig. 6.1 (right) two dead-end nodes from different branches (nodes β and γ) and the most closeness central node, α, were chosen. Clearly, the node β is a troublemaker by exceeding the frequency threshold most. The emergence of different TI values for each branch in the network is remarkable. Even for a microgrid with homogeneous power distribution the network topology seems to play an important

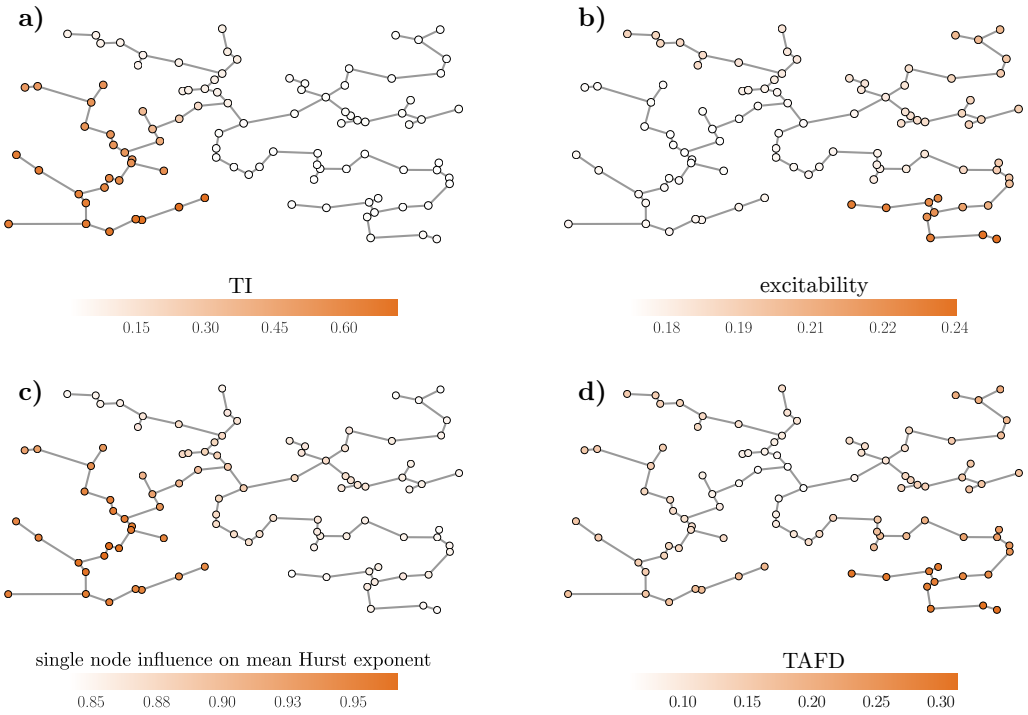

Figure 6.3: **Network plots of stochastic stability measures for an example microgrid.** Network plot of **a)** Troublemaker index (TI, see (3.5)), **b)** excitability (see (3.6)), **c)** single node influence on mean Hurst exponent, see (3.8) and **d)** time average of grid's frequency spread (TAFD, see (3.7), normalized to average mean deviation) as coloring.

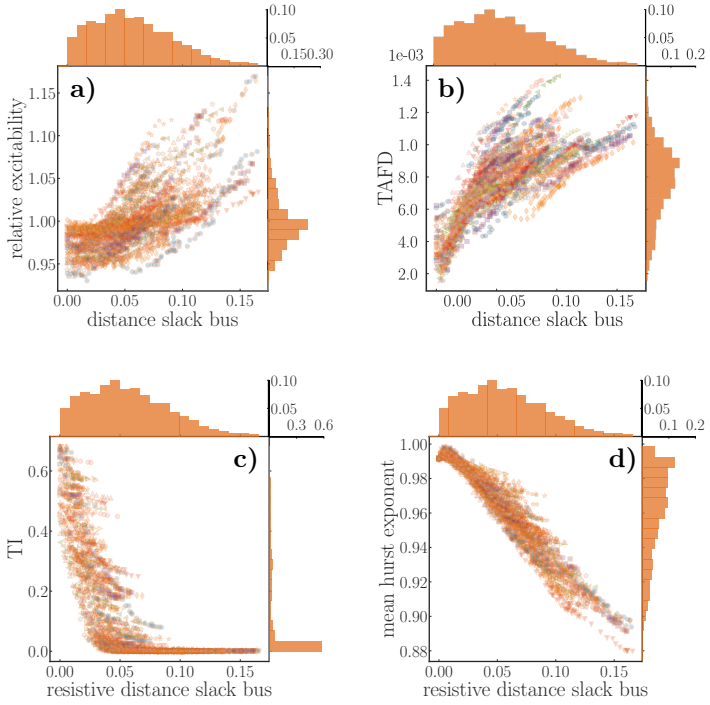

Figure 6.4: **Scatter plots of stochastic stability measures for ensembles of MV grids.** Scatter plots of **a)** relative excitability (excitability from (3.6) normed to the mean of each network simulation), **b)** time average of frequency dispersion (see TAFD in (3.7)), **c)** troublemaker index (see TI in (3.5)) and **d)** mean hurst exponent (see (3.8)) over the resistive distance towards the slack bus. Different colors represent different networks from a 30 MV grid ensemble.

role. For an exemplary microgrid, the top row of Fig. 6.3 shows branches of troublemakers (with relatively high TI) and branches of vulnerable nodes (with relatively high excitability, see eq. (3.6)). Comparing Figs. 6.3a and 6.3c additionally tells that TI and the mean Hurst exponent (see eq. (3.8)) are strongly correlated. Thus, nodes causing frequency fluctuations above threshold in the whole grid are exactly those that are able to maintain temporal correlations in the frequency time series, $\Delta f_i(t)$, over all grid nodes i. At the same time, nodes reacting strongly to intermittent power infeed, $\Delta P(t)$, at whatever node in the grid, themselves, show little ability to be drivers of exceedance. Instead, fluctuations at such nodes lead to large frequency incoherencies or frequency spread (TAFD, see eq. (3.7)) among the nodes (see Fig. 6.3d), even if the frequency is mostly in the bulk regime (Zhang et al. 2017). Hence, high TI does not necessarily mean high frequency spread and vice versa. Nodes that destabilize the grid, causing large fluctuations at all nodes, are not the same nodes that make the grid incoherent. On the other hand, high TI nodes are the same nodes that pass on temporal correlations to the other grid nodes.

For the case of a typical MV grid Fig. 6.2 demonstrates how the slack bus dominates the overall grid dynamics. It is clearly visible how the trouble-maker nodes are in close proximity to the slack bus. This means, the closer a disturbed node is to the high-inertia center or the High-Voltage connection point, the more the whole network follows the perturbation. This is clearly visible in the time series of two representative nodes of the network. Disturbing node α, sitting on the same branch as the slack bus, forces all nodes on a similar trajectory, following the power fluctuation almost one to one. Whereas exerting the fluctuations on node β still gives a high spread in frequency deviation between the nodes (or TAFD) and the frequency fluctuations are much more dispersed. This impression from the frequency time series is supported by Fig. 6.4b and illustrates how the proximity to the slack bus influences frequency dispersion within the network. Perturbations close to the slack bus lead to bulk grid oscillations whereas perturbations far away from the heavy node can not force all nodes on a similar frequency trajectory. As in the microgrid case, Fig. 6.4a shows how nodes with high excitability have little ability to drive exceedance, they have low TI (see 6.4c). Instead, fluctuations at such nodes show high frequency spread (high TAFD) among the nodes.

Not only the spatial but also the temporal correlation is determined by a node's position relative to the slack bus. Figure 6.4d shows the network's mean correlation in time derived from the frequency time series and expressed with the mean Hurst exponent. The temporal correlation with a mean Hurst exponent close to 1 is part of the intermittent nature of RES fluctuations. It is preserved for disturbing nodes close to the slack and reduces linearly with increasing distance from the heavy node. The same holds for troublemakers where TI decreases moving away from the slack bus. Then above a certain threshold distance far away from the slack bus, it drops to zero. Power fluctuations close to the slack bus and on the same branch as the slack bus result in highest TI values.

Hence, distances play a central role in lossy MV networks. All observed stability can be related to a node's distance towards the slack bus where half the system's inertia accumulates.

Losses cause differences in stability. A first important result is that this interplay, and the dependence on the position of nodes, at which power infeed is fluctuating, only appears due to the losses in distribution grids. This applies to both model cases. Generally, losses increase the absolute value of and the differences in exceedance. Also, differences in troublemaking only appear in the presence of losses (see Fig. 6.5 and Fig. 6.6).

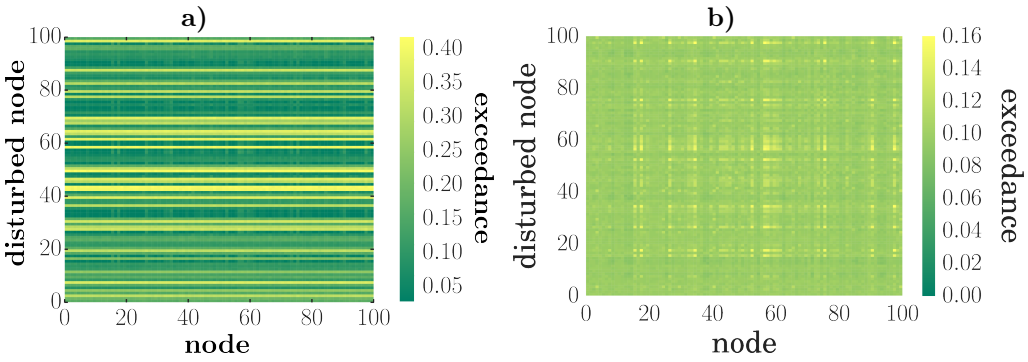

Figure 6.5: **Exceedance colorplots for a microgrid with and without losses.** Colorplot of single node exceedances (see (3.4)) for each simulation run or disturbed node (y-axis) and each node in the network (x-axis) with 10% coupling strength (see K_{ij} in (6.2)) for **a)** lossy lines ($Z = (0.4 + 0.3j)\Omega/km \cdot l$) and **b)** non-lossy lines ($Z = (0 + 0.3j)\Omega/km \cdot l$ with link length l). The same plot for a 100% coupling strength leads to $E_{ij} \approx 0.16\ \forall i, j$

A normally coupled lossless microgrid reacts as one and identically to perturbations, no matter where they occur. The exceedance plot is homogeneous. The network and position of the perturbation play no role here. As can be seen in Figure 6.5b, a lossless microgrid with relatively weak lines will lead to strongly and weakly interacting nodes. In any pair of nodes i, j, the reaction of node i to perturbations at node j is identical to the reaction of j to perturbations at i. The exceedance plot is symmetric in this case. However, the differences in exceedance remain relatively small, even in this case.

Similarly, for the MV grid case the losses cause the nodal differences in stability. This is illustrated for the troublemaker index in Fig. 6.6. It shows how increasing values of resistance and thus losses lead to a spread in trouble-maker index. For some node losses on the lines may also reduce TI and can contribute to stability for such nodes. For zero losses, all nodes act equally.

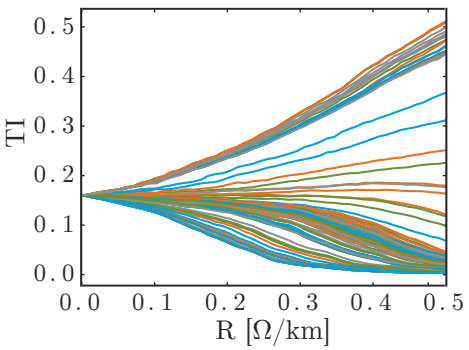

Figure 6.6: **Troublemaker index for increasing losses for an example MV grid** Plot of TI, see (3.5), for all network nodes (in different colors) for increasing resistance R.

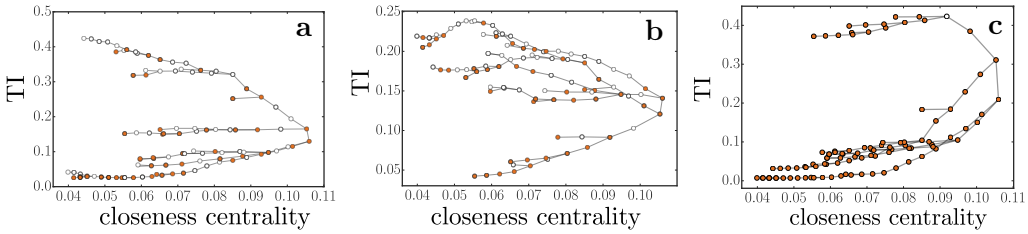

Figure 6.7: **Troublemakers and their relation to closeness centrality for the MV and microgrid case** with TI over closeness centrality, cc. **a)** and **b)** Microgrid example with different power input configurations (different realizations of the distribution of consumers and producers). **c)** MV grid case. White and orange node represent consumers and producers, respectively.

After these first insights, I want to develop a better understanding of how the network structure may provoke branches of high TI and excitability in Sections 6.2.2 and 6.2.3, respectively.

6.2.2 The Troublemaker Tale - an Empiric Analysis

From Figure 6.7 a clear but non-trivial relationship between TI and closeness centrality is visible, which holds for microgrids and MV grids (see Figs. 6.7a,b and Figure 6.7c, respectively). The closeness centrality, cc_i, of node i is defined as the inverse sum over all shortest paths between node i and all other nodes j of the network (Newman 2003). Therefore, a large cc value characterizes a node with short distances to all other nodes of the network. Connecting nodes adjacent to each other in the TI(cc)-plot gives additional information (see Figure 6.7). It underlines how branches of high TI are actual physical network branches. The highest centrality node separates the network into branches of troublemaker nodes and low TI branches. Hence, intermittent RES at certain but not all nodes may induce relatively strong frequency fluctuations. In a microgrid, going away from the most-cc node increases values of TI if there are more producers than consumers downstream, and vice versa (see Figs. 6.7a and 6.7b). Due to the losses that are compensated by an equal extra production by all nodes, there is a small asymmetry between consumer and producer power inputs. For the MV grid case the branch that holds the slack bus is the high TI network branch (see 6.7c).

From Fig. 6.7 it becomes evident that different power input configurations play a central role in this phenomenon because a change in the power input configuration alters the branches' TI values. Since the power input configuration changes the power flow across the network, the steady-state

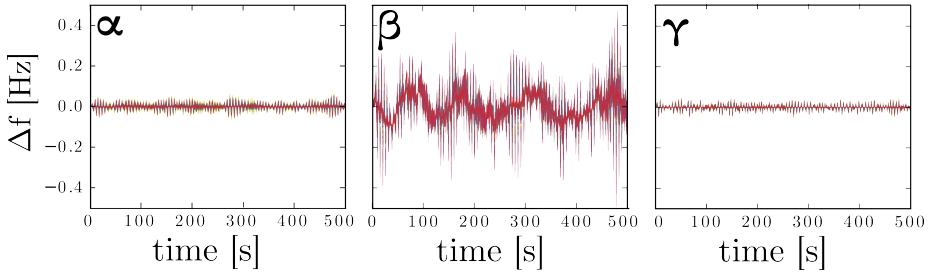

Figure 6.8: **Frequency time series for a microgrid with relatively low coupling strength.** Frequency time series for all network nodes for disturbances at the nodes α, β and γ. The coupling strength is reduced to 10% compared to Fig. 6.1 of the same distribution grid with identical power input configuration.

voltage phases of the nodes relative to each other seem to influence what node may act as a troublemaker and which not.

6.2.3 High Excitability and Network Eigenmodes

At first sight, equally reducing the coupling strength leads to much more difference for exerting single-node perturbations to different nodes concerning the network frequency time series (see Fig. 6.8). For better comparability, the same nodes as in Fig. 6.1 were chosen. Compared to node α and γ, the frequency fluctuations of node β are enormously high. For sure, node β is a troublemaker because fluctuations at this node lead to all network nodes to be on average 90% outside the given frequency band (TI value of 0.9). However, this node has been known as a troublemaker before, for higher coupling strength. The color plots of Fig. 6.9 illustrate how the reduction of coupling strength (columns of Fig. 6.9) also brings another aspect into play. For high coupling strength it is clearly visible how some nodes are the driver of high single node exceedance values for all nodes in the network (see Fig. 6.9 II.a). Now, lowering coupling strength results in two node classes. For low coupling strength there are drivers of instability and nodes that generally tend to be unstable irrespective of which node was initially perturbed. This is underlined by the excitability network plot of Fig. 6.1.

This is particularly interesting taking into account the power spectrum of the power fluctuations from wind and solar generation and comparing these with the eigenfrequencies of the Jacobian (see J_{ij} of (6.10)) of the distribution grid dynamics (see Fig. 6.9 I.a-c). Lowering coupling strength then shifts more and more eigenfrequencies into the power spectrum range of the power fluctuations. Thus, the fluctuations more and more hit the so-called resonant regime mentioned in Zhang et al. 2017. This insight is a

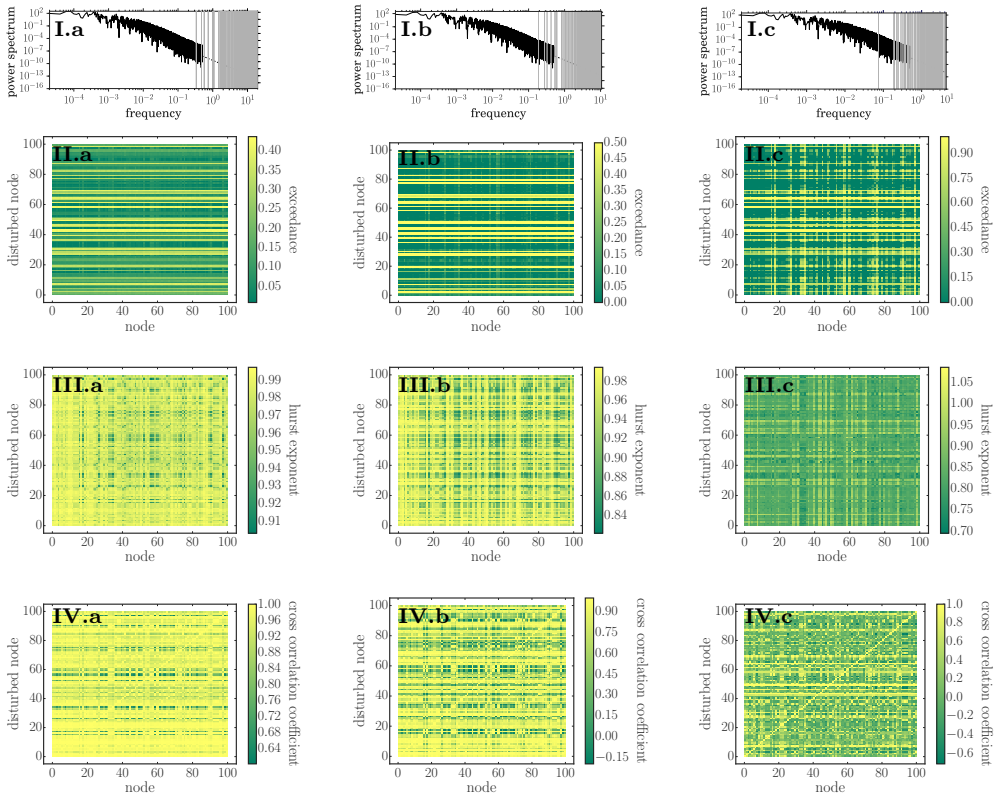

Figure 6.9: **Stochastic stability measures, cross correlation and eigenfrequency spectra for a microgrid with decreasing coupling strength. I**: Power spectrum of power fluctuations (black) with network eigenfrequencies (grey vertical lines). The black dashed line shows how the wind and solar power spectrum continues below the simulation's time resolution. Color plots, with disturbed node on the y-axis and reacting nodes of the network on the x-axis, of **II** single node exceedance, **III** hurst exponent and **IV** cross correlation coefficient for a microgrid example. From **a** to **c** the coupling strength (see (8.1)) is scaled with factor 1.0, 0.3, and 0.1. Please note the different color scales. All plots show an example microgrid.

basis for developing an analytic predictor for excitable nodes (see Section 6.3)

Concerning the Hurst exponent (Fig. 6.9 III.a-c), it is symmetric towards the perturbed and reacting nodes. This means thatthe correlation in time is preserved for certain nodes irrespective of what node is perturbed initially. With lower coupling strength the correlation in time decreases symmetrically.

The cross correlation between the time series of the disturbed node and all other nodes for different coupling strengths (Fig. 6.9 IV.a-c) shows

how for larger coupling strength cross correlation is generally higher than for networks with lower coupling strength, as can be expected. Hence, for higher coupling strength the network reacts as one whereas the node dynamics for low coupling may even become anti-correlated.

6.3 Predictors for Troublemakers and Excitable Nodes

As the previous sections showed, the introduction of lossy lines for the analysis of distribution grid stability had a surprisingly strong effect on the stability of each node towards local fluctuations. Hence, the interpretation of these results must be closely related to the losses and how they eliminate the symmetry of the Laplacian matrix in the model system. Instead of the usual eigenvalue/eigenvector analysis, here, it is necessary to distinguish between left and right eigenvectors for the non-symmetric Laplacian. In the following, I shortly introduce the specific mathematics of non-symmetric Laplacians which is necessary for the analysis of distribution grid systems. Then, this section shows how troublemaker relate to the left and excitable nodes to the right eigenvectors, respectively.

Some notes about non-symmetric Laplacians. Non-symmetric matrices, such as the Laplacian of the lossy distribution grid dynamics, have left and right eigenvectors:

$$\sum_m L^{km} v_r^{mj} = \lambda^j v_r^{kj}, \tag{6.3}$$

$$\sum_k v_l^{kj} L^{km} = \lambda^j v_l^{mj}. \tag{6.4}$$

They are orthonormal to each other but not orthonormal within themselves. Also, left and right eigenvector appear in pairs with the same corresponding eigenvalue:

$$v_r^i \cdot v_l^j = \delta^{ij},$$
$$L^{km} = \sum_i v_r^{ki} \lambda^i v_l^{mi}.$$

Thus, for the vector $x_0^{km} = \sum_i c_i v_r^{ki}$ holds the following

$$L^{km} x_0^{km} = \sum_{i,m} v_r^{ki} \lambda^i \underbrace{v_l^{mi} \cdot x_0^{km}}_{c_i}, \tag{6.5}$$

$$= \sum_i c_i v_r^{ki} \lambda_i. \tag{6.6}$$

I will always order the eigenvalues from largest to smallest: $\lambda_0 \geq \lambda_1 \geq \lambda_2 \cdots > \lambda^{N-1}$. The graph Laplacian always has a largest eigenvalue equal to zero: $\lambda_0 = 0$.

$$e^L v_r^i = e^{\lambda_i} v_r^i \tag{6.7}$$

In matrix writing the Laplacian can be decomposed as

$$L = v_r \cdot D \cdot v_l^T \tag{6.8}$$

with

$$D_{ij} = \begin{cases} \lambda_i & \text{for } i = j, \\ 0 & \text{for } i \neq j. \end{cases} \tag{6.9}$$

Having defined the Laplacian and its corresponding eigenvalue-eigenvector pairs allows to determine the resulting Jacobian:

$$\mathbf{J} = \begin{bmatrix} \frac{\partial \dot{\phi}_i}{\partial \phi_j} & \frac{\partial \dot{\phi}_i}{\partial \omega_j} \\ \frac{\partial \dot{\omega}_i}{\partial \phi_j} & \frac{\partial \dot{\omega}_i}{\partial \omega_j} \end{bmatrix} = \begin{bmatrix} \mathbf{0}_{N\times N} & \mathbf{1}_{N\times N} \\ \frac{1}{H}\mathbf{L} & -\frac{\alpha}{H}\mathbf{1}_{N\times N} \end{bmatrix}, \tag{6.10}$$

which holds for homogeneous inertia $H_i =: H$ and damping $\alpha_i =: \alpha$. With obvious modifications (6.10) can also be derived for heterogeneous inertia and damping. With (6.10) the Jacobian's eigenvalues σ^i can be expressed in terms of the eigenvalues of the Laplacian:

$$\sigma_{1/2}^i = -\alpha/(2H) \pm 1/H \sqrt{\alpha^2/4 + \lambda^i} \tag{6.11}$$

Hence, the imaginary part of the Jacobian eigenvalues derives from the negative real eigenvalue of the Laplacian eigenvalues.

Illustrative example. The definition of the Laplacian in terms of left and right eigenvectors enables to relate the left eigenvectors with the troublemaker index and the right eigenvectors with the excitable nodes, respectively. A helpful example is the simple first-order equation which has similarities with linear power grid system:

$$\begin{aligned} \dot{x}(t) &= Lx \\ x(t) &= e^{Lt} x_0 \\ x(t) &= \sum_i v_r^i \, e^{\lambda_i t} \, v_l^i \cdot x_0 \end{aligned} \tag{6.12}$$

which allows to interpret v_r^i as the shape of the mode, $e^{\lambda_i t}$ as the dynamics of the mode and $v_l^i \cdot x_0$ as the strength with which the mode is excited.

Introducing a perturbation, p, allows a better understanding of how the different modes are excited and what role left and right eigenvectors play. As a high autocorrelation plays a role in troublemaker index, I consider the example of a continuously displaced system.

$$\begin{aligned} \dot{x}(t) &= Lx + p \\ x(t) &= e^{Lt}x_0 + \int_0^t e^{Lt'} p \, dt' \\ x(t) &= \sum_i v_r^i \, e^{\lambda_i t} \, v_l^i \cdot x_0 + \sum_i \int_0^t v_r^i e^{\lambda_i t'} v_l^i \cdot p \, dt' \end{aligned} \tag{6.13}$$

Assuming $\lambda_0 = 0$, and $\lambda_i \neq 0$ for $i > 0$ gives

$$x(t) = \sum_i v_r^i \, e^{\lambda_i t} \, v_l^i \cdot x_0 + v_r^0 v_l^0 \cdot pt + \sum_{i>0} v_r^i \frac{e^{\lambda_i t} - 1}{\lambda_i} v_l^i \cdot p \tag{6.14}$$

Thus for long times, the zero mode diverges and will tend to dominate the dynamics.

Left Eigenvectors and Troublemakers. The conclusion from this illustrative example is that strongly autocorrelated drivers of instability or troublemakers are most visible in the zero mode. This is expressed by the term $v_r^0 v_l^0 \cdot pt$ in (6.14). Hence, the troublemaker index is approximately proportional to the left eigenvector of the zero eigenmode:

$$Pred_{\mathrm{TI}} = v_l^0 \, . \tag{6.15}$$

This means, as I vary p to hit different nodes, the size of the term will vary with the zero-component of v_l, and hence v_l^0 is a predictor for the TI-index

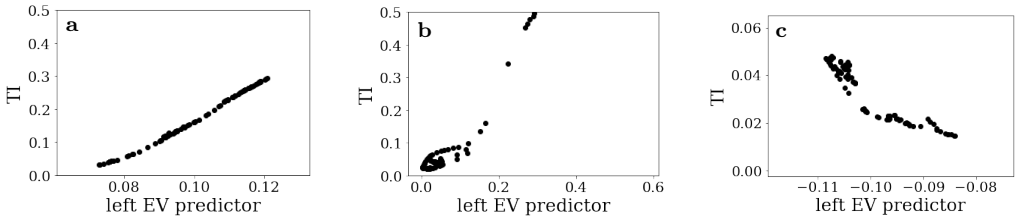

Figure 6.10: **Comparison of model results with predictor for the troublemaker index.** Plot of troublemaker index over the predictor (see (6.15)) based on the zero mode of the Laplacian's left eigenvector for **a)** an exemplary tree-like microgrid, **b)** a MV grid and **c)** a meshed microgrid.

of a node. Heuristically, this can be understood in the following way: In order to get a large frequency deviation, it requires a sustained displacement of the system. The zero eigenmode is the only one that does not lead to oscillations of the system which cancel each other out. This holds if the system is not overdamped and $|\lambda_i| > \alpha^2/4$. Thus, there is only a chance of a sustained perturbations for the zero mode.

This interpretation is supported by the model results (see Fig. 6.10). For both the micro- and the MV grid the predictor gives an excellent correlation with the troublemaker index from the simulation results. Despite the heterogeneity of damping and inertia in the MV grid case this predictor works astonishingly well for this model case (see Fig. 6.10b). The results from the meshed microgrid in Fig. 6.10c show that this analysis does not only apply to tree-like networks but may also be extended to other grid topologies. At the same time, the meshed topology's troublemaker index is about a factor 10 smaller than the microgrid and MV grid case with same coupling strength. This shows how the addition of lines is able to reduce the risks for stability occurring from fluctuating power input. Hence, the troublemaker predictor works well for all model cases: for the microgrid case, the MV grid example and even for a meshed microgrid.

Right eigenvectors and excitable nodes. Conversely, Figs. 6.3 and 6.4 showed that temporal correlations play no such prominent role when considering excitability. Instead, the spatial structure of the modes becomes relevant. Hence, I will consider the right eigenvectors, v_r^i, of the Laplacian, which encode the spatial structure. A simple guess is that a predictor for excitability therefore needs to contain the sum over all right eigenvector modes since it gives insights on how strong each node is excited on average. Because intermittent RES fluctuations show a turbulent power spectrum, with the Kolmogorov exponent of $-5/3$, not all network modes are excited equally strong and the right eigenvectors needs to be weighted. Then, the excitability predictor $\mathrm{Pr}_{\bar{E}_m}$ of node m is defined as

$$\mathrm{Pr}_{\bar{E}_m} = \sum_i |v_r^{m,i}| n(\lambda_i) \tag{6.16}$$

where

$$n(\lambda) = \begin{cases} |\lambda|^{-5/3} & for\ \lambda \neq 0, \\ 0 & for\ \lambda = 0. \end{cases} \tag{6.17}$$

The estimator for excitability makes two assumptions. First, each mode is excited with an amplitude proportional to the power spectrum of the feed in

fluctuations and second, each mode contributes its amplitude independently to the overall amplitude of a node. Justifying and improving these two assumptions is part of future work.

Again, this predictor correlates well with the simulation results, as shown in Fig. 6.11. This applies for all model cases: the homogeneous and purely tree-like microgrid, MV grid example and the meshed microgrid. Since the predictor is an estimator, more complex power flow patterns with several fix point solutions, as they appear in meshed grids, hamper the agreement of simulation results and predictions but nevertheless, give a great qualitative understanding of which network regions are weakly or strongly excited by fluctuating input. In the case of heterogeneous damping and inertia, such as in the MV grid case, eigenvalues of the Laplacian are not directly translatable into eigenvalues of the Jacobian. This makes the well correspondence of model results and predictor rather astonishing.

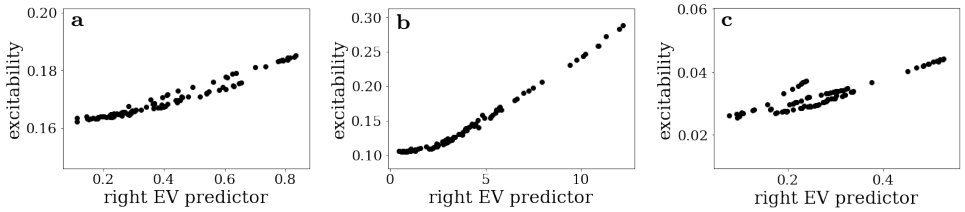

Figure 6.11: **Comparison of model results with predictor for excitability.** Plot of excitability over the predictor (see (6.16)) based on the right Laplacian EV predictor for **a)** an exemplary tree-like microgrid, **b)** a MV grid and **c)** a meshed microgrid.

6.4 Discussion of Fluctuation Analysis

This chapter showed the importance of the network position for single-node fluctuations and different model cases in terms of its influence on the overall stochastic stability of lossy DGs. There is a remarkable and subtle but robust interplay of dynamical and topological properties, even in the case of a microgrid with a homogeneous distribution of identical net consumers and producers. This interplay is largely absent for lossless grids. Without the correct representation of distribution grids as lossy networks, this effect would therefore have stayed undiscovered.

Drivers of instability, the so-called troublemakers and fluctuation sensitive nodes appear on branches, which demonstrate coherent behavior within themselves and thus network neighbors behave alike. Such troublemakers tend to pass on the temporal correlation of the intermittent power time series to the other grid nodes. Which branches turn out to be instable ones

is determined by the power input configuration and thus the power flow on the network.

At the same time, especially at low coupling strength generally fluctuation sensitive nodes emerge. Such nodes of high excitability themselves have little capability to act as troublemakers. Instead they cause large frequency incoherencies.

Generally, I conclude that the left eigenvectors of the Laplacian determine which modes are excited by how much. In order to get a large deviation from synchrony, a large sustained displacement of the system is required. The zero eigenmode is the only one that does not lead to oscillations of the system which cancel themselves out. Strongly autocorrelated drivers of instability or troublemakers are most visible in the zero mode. Hence, the zero mode entry of the left Laplacian eigenvector is a predictor for troublemaking.

Whereas the right eigenvectors says what the modes look like and serve as excitability predictor. The excitation of the network's eigenmodes happens in the case of a strong overlap of the network's eigenfrequencies and the wind and solar power spectrum for low coupling strength. The overlap leads to large entries in the corresponding Kolmogorov weighted sum of the Laplacian's right eigenvectors that enables to identify the most excitable or fluctuation sensitive nodes. The corresponding analytical predictor permits to identify network regions that are especially effected.

Meshed grids show the previously described effects, only less pronounced and with reduced values in exceedance. Hence, these findings are not restricted to pure tree-like networks. Still, a more detailed investigations of meshed grids shall follow, especially targeting at the question how the smart placement of a few additional lines may eliminate troublemakers.

Despite the conceptual modeling approach, I would like to be make a few careful distribution grid design recommendations. As the issue of excitable nodes in lossy grids increases with reduced coupling strength, long lines and cables are especially affected and thus, are to be avoided in distribution grids. Also, the issue of troublemakers and can be overcome with low resistance lines. However, the placement of RES at nodes that are no troublemakers would be the cheapest solution, if possible. The addition of new links to distribution grid trees significantly reduces the occurrence of troublemakers and the risks from eigenmode excitations at the same time.

The simple form of the predictors found in this work, strongly suggests that future analytic work will be able to actually derive these predictors precisely. The relevant features of the noise and system, that drive the various observations have been identified, provide a roadmap for future investigations. A related publication is in preparation and to be published

after the submission of this thesis. Also, a study on multiple node fluctuations shall follow, which asks for a better understanding of the spatial correlation between fluctuations in renewable energy production. To capture the effect of future voltage issues, as a next step, the voltage dynamics shall be introduced in the current model setup.

There is little known about the influence of RES fluctuations on frequency dynamics in distribution grids. However, results of this and related work help to reduce balancing needs and improve the placement of network stabilizing power balancers and cost-efficient control techniques.

Chapter 7

The Impact of Delayed Reaction

In this chapter, with the example of DSGC, I present the impact of delayed reaction on power grid stability. This research relates to the question of how to enable a dynamically stable integration of renewable energies (see Sect. 1.5). First, Section 7.1 demonstrates why it is relevant to investigate delays in power grid dynamics. Section 7.2 recalls the model description from Sect. 2.3 and introduces different network motifs as model cases. For a star motif, in Section 7.3, I show the appearance of destabilizing resonances and possibilities to maintain stable grid operation. Further, I investigate the effect of decentralized power generation in cyclic and square lattice grid motifs in Section 7.4. Much of this chapter is based on **Schäfer, Grabow, Auer, et. al.**[1] where I helped to design the study, interpret the results and aided the model implementation.

7.1 Why Delays are Relevant

In future smart grids household may not only consume power but also generate electricity, e.g. through roof-top PV generation. Thus, in such a scenario consumers may act as producers and consumers at the same time, so-called *prosumers* (Kotler 1986). As a result, both consumption and production may be controlled by power electronic devices. These do not react inherently through the laws of physics as the rotating masses of synchronous machines do. Instead, they need to measure grid variables such as frequency and voltage and react with adequate, predetermined control schemes. These measurement and reaction times introduce delays into the power grid dynamics. Both, the concept of Decentral Smart Grid Control

[1]

(DSGC, see Sect. 2.3) and grid-following inverter control (see Sect. 2.2.3.1) may provoke such delays.

In current (European) power plants the initial delays have to be smaller than 2s according to European regulations (ENTSO-E 2016), in practice they will be significantly smaller. However, in future power grids additional communication delays (Naduvathuparambil et al. 2002) of the order of several hundred milliseconds might arise in addition to delays of unknown magnitude caused by demand response and additional power electronics. Hence, the following investigation considers a large range of potential delays $\tau \in (0, 5)$s looking for the boundary of acceptable delays.

7.2 Model Description

The equation of motion for power system dynamics with delayed control was derived in Section 2.3 by introducing a power adaption term with time lag τ:

$$\frac{\mathrm{d}^2\phi_i}{\mathrm{d}t^2} = P_i - \alpha_i \frac{\mathrm{d}\phi_i}{\mathrm{d}t} + \sum_{j=1}^{N} K_{ij} \sin(\phi_j - \phi_i) - \gamma_i \frac{\mathrm{d}\phi_i}{\mathrm{d}t}(t-\tau) \quad \forall i \in \{1, ..., N\}. \tag{7.1}$$

The moment of inertia is assumed to be identical for all machines and hence I eliminate such moments of inertia in the equation of motion for simplicity of presentation (Schäfer, Matthiae, Timme, et al. 2015). As a further simplification, ohmic loads are neglected as they should be small compared to shunt admittances (Hertem et al. 2006) for the dynamics I consider. The parameters of the swing equation are calculated from standard literature values (Machowski et al. 2011; Schultz, Heitzig, et al. 2014a).

Delayed differential equations need a history function as initial condition that describes the system dynamics for the time interval $[-\tau, 0]$:

$$\omega(t < 0) = \omega_0(1 + 0.1 \tanh(t/2)). \tag{7.2}$$

The simulation results do not change significantly with different history functions such as $\omega(t < 0) = \omega_0$. Though, the choice of (7.2) has the advantage to be smooth, non-constant and thus more realistic.

In Schäfer, Matthiae, Timme, et al. 2015, it was already shown that such a delayed system poses risks to the stability of the power grid for certain delays τ. Hence, an extension using frequency measurements averaged over time intervals of lengths T was introduced to stabilize the power grid regardless of the specific delay. Such averaging yields

$$\frac{\mathrm{d}^2\theta_i}{\mathrm{d}t^2} = P_i - \alpha_i \frac{\mathrm{d}\theta_i}{\mathrm{d}t} + \sum_{j=1}^{N} K_{ij} \sin(\theta_j - \theta_i) - \frac{\gamma_i}{T} \int_{t-T}^{t} \frac{\mathrm{d}\theta_i}{\mathrm{d}t}(t' - \tau)\mathrm{d}t' \tag{7.3}$$

$$= P_i - \alpha_i \frac{\mathrm{d}\theta_i}{\mathrm{d}t} + \sum_{j=1}^{N} K_{ij} \sin(\theta_j - \theta_i) \tag{7.4}$$

$$- \frac{\gamma_i}{T} \left(\theta_i(t-\tau) - \theta_i(t-\tau-T)\right) \quad \forall i \in \{1, ..., N\}. \tag{7.5}$$

For what follows, I choose homogeneous averaging time T for all machines, as well as similar delays τ for all nodes. In addition, I use homogeneous capacities $K_{ij} = K$ for all lines as well as same α and γ for all nodes to simplify the calculations. In the following sections the delayed equations (7.1) and (7.3) are applied to different network topologies and evaluated according to their stability as a function of the delay τ with different averaging times T. I hereby treat the averaging time T as a control parameter that can be chosen when setting up the system, while the delay τ remains as an exogenous parameter introduced by the consumers and producers.

The model cases are different network motifs. The four-node star motif (see Fig. 7.1 (a) for an illustration) constitutes a conceptualization of the main building blocks of power grids. In principle, their effective topology locally resembles a star, the central node being a large power plant that supplies the regional consumers in its vicinity (50Hertz et al. 2012; Rohden et al. 2014). The cycle network and lattice-like topology, for which the effect of decentral vs. central production is investigated, conceptually implement cycle and meshed grid topologies.

The Linear Stability Analysis of delayed dynamical systems is determined via the eigenvalues λ of Jacobian $\mathbf{J}$ (see Section 3.3) of both the non-delayed

$$\mathbf{J_0} = \begin{bmatrix} \frac{\partial \dot{\phi_i}}{\partial \phi_j} & \frac{\partial \dot{\phi_i}}{\partial \omega_j} \\ \frac{\partial \dot{\omega_i}}{\partial \phi_j} & \frac{\partial \dot{\omega_i}}{\partial \omega_j} \end{bmatrix} = \begin{bmatrix} \mathbf{0}_{N\times N} & \mathbf{1}_{N\times N} \\ \mathbf{L} & -\alpha \mathbf{1}_{N\times N} \end{bmatrix}. \tag{7.6}$$

and delayed system (Roussel 2005; Schäfer, Matthiae, Timme, et al. 2015)

$$\mathbf{J}_\tau = \begin{bmatrix} \frac{\partial \dot{\phi_i}}{\partial \phi_j^\tau} & \frac{\partial \dot{\phi_i}}{\partial \omega_j^\tau} \\ \frac{\partial \dot{\omega_i}}{\partial \phi_j^\tau} & \frac{\partial \dot{\omega_i}}{\partial \omega_j^\tau} \end{bmatrix} = \begin{bmatrix} \mathbf{0}_{N\times N} & \mathbf{0}_{N\times N} \\ \mathbf{0}_{N\times N} & -\gamma \mathbf{1}_{N\times N} \end{bmatrix}. \tag{7.7}$$

From these the characteristic equation reads as

$$p(\lambda) = \det(J_0 + e^{-\lambda\tau} J_\tau - \mathbf{1}\lambda) = 0 \tag{7.8}$$

$$= \det \begin{bmatrix} -\lambda \mathbf{1}_{N\times N} & \mathbf{1}_{N\times N} \\ \mathbf{L} & (-\alpha - \gamma e^{-\lambda\tau} - \lambda)\mathbf{1}_{N\times N} \end{bmatrix} = 0. \tag{7.9}$$

7.3 Delays and Network Resonances

This section presents the stability impact of delays for a four-node star motif and compares the results of linear stability and basin stability analysis (see Sect. 3.3). Hereby, I discuss the destabilizing effects of resonances and the "rebound effect" for large delays and present how intermediate delays τ benefit the stability.

Delays induce destabilizing resonances. Networks with star topology (Fig. 7.1a) exhibit stability properties that depend crucially on the delay and the averaging applied (Fig. 7.1b). Without any averaging (Fig. 7.1b dark blue curve), there are delays τ for which the fixed point is linearly unstable, i.e., there are eigenvalues with a positive real part $\mathrm{Re}(\lambda) \geq 0$. Those eigenvalues exhibit a periodic behavior with respect to the delay τ. Operating the power grid at a delay τ, e.g. $\tau \approx 1$s for which the real part of the eigenvalue is positive, is equivalent to resonantly driving the power grid

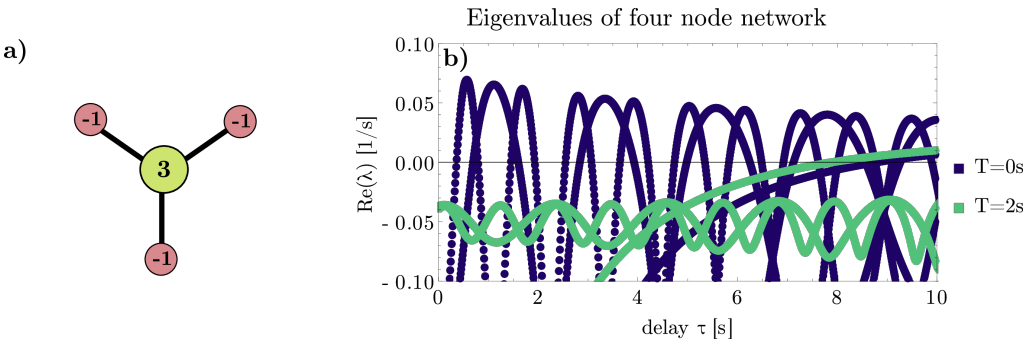

Figure 7.1: **Resonances and large delays τ destabilize the four-node system. a)** An elementary building block in a power grid with centralized production is shaped like a star. The network is formed of one producer (green) in the center with power $P_{\text{producer}} = 3/\text{s}^2$ and three consumers (red) with power $P_{\text{consumer}} = -1/\text{s}^2$ each. **b)** Plotted are the eigenvalues with the largest real part as functions of delay τ. For no averaging (dark blue curve), stable and unstable regions exist. For an averaging of $T = 2$s, the system is stable for all delays below a critical $\tau_c \approx 8$s. In (7.3) parameters $\alpha = 0.1/\text{s}$, $K = 8/\text{s}^2$ and $\gamma = 0.25/\text{s}$ were applied. Figure b) is taken from Schäfer, Matthiae, Timme, et al. 2015.

away from the fixed point instead of damping it towards stable operation. These destabilizing delays are linked to the eigenfrequency of the oscillators in the power grid. If the delay is half the eigenoscillation duration, then it increases amplitudes of perturbations instead of damping them. This destabilization only occurs for $\alpha < \gamma$ because the resonant driving has to be larger than the intrinsic damping of the system, see also Schäfer, Matthiae, Timme, et al. 2015. Introducing sufficiently large averaging times into the control cures these instabilities (Fig. 7.1b green curve); the unstable regions vanish for all delays $\tau < 7$s.

Rebound effect for large delays. For delays larger than a critical delay $\tau > \tau_c \approx 8.7$s the system always gets destabilized, i.e., there is an eigenvalue with $\mathrm{Re}(\lambda) > 0$. This rebound effect acts on a longer time scale than the intrinsic oscillations of the power grid system and originates from an overreaction of the attempted damping as I explain below. The existence of such a rebound effect is independent of averaging T (Fig. 7.1). I determine the critical delay without averaging τ_c to be

$$\tau_c = \frac{\arccos\left(-\frac{\alpha}{\gamma}\right)}{\sqrt{\gamma^2-\alpha^2}} + \frac{2\pi n}{\sqrt{\gamma^2-\alpha^2}},\ n \in \mathbb{Z}. \tag{7.10}$$

This result is obtained by the following considerations. For $T = 0$, the sum of all angles, defined as $\Sigma\phi := \sum_{i=1}^{N} \phi_i$. The corresponding equation of motion is obtained by using (7.1) as

$$\frac{\mathrm{d}^2}{\mathrm{d}t^2}\Sigma\phi(t) = -\alpha\frac{\mathrm{d}}{\mathrm{d}t}\Sigma\phi(t) - \gamma\frac{\mathrm{d}}{\mathrm{d}t}\Sigma\phi(t-\tau). \tag{7.11}$$

The characteristic equation of this equation reads

$$p\,(\lambda) = -\alpha - \gamma e^{-\lambda\tau} - \lambda = 0, \tag{7.12}$$

where the zero eigenvalue $\lambda = 0$ is eliminated which arises due to the possibility to shift all angles by a constant. For $\tau = 0$ the eigenvalue $\lambda = -\alpha - \gamma$ is negative as $\alpha > 0$ and $\gamma > 0$ and hence the system is stable with respect to the sum $\Sigma\theta$. For larger delays $\tau > 0$ I set $\lambda = i \cdot \xi$ to obtain the delays for which the stability changes. This leads to

$$-\alpha - \gamma e^{-i\xi\tau} - i\xi = 0. \tag{7.13}$$

Applying complex expansion and separating into real and imaginary results in

$$-\alpha - \gamma\cos(\xi\tau) = 0, \tag{7.14}$$

$$\gamma\sin(\xi\tau) - \xi = 0. \tag{7.15}$$

These equations can be solved for τ and ξ to yield the critical delay as in (7.10). Note that a critical delay τ_c only exists, if the price adaptation is larger than the intrinsic damping of the system $\gamma > \alpha$. Following straight-forward calculations I can prove that eigenvalues obtained from (7.12) always destabilize the system, i.e., their real parts are positive for all delays larger than the critical one,

$$\mathrm{Re}(\lambda(\tau)) > 0 \quad \forall \tau > \tau_c. \tag{7.16}$$

These results hold for all network topologies, since they required no assumptions regarding the coupling matrix K_{ij} or the power production P_i. Predicting the precise scaling of the critical delay as a function of the averaging time T is not easily possible but an approximation for small ξT is obtained as

$$\tau_c(T) \approx \frac{\sqrt{T^2\gamma^2 - 4}\arctan\left[\frac{(\alpha+\gamma)\sqrt{T^2\gamma^2-4}}{(2+T\gamma)\sqrt{\alpha^2-\gamma^2}}\right]}{\sqrt{\alpha^2-\gamma^2}}, \tag{7.17}$$

which is a decreasing function in T for parameters $\alpha, \gamma, T > 0$. Hence, increasing averaging time T causes the rebound effect to occur for smaller delays τ.

I conclude that the delay τ has to be smaller than a critical value τ_c to ensure stability. This critical value depends only on the intrinsic damping α and the price adaptation γ and decreases for increasing averaging T, while it is valid for all network topologies. Hence, to avoid problems with large delays, all actors of the power grid have to react within less than this critical delay τ_c. Or they need to ensure that the intrinsic damping is larger than the price adaptation: $\alpha > \gamma$. For the next section, I restrict the delay to the interval $\tau \in [0, 5]$s to avoid this destabilizing rebound effect.

Intermediate delays benefit stability. With the help of linear stability I observed that delays induce destabilizing resonances which can be suppressed by prosumers responding to averaged frequency measurements. At the same time large delays destabilize the system by introducing a rebound effect. These results are supplemented by information from the basin stability analysis. For DSGC with averaging (Fig. 7.2b and c), I demonstrate how intermediate delays τ are beneficial for the stability of the system. Basin stability increases with greater delay $\mu_B(\tau > 0) > \mu_B(\tau = 0)$ until, for delays $\tau \approx 4$s, it is close to perfect stability with $\mu_B \approx 1$ both for an averaging $T = 1$s and $T = 2$s. In the previous paragraph I demonstrated that high averaging times and large delays always destabilize the power grid.

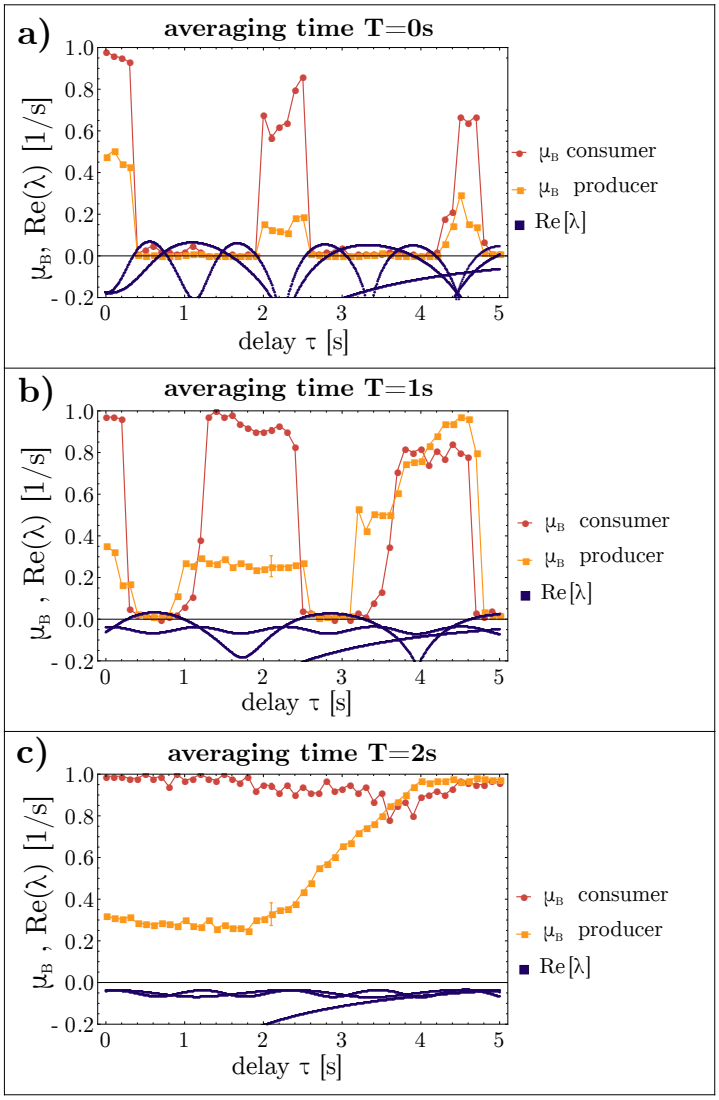

Figure 7.2: **Linear stability and basin stability analysis for the star topology** (see Fig. 7.1). Intermediate delays result in high values of basin stability if averaging is switched on. Shown are the real parts of the eigenvalues for the 4 node star motif (dark blue) as well as the basin stability of the producer (orange) and of one consumer (red) as functions of the delay τ for different averaging times: **a)** $T = 0$s, **b)** $T = 1$s, **c)** $T = 2$s. Parameters $\alpha = 0.1/\text{s}$, $K = 8/\text{s}^2$ and $\gamma = 0.25/\text{s}$ were applied. For delay $\tau = 2.1$s simulations were repeated 21 times, averaged and the standard deviation is shown as a typical error bar. Figures are taken from Schäfer, Matthiae, Timme, et al. 2015.

Hence, I observe a trade-off in curing resonances with averaging and avoiding the rebound effect for delays larger than a critical value τ_c. Furthermore,

basin stability reveals that disturbances in a consumer node are less likely to destabilize the system than perturbations of the producer (compare dark red and light orange curves in Fig. 7.2). This is intuitively clear as there is only one producer and the topology increases its importance even more.

I conclude that Decentral Smart Grid Control can be applied to the star motif if an averaging time of at least $T = 2$s is used or the price elasticity is smaller than the intrinsic damping $\gamma < \alpha$. Additionally, intermediate delays $\tau \approx 4$s incorporate the trade-off between curing either destabilizing resonances or rebound effects. They increase the basin stability of the system and thereby benefit the overall stability of the power grid.

7.4 Effect of decentralized production

In this section I demonstrated that switching from central to decentralized production improves the linear stability in the power grid topologies I investigate for small and intermediate delays. Specifically, I analyzed linear stability for moderately sized lattice and cycle networks for different central and decentralized power production.

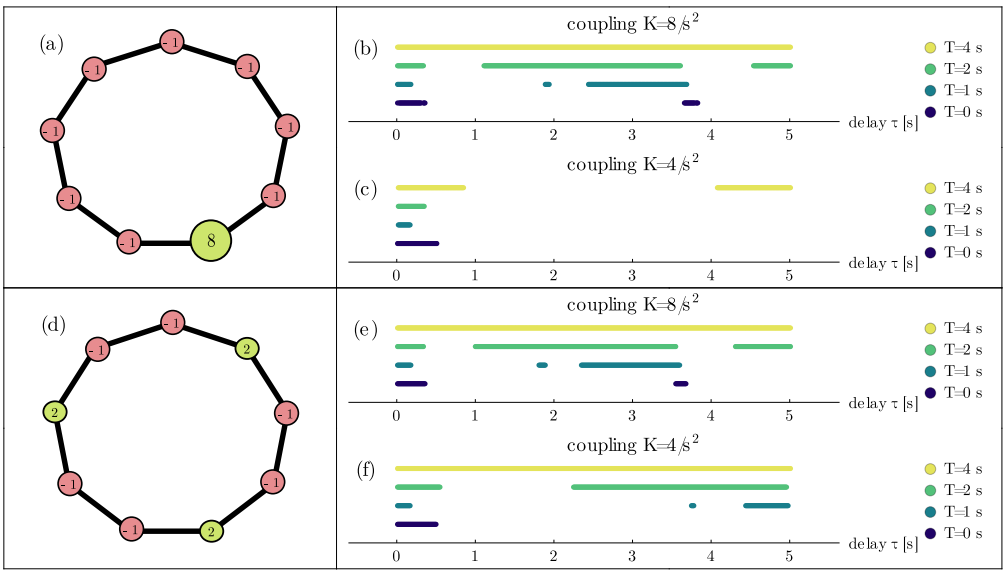

Figure 7.3: **Central power production in a circle network requires larger capacity K than in decentralized power grids.** Shown are the ranges of delay τ for which the power grid motifs with central production (a) or decentralized production (d) are linearly stable. Panels (b) and (e) present ranges for a high capacity $K = 8/\text{s}^2$, whereas (c) and (f) for $K = 4/\text{s}^2$. Overall, the regions of stability tend to become larger, the larger the average time T. Parameters $\alpha = 0.1/\text{s}$ and $\gamma = 0.25/\text{s}$ were applied. Figures are adapted from Schäfer, Matthiae, Timme, et al. 2015.

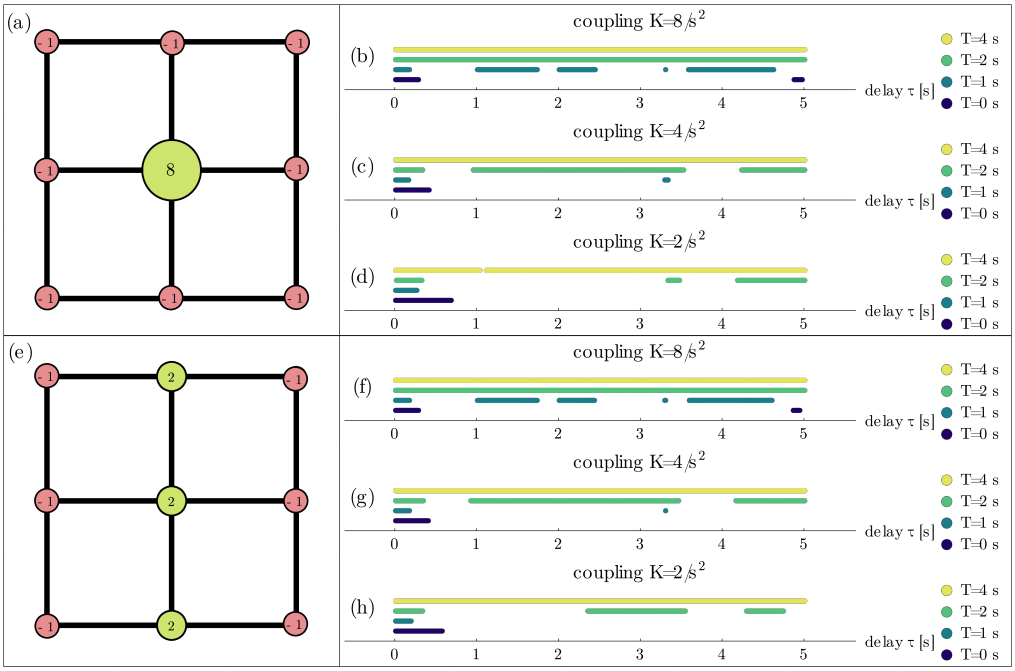

Figure 7.4: **Central and decentralized power production in a lattice-like topology lead to similar stability.** In contrast to the cycle network, the lattice-like topology is stable for lower coupling K. Shown are the ranges of delay τ for which the power grid motifs with central production (a) or decentralized production (e) are linearly stable. Panels (b) and (f) present ranges for a high capacity $K = 8/\mathrm{s}^2$, (c) and (g) for an intermediate capacity $K = 4/\mathrm{s}^2$, finally (d) and (h) for $K = 2/\mathrm{s}^2$. Overall, the regions of stability tend to become larger, the larger the average time T. Parameters $\alpha = 0.1/\mathrm{s}$ and $\gamma = 0.25/\mathrm{s}$ were applied. Figures are adapted from Schäfer, Matthiae, Timme, et al. 2015.

For a cycle network decentralization enhances stability significantly (Fig. 7.3). For a power line coupling of $K = 8/\mathrm{s}^2$ centralized and decentralized production result in similar stability (Fig. 7.3b and e). However, for the critical coupling of the cycle network, i.e., the minimal coupling needed so that there exists a fixed point (Rohden et al. 2014), $K = 4/\mathrm{s}^2$, the cycle with central production cannot be stabilized for all considered delays. Whereas this is possible for decentralized production (Fig. 7.3c and f).

A lattice-like topology for power grids allows stable operation with central power production (Fig. 7.4). Choosing large couplings of $K = 8/\mathrm{s}^2$ (Fig. 7.4b and e) or even $K = 4/\mathrm{s}^2$ (Fig. 7.4c and g), decentralized and centralized production result in very similar stability. Even when operating at the critical coupling of the lattice-like topology $K = 2/\mathrm{s}^2$, the central power production can be stabilized for sufficiently large averaging time $T = 4\mathrm{s}$ (Fig. 7.4d and h).

Note that I chose $\gamma_i = 0.25/\mathrm{s}$ for all nodes in the networks. Hence, the large producer with $P_{\mathrm{large}} = 8/\mathrm{s}^2$ adapts relatively less compared to the smaller producers with $P_{\mathrm{small}} = 2/\mathrm{s}^2$. Nevertheless, the overall adaptation of the whole network is

$$\Delta P = \sum_{i=1}^{N} \gamma_i \cdot |\Delta\omega|, \tag{7.18}$$

with $|\Delta\omega|$ being the maximal angular frequency deviation. Hence, the maximal adaptation ΔP is independent of the power distribution.

I conclude that a centralized power production requires larger transmission capacities compared to a decentralized power production to guarantee stable power grid operation. An averaging time of $T \approx 4\mathrm{s}$ stabilizes the power grid with Decentral Smart Grid Control for all considered delays. Note that the decentralized production has only short distances to the consumers. Decentralized power production tends to allow smaller averaging times, thereby offering a greater safe operating space. In addition, a highly connected topology like a lattice outperforms the less connected cycle in terms of stability.

7.5 Summary

In this article I showed the impact of delayed control with the application of "Decentral Smart Grid Control" (DSGC), as proposed in Schäfer, Matthiae, Timme, et al. 2015. The stability analysis has been undertaken for different motifs and small networks.

I first determined both the linear stability and the basin stability of a four-node-star motif in dependence on the delay time τ (see equation 7.1) and for fixed averaging times T (see equation 7.3). Linear stability analysis reveals two destabilizing effects for the power grid. First, resonance catastrophes destabilize the system periodically. This instability can be cured by applying sufficient averaging (Fig. 7.1). Secondly, a rebound effect emerges for large delays and destabilizes the system regardless of averaging. The rebound effect sets an upper limit for the delay $\tau = \tau_c$ and magnitude of adaptation response γ as it has to be smaller than the intrinsic damping of the system α. The basin stability analysis gives further probabilistic insight on how well DSGC tames grid instabilities. For large averaging times T and intermediate delays τ, basin stability approaches unity (Fig. 7.2). Hence, for DSGC exists a trade-off in curing resonances with averaging and larger delays and avoiding the rebound effect for delays larger than a critical value τ_c.

Summarizing the results from linear and basin stability analysis, adaptation has to be smaller than the intrinsic damping of the system ($\gamma < \alpha$) or the demand response time needs to be located in a delay window of safe operation ($\tau < \tau_c$). For values above the critical delay τ_c the system becomes always destabilized, regardless of the averaging time. At the same time, averaging and increasing delay is beneficial for system stability in terms of basin stability. These results have strong implications on how parameters has to be set for real world applications of DSGC.

In the last section of this chapter, I demonstrated the usefulness of DSGC with centralized and decentralized power production. While it works in both cases, central production requires larger line capacities K. For the lattice-like topology, this effect can be compensated by using longer averaging times. But decentralized power production is clearly advantageous.

As a next research step, this analysis shall be repeated with the fourth-order model (see Sect. 2.2.2.2). Chapter 4 presented it as the necessary model detail for basin stability assessment. It is also relevant to consider heterogeneous networks, i.e. the use of different τ, γ, T values for individual nodes, modifying the averaging method, e.g., to a discrete time window and extending the DSGC framework to larger network topologies. In this context, there remain a couple of open questions that will have to be investigated in more detail, namely: What is the reason that delays τ for which $\mu_B(\tau) > \mu_B(\tau = 0)$ exist, in particular for larger averaging times? Do larger networks required even larger averaging times T? How large is the safe operating space to cure instabilities by resonances while avoiding the rebound effect for different networks? These are all widely open questions.

In this chapter, I have demonstrated that Decentral Smart Grid Control constitutes a promising control concept, in particular for future power grids that will be more decentralized than the present one.

Chapter 8

Decentral Electric Vehicle Control

Today, in Germany 90% of RES are installed in distribution grids (BMWi 2014). Intermittent RES have strong power output fluctuations challenging the dynamical stability of power grids (Rohden 2015; Schäfer, Grabow, et al. 2016; Short et al. 2007; Troester 2009). In this chapter, I show how the dynamic stability of distribution grids can be restored by concepts of electric vehicle (EV) demand control. This relates to the question of how to enable a dynamically stable integration of renewable energies (see Sect. 1.5). To a great extent this chapter is based on **Auer, Roos, et al. 2017**.

The goal of this work is to find an optimal parameterization for decentral EV control in a modeling scenario with strong Photovoltaic (PV) penetration (Roos 2016). The parameterization shall improve the dynamical stability of the power grid, minimize the amount of battery switching events to avoid battery degradation, and ensure an effective control at the same time. In addition, I test whether randomization will be useful in order to prevent undesirable demand synchronization as observed in Krause et al. 2015; Moghadam et al. 2016; Mohsenian-Rad et al. 2010; Short et al. 2007.

This chapter is organized as follows. First, Section 8.1 introduces to the concept of EV control. Section-8.2 presents parameterization of the chosen grid, of the inverter dynamics and the EV control and the performance measures to evaluate the different parameterization scenarios. The results section, 8.3, starts with investigating a base scenario without EV control. Then I test different EV parameterizations or control strategies and their robustness. Section 8.3 closes with a comparison of decentral vs. central control.

8.1 Introduction to Electric Vehicle Control

To maintain the grid's dynamical stability, Schäfer, Matthiae, Timme, et al. 2015 suggested the concept of Decentral Smart Grid Control (DSGC), where power consumers adjust their demand according to the locally measured grid frequency (see Chapter 7). The use of the locally measured grid frequency for DSGC has the advantage that the electrical appliances can be automated with load controllers, such as the Distributed Intelligent Load Controller (DILC) (Ian et al. 2003; Short et al. 2007). These load controllers then adjust the power demand of an electrical device with a certain control strategy or heuristic (Short et al. 2007).

In order to balance fluctuations locally where they appear, EVs and their battery storage systems would present an ideal use case for DSGC (Liu et al. 2013; Pillai et al. 2010). EVs can adjust their power demand within milliseconds and have the capability to deliver power back into the grid, also known as *vehicle to grid* (V2G) power transfer and vice versa simply charge – *grid to vehicle* (Pasaoglu et al. 2013; J. Wang et al. 2011).

With a frequency control strategy, EVs essentially act as primary frequency control reserves, since they autonomously assist in stabilizing the grid frequency (Liu et al. 2013; Pillai et al. 2010). The fact that 94% of all U.S cars are parked at noon time of a typical day (Van Haaren 2011) shows the great potential for EV control. Instead of installing additional expensive balancing hardware, the anyways idle EVs may be used for grid control purposes.

A control strategy that has been suggested and used in order to maintain dynamical grid stability is the *band gap* strategy (Almeida et al. 2011; Karki et al. 2014; Liu et al. 2013). A band gap is the frequency interval between the battery thresholds for positive and negative frequency deviations, $f_{\min}$ and $f_{\max}$ (see Fig. 8.1), also called deadband. It defines the frequency range where no power is transferred between the EV and the power grid, at least relative to the base charging scenario. As small frequency deviations are considered to be part of normal operation, the deadband reduces unnecessary battery stress. When the frequency deviations are out of this band gap, the EV and power grid exchange an amount of power that depends on the magnitude of the deviation from the band gap and a predefined rate of power transfer called the ramping rate, r. Thus, this rate of power transfer and the frequency band gap are the parameters which determine the sensitivity of this control strategy.

8.2 Model Description

In contrast to previous works (Almeida et al. 2011; Karki et al. 2014; Liu et al. 2013; Pillai et al. 2010), I explicitly model the network structure as a complex network. This allows to investigate the influence of decentral vs. central control and model the interaction of appliances via the power grid. In addition, stochastic models reproducing solar power fluctuations are very recent (Anvari, Lohmann, et al. 2016) and I am the first to incorporate the intermittent nature of fluctuations from RES in such a EV control study.

The model is designed to represent distribution grids. Thus, I chose tree-shaped networks as the underlying network topology (generated with a random growth model (Schultz, Heitzig, et al. 2014b). I introduce lossy lines, since the common assumption of non-lossy lines for transmission grids does not hold for distribution grids. As a simplification, all nodes in the network have the same absolute power and inertia to exclude any side effects from network heterogeneities that make the evaluation of different control strategies more difficult (see the medium-voltage grid case described in Sections 2.1.4 and 6.1). The model uses discrete time steps of 0.01 seconds, and each control strategy was simulated on 15 different power grids to average out the influence of one specific network structure.

In the following, I elaborate on the modeling assumptions concerning the type of node dynamics as well as the medium-voltage (MV) grid and EV parameterization. Then, I describe what measures I use to evaluate the performance of different heuristics.

Inverter-dominated grids. As a model case, I choose a MV grid region with high PV penetration which makes the grid dynamics inverter-dominated. Most PV and wind power plants are connected to the grid via grid-feeding inverters. However, grid-forming inverters are important for dynamic stability (Schiffer, Zonetti, et al. 2016). Thus in this scenario, which is meant to represent future MV grids, I assume that effective grid nodes representing an accumulation of production from the Low-Voltage (LV) level where each node has at least one grid-forming inverter. This type of inverter is able to provide virtual inertia whereas grid-feeding inverters contribute no inertia. Grid-forming inverters and their power electronics may be programmed as Virtual Synchronous Machines, as mentioned in Section 2.2.3.1, by using a smooth droop control. This then leads to the same equations for the voltage angle ϕ and angular frequency (in the co-rotating frame), $\omega = 2\pi f$, in terms of the (virtual) inertia H_i (Schiffer, Goldin, et al. 2013), power infeed P_i, (virtual) damping α, line susceptibil-

ities, $Y = G + jB$, and voltage magnitudes U_i for each node i:

$$\begin{aligned}\dot{\phi}_i =&\omega_i,\\ \dot{\omega}_i =&\frac{1}{H_i}(P_i + \delta P_i(t) - \alpha\omega_i - b(f_i) - \sum_k U_i|Y_{ik}|U_k \sin(\phi_i - \phi_k + \phi_{ik})).\end{aligned} \tag{8.1}$$

where $b(f)$ is the function of the bandgap strategy illustrated in Fig. 8.1a and equals

$$b(f_i) = \Theta(|f_i| - f_{min})sign(f_i)(|f_i| - f_{min})r \tag{8.2}$$

with the Heaviside step function Θ and the sign function $sign$. The power ramping slope of the EV batteries is given by

$$r = \frac{p_{max}}{f_{max} - f_{min}} \tag{8.3}$$

where $p_{max} = 3.7$kW is the maximum charging power.

The virtual inertia and damping for the network model are calculated as shown in Section 2.2.3.1. As I am interested in the low inertia case, with few low powered grid forming inverters at each node, I assume a weakly reacting, strongly smoothed system. This leads to consider $\alpha = 0.01s$ and $H = 0.05s^2$. Please note that the results are not sensitive to the exact choice of α and H.

Medium-voltage (MV) grid parameterization. The MV-grid is a good testing case for modeling EV frequency control as a reaction to power fluctuations caused by a high PV penetration. This is the case because most PV power plants are connected to LV or MV levels. This modeling scenario is an extension of the MV grid case presented in Section 6.1. Again, all nodes have the same amount of inflexible load and production which a strong assumption in favor of homogeneity that allows to attribute any difference in performance of EV control at different network nodes purely to the chosen control strategy in combination with the nodes' network properties.

For the inflexible load and average PV power generation a challenging 2050 scenario was assumed, where the power production from PV is two times larger than the inflexible load in the MV nodes. Here, I assume 0.268 MW solar production for each MV node. This is a challenging, but realistic scenario, as the installed PV capacity in some LV grids in south Germany can already exceed the peak load by a factor of ten (Appen et al. 2013). The inflexible load of each node was 0.168 MW, as the peak load in 2014 of 84 GW in the German grid was equally divided among the

MV nodes (Bayer 2015). This peak load is assumed to remain unchanged until 2050, although it included the additional load from EVs. This is the case since Smart Charging of EVs and the improved energy efficiency are expected to compensate for additional loads from the growing amount of EVs (Boßmann et al. 2015). Hence, the effective power input P_i, the power which is injected into the grid, equals $P_i = 0.1$MW. The frequency time series for this base scenario is shown in Fig. 8.1b.

EV parameterization. The EVs' maximum charging/injection power transfer rate is assumed to be 3.7 kW (230V/16A), also referred to as private home charging, since this type of EV charging is expected to have a market share of 64,8% in Germany by 2050 (Madina et al. 2016; Richter et al. 2010). The total battery capacity of an EV was 90 kWh, equal to the maximum capacity of a Tesla model S (Tesla Motors 2016). The energy consumption during a driving event is assumed to be 6.7 kW according to Metz et al. 2012; Silva et al. 2009. At the beginning of each simulation 94% of the EVs were available, in compliance with the findings from Van Haaren 2011,which documented that 94% of all U.S cars were parked at noon on a typical day. The 6% of unavailable EVs were randomly distributed among the MV nodes in the model.

The initial charge of all EVs is 72 kWh representing a state of charge

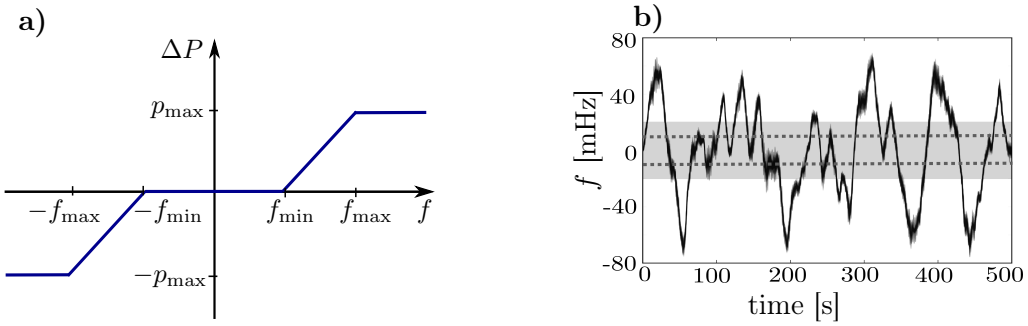

Figure 8.1: **Scheme of electric vehicle control and frequency time series without such control. a)** Scheme of battery ramping. $[-f_{min}, f_{min}]$ is the frequency dead band for which the battery stays idle. For $\Delta P = 0$, no frequency control is provided. f represents the frequency in the co-rotating frame. f_{min} and f_{max} determine the ramp at which the battery charges ($\Delta P > 0$) or discharges ($\Delta P > 0$). $\pm p_{max}$ are the upper limits for charging and discharching. **b)** Time series of all nodes' frequency trajectories for the base scenario of an example grid with power production of 0.268 MW and 0.168 MW demand. The exceedance is calculated as the time share of frequency trajectories outside the grey safety band of ±20 mHz. The dark grey dotted line at ±10 mHz marks the threshold for battery control.

(SOC) of 80%. For the EV battery threshold, I assume: $f_{min} = 0.01$ (see Fig. 8.1), which corresponds to the so-called dead band from the German transmission code and defines at which frequency primary control actions kick in to balance deviations from the desired 50Hz set point (Verband der Netzbetreiber e.V. 2007).

Performance Measures. The stability measures typically used in power grid synchronization analysis are not applicable to stochastic system (Auer, Kleis, et al. 2016; Belykh et al. 2004; Hellmann et al. 2016; Menck, Heitzig, Marwan, et al. 2013; Nishikawa et al. 2006; Pecora et al. 1998). Here, I use the *exceedance* measures, which is the time share the frequency spends outside a given safe band (see Sect. 3.4 for a detailed explanation).

Besides frequency stabilization the performance of the proposed heuristics are evaluated with respect to their influence on battery degradation. Hence, the *Switching events* are recorded. They include the battery action changes: decharging to idle, charging to idle, idle to charging and idle to decharging. Note that I evaluate switching only for the primary control. However, the background charging for battery refilling is assumed to be fulfilled in the power balance and considered to be a problem of secondary or tertiary control.

8.3 Performance Analysis of Electric Vehicle Control.

The starting point of my investigations is the base scenario in order to gather an understanding of how the power system behaves with increasing power

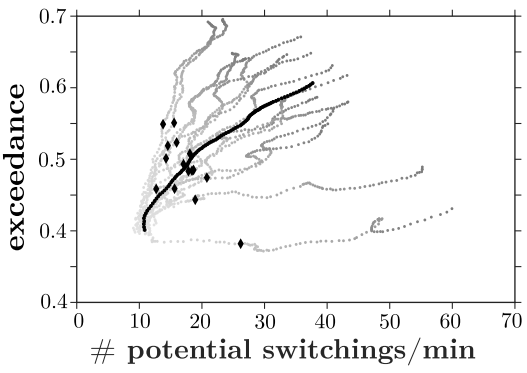

Figure 8.2: **Sensitivity of base scenario (no EV control).** Exceedance (averaged over all nodes) plotted over the potential average number of battery switchings for increasing power production from 0.17 to 0.5 MW. The grey dotted lines (darker grey for greater power production) show a network sample of 15 random medium-voltage topologies with the black line representing the ensemble average. The black diamonds mark the chosen base scenario.

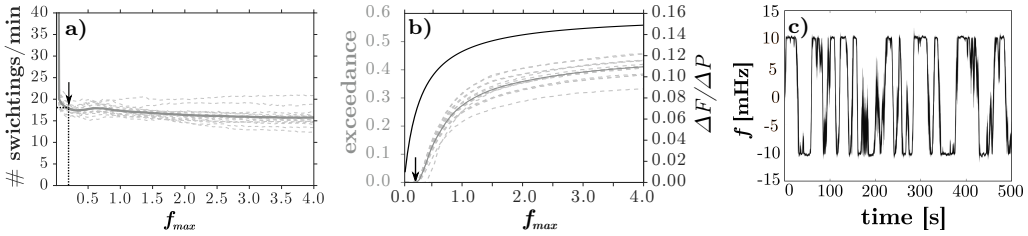

Figure 8.3: **Parameterization of EV ramping. a)** Average number of nodal battery switchings and **b)** average nodal exceedance plotted over different ramping slopes, r, for 15 different networks (grey dashed lines). For $f_{max} = 0.01$ Hz switching events go up to 500. The solid grey line represents the ensemble average for both, a) and b). The second y-axis of the b) shows the analytic result for global frequency offset ΔF caused by a global power unbalance ΔP (see (8.4)). **c)** Frequency time series for $f_{max} = 0.02$ Hz.

production from RES without any EV primary control present. Section 8.2 presented the chosen base scenario for the EV DSGC. Nevertheless, at first I want to better understand how larger or lower values of RES production influence the power system stability measures. Then, I identify the battery ramping slope that is necessary to prevent frequency from exceeding the chosen safety margin of ±0.02Hz. In order to identify not only a grid- but also battery-friendly control mechanism, I apply a suitable battery threshold randomization. I compare this strategy with the alternative approach of averaging over past frequency values in order to overcome fast switching. Finally, the importance of decentral control is investigated more closely with respective to its effectiveness.

Base scenario - no EV control. Fig. 8.2 shows how an increase in production equally leads to higher values of exceedance and potential switching events. However, to what extent this happens, strongly depends on the chosen type of network. A concise classification of networks with respect to their robustness towards fluctuations will be an interesting research problem for future work.

In this base scenario the EVs do not participate in frequency control. However, by measuring how many times f_{min} was crossed, the potential switching events are determined. In order to challenge EV grid control, as previously mentioned, I have picked a case of relatively high production, $S_i = 0.268$MW (marked by black diamonds for each network in Fig. 8.2). Fig. 8.1b shows the frequency evolution for all 100 network nodes for this model setup. The frequency safety band illustrates how much time the nodal frequencies spend outside the given safety band of ±20mHz. The grey dotted lines show where the EV control would be triggered, if enabled. The dead band of ±10mHz is in accordance with the present frequency reg-

ulation scheme where primary control kicks in (Verband der Netzbetreiber e.V. 2007).

How to avoid demand synchronization catastrophes with EV ramping. The advantage of EVs for grid control, compared with devices that have a fixed runtime, is the possibility to smoothly ramp control up and down at any time. The need for battery charging is left to an investigation of secondary and tertiary grid control. In this work, the focus is on primary control balancing of short-term fluctuations centered around a zero frequency deviation mean value.

In the following, different parameterizations of ramping slopes, r (see eq. (8.3)), are tested. For that I vary f_{max} and keep $f_{min} = 0.01$Hz fixed (see Fig. 8.1). For an ensemble of 15 networks, Fig. 8.3a shows how different ramping slopes perform with respect to the number of switching events, that happen on average at each node and how many times a node on average exceeds the given frequency threshold band. In the steady state, $\dot{\omega}_i = 0$, the latter mean exceedance can be related to the global frequency deviation ΔF which again can be defined as a function of f_{max}. By summing over all indices i, results in:

$$0 = \sum_{i=0}^{N-1} \frac{1}{H_i} \left[\delta P_i - 2\pi\alpha_i \Delta F - (\Delta F - f_{min}) \frac{p_{max}}{f_{max} - f_{min}} \right].$$

Thus, the shape of the exceedance over f_{max} function can be easily reproduced analytically (shown in black in Fig. 8.3b):

$$\Delta F = \frac{\Delta P/H(f_{max} - f_{min}) + c \cdot f_{min}}{d(f_{max} - f_{min}) + c}, \tag{8.4}$$

where $c = N p_{max}$, $d = \sum_i 2\pi\alpha_i/H_i$ and $\Delta P = \sum_{i=1}^{N-1} \delta P_i$ is the absolute power mismatch in the grid with contributions δP_i from all nodes but the slack bus, $i = 0$, and thus $H = H_i, \forall i = \{1, .., N\}$. With the probability distribution of ΔP values over time a ΔF-distribution could be derived and the integral over all values above $\Delta F = 0.02$Hz would result in the exceedance values. This calculation shows that transient frequency dynamics settle fast in the new equilibrium. Hence, the global equilibrium, which is determined by the average global frequency offset, at each point in time is sufficient to reproduce the evolution of exceedance. From Fig. 8.3b I conclude that at least $f_{max} = 0.02$Hz is necessary to reduce the exceedance probability to zero. Compared to other approaches, this control scheme does not lead to an increased probability of large frequency peaks (Tchuisseu et al. 2017).

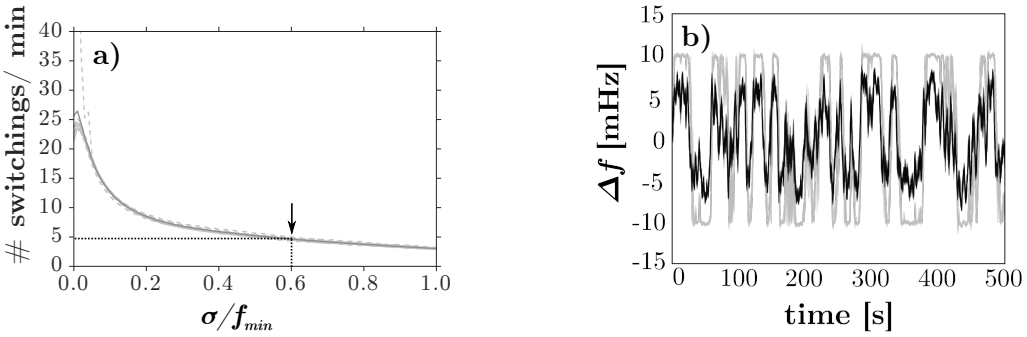

Figure 8.4: **Reduced switchings through randomization. a)** Number of switchings per minute over normalized variance, σ/f_{mins}, of the battery threshold $f_{min} = 10$mHz for a 15 network ensemble. The dashed grey lines represent different networks, the solid grey line the ensemble average. The dotted black line shows the chosen variance. **b)** Frequency trajectories for all nodes of an example network for a normalized variance of 0% (grey) and 60% (black).

The switching events are relatively insensitive to a variation in ramping slope. Only for $f_{max} = 0.01$Hz where batteries are charging and decharging with an infinitely large ramping slope, switchings shoot up to more than 500 per minute. Nevertheless, in the zero exceedance range of $0.01 < f_{max} < 0.02$Hz the number of switching events (with a mean of about $18/min$) is very high. The frequency trajectories (in grey) of Fig. 8.3c illustrates why this is the case. The frequency is fluctuating around the battery treshold because all batteries react almost simultaneously to the treshold crossings. Small differences in local frequency signals are not enough to prevent the build-up of such an undesirable feedback.

How to ensure sustainable battery operation with EV randomization. To reduce switching events, as previous work suggested, I randomize battery thresholds f_{min} (Moghadam et al. 2016; Mohsenian-Rad et al. 2010; Short et al. 2007). Fig. 8.3a illustrates how a high ramping slope is able to push exceedance down to zero. However, an undesirably large number of switching events exists which would lead to fast battery degradation (see Fig. 8.3a). Thus, I draw the battery threshold for each EV from a Gaussian probability distribution centered around $\bar{f}_{min} = 0.01$Hz. With this randomization, I prevent all EVs from switching on and off at the same time which leads to a negative feedback and oscillations around the battery threshold. Fig. 8.4a demonstrates how the switching events at first peak for very small variance and then rapidly decrease. Already for 20% of variance, switching events are reduced by around 60%, for 60% variance they are down to 20% of its value without randomization. The power input evolution over time re-

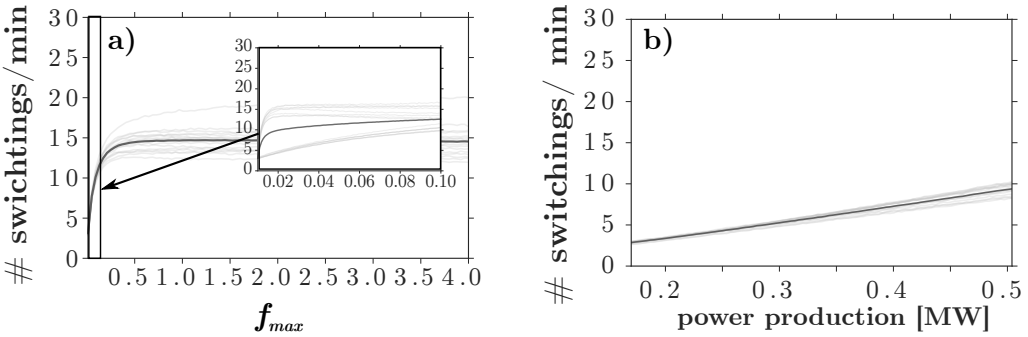

Figure 8.5: **Robustness of the chosen EV control scheme. a)** Number of switchings for varying ramping slopes and **b)** for increasing power production with 60% normalized variance in f_{min}. The light grey lines for both plots represent the 15 network ensemble. The dark grey line is the ensemble average. a) has an inlay which is a zoom of the frequency range $f = [0, 0.01]Hz$.

veals another side effect. In addition to the switching events also the peaks in absolute power changes are reduced. Finally, in frequency trajectories with randomization there are no oscillations around the battery threshold anymore and a normal distribution of the battery threshold around 0.01Hz results in frequency fluctuations much below this value (see Fig. 8.4b).

Because I still want to keep a dead band for all EV batteries, in the following I will choose the 60% variance as the standard model setup. For larger variances in f_{min} a number of EVs would already start their control at very small frequency deviations or even close to zero.

Robustness of control setup. With this choice of EV control parameterization, the ramping slope and input power variation is repeated in order

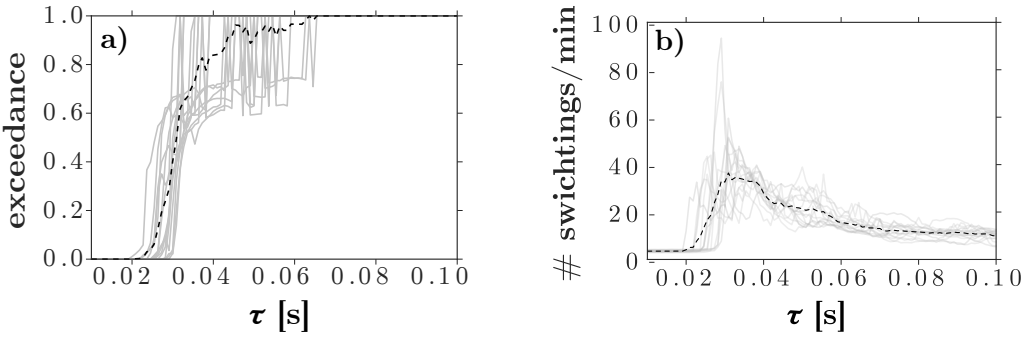

Figure 8.6: **Influence of input signal averaging.** Averaging over the input frequency signal for different interval lengths τ (or averaging times) changes **a)** exceedance and **b)** number of switchings. An ensemble of 15 networks is shown as gray lines with the ensemble average as black dashed line.

to check for any improvements. Indeed, for immediate ramping (with infinite ramping slope) the strong repeated switching is suppressed and reduced by a factor 100 (see Fig. 8.5a). However, in the evolution of exceedance over f_{max} (not shown here) there are no changes. According to Fig. 8.5b even with the randomization approach a light increase in switching events is unpreventable. At the same time, with respect to the frequency exceedance, the model setup is pretty robust towards increasing power fluctuations.

Destabilizing effect of input signal averaging. As an alternative to randomization, an input signal averaging approach was considered in order to reduce battery switchings. The influence of averaging on exceedance and switchings, without any randomization is shown in Figs. 8.6a and b, respectively. At averaging times around $\tau = 0.02$s the frequency fluctuations grow in time. Not only that the frequency safe-band is exceeded but the frequency is completely driven out of its stable state. Normally distributing the battery threshold around $f_{min} = 0.01$Hz does not eliminate the destabilizing effect of averaging.

I suspect that this is due to the introduction of delays into the system (Schäfer, Matthiae, Timme, et al. 2015; Schäfer, Grabow, et al. 2016; Yu et al. 2016), the further study of which is outside the scope of this work.

How to ensure effective control – Central vs. decentral EC control. I set up a control system that both brings down the exceedance to zero and reduces switching events through randomization. In the following, I want to test the robustness of my proposed control scheme against a changing number of EVs in the power system and compare how central vs. decentral control performs. This is realized by either distributing a number of M EVs homogeneously or inhomogeneously in the power grid. In the decentral case all nodes have the same number of EVs whereas in the centralized approach all nodes except the slack bus have only one EV. The number of EVs place at the slack bus is then $M - (N - 1)$. It can be positively emphasized that both regional distributions are able to bring down exceedance when there are more than a total of about 400 EVs in the system (see Fig. 8.7a). Thus, above a minimum number of EVs the exceedance of the 0.02 Hz-threshold is independent of the way EVs are distributed. However, concerning the switching events, there is a considerable difference in performance of both model cases. For the central distribution the mean switching number is one order of magnitude higher than for the homogeneous distribution and the variance in the performance for different networks is very large, as Fig. 8.7b shows.

The frequency trajectories for either a central or decentral distribution of a total of 10,000 EVs for an exemplary time frame of 50s is illustrated in Fig. 8.7c. The frequency fluctuations for the central case are up to three times larger for a few nodes. Because all 100 nodes' frequency trajectories are plotted, these visible large fluctuations may be attributed to only a few nodes in the network. Indeed, it is clearly visible how the decentral EV control is able to better equally reduce frequency fluctuations among all network nodes, whereas the central control scheme is not able to handle frequency fluctuations at nodes further away from the slack bus. For stricter exceedance thresholds this would lead to notable differences in exceedance values for high numbers of EVs (see Fig. 8.7d). Fig. 8.8 compares both cases by illustrating the maximum frequency deviation for each node over the whole time horizon in different coloring.

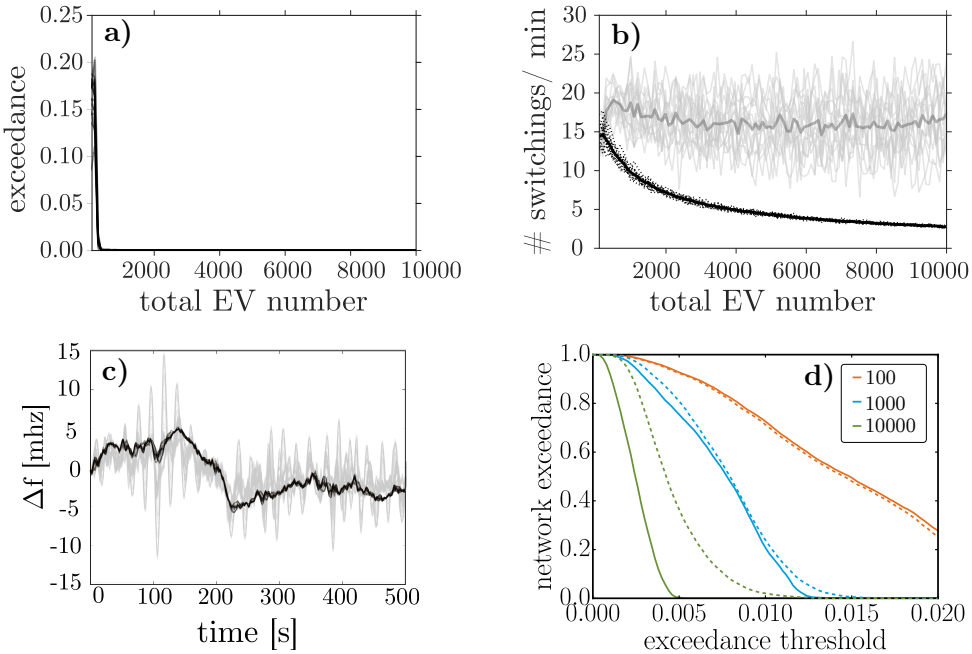

Figure 8.7: **Decentral vs central control. a)** Single node exceedances and **b)** nodal average of battery switching events for an increase in the total number of EVs for a homogeneous (black dotted lines) and an inhomogeneous (grey solid) EV distribution. The mean values are plotted with a darker color gradient. In the decentral case all nodes have the same number of EVs, whereas in the centralized approach each node but the heavy node has only 1 EV, all the other EVs are connected to the heavy node. **c)** Exemplary 50s time frame of frequency trajectories (from 100-node example network) of an overall simulation time of 500s for the decentral (black) and central (grey) EV distribution for the same total number of 10,000 EVs. **d)** Varying exceedance threshold and overall network exceedance for central (dashed) and decentral (solid) control and different total EV number (see legend) for an example grid.

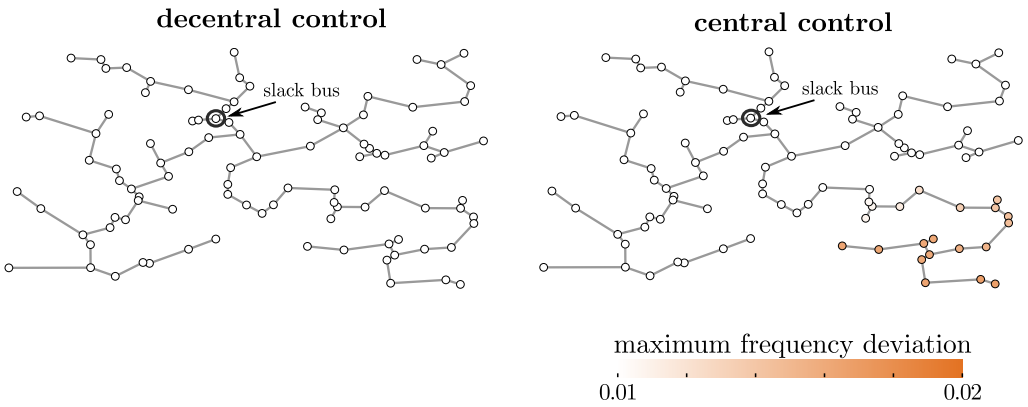

Figure 8.8: **Maximum nodal frequency deviation for decentral and central EV control** for an example MV-grid with a total of 10,000 EVs. In the decentral case all nodes have the same number of EVs, whereas in the centralized approach each node but the heavy node has only 1 EV, all the other EVs are connected to the slack bus.

8.4 Summary

In this chapter, I demonstrated the feasibility and advantages of decentral EV control for MV network ensembles with high shares of solar production and thus, strong intermittent power fluctuations. Here, I incorporated a highly realistic stochastic representation of RES fluctuations and focused on the issue of primary control of short-term frequency fluctuations centered around a mean of 50Hz, the stable set point of frequency synchronization. I explicitly model the network structure instead of following a copper-plate approach which allows to compare the performance of decentral vs. central control by modeling the interaction of all EV devices via the power grid infrastructure.

In my analysis, I followed the three main aims of ensuring dynamic grid stability within a frequency safe band, engineering EV control for a sustainable battery operation and designing grid control in an effective manner. In order to ensure grid stability, I find a maximal necessary (critical) ramping rate to completely suppress threshold exceedance. The influence of the ramping rate on the exceedance can be reproduced analytically. The ability of battery devices to be adjustable in their ramping as well as charging and decharging times prevents an undesired synchronization catastrophe caused by negative feedback loops. Hence, the here suggested control scheme does not lead to an increased probability of large frequency peaks (Tchuisseu et al. 2017).

Nevertheless, using the same ramp for all EVs leads does not cause a synchronization catastrophe, as expected. It is able to suppress frequency

fluctuations, however, at the cost of a large number of battery switching events. To overcome this effect and prevent battery degradation, I introduced a variance in battery threshold and randomize the switching of the different EV devices. To my knowledge, this combination of ramping slope and randomized battery threshold, performs best to jointly reduce exceedance and switching events. This control strategy parameterization is relatively robust against a further increase in power production and thus fluctuations. The exceedance stays at zero level and switching events only increase slightly.

In contrast to the randomization, an averaging approach destabilizes the system. This highlights the need for further research into the interaction of decentral frequency control and delayed control actions.

Another important finding is the advantage of decentral over central control for a more effective frequency balancing. While both control measures succeed in keeping fluctuations within a given safe band, the decentral control leads to an order of magnitude lower switchings and thus, allows for a more sustainable battery operation. At the same time, the central control would introduce a strong heterogeneity in the fluctuation amplitudes among the network nodes.

For further work, I see a great potential in the extension of this model setup to secondary and tertiary control. This would also allow to incorporate EV control into a realistic case study and compare it with other balancing techniques with respect to their technical and economic feasibility. Related to this issue is the interaction of EV control with different inverter types and their individual control schemes.

Generally, electric vehicles are an opportunity for the decarbonization of both the electricity and traffic sector, especially by interconnecting the two. The use of state-of-the-art battery technology increases the availability of storage for the eradication of mid- and short-term power fluctuations, e.g. from RES deployment. With my holistic network modeling approach, I demonstrated the technical feasibility of interconnected EV control devices but, there is much more work to follow to understand the risks and potential of decentral EV grid control.

Chapter 9

Summary and Discussion

This PhD thesis is centered around the "Stability and Control of Power Grids with high Renewable Energy Share" and makes contributions to the three overarching questions related to the challenges of future power grids' stability. With my thesis I aim to bridge the gap between the research of the electrical engineering and the theoretical physics community. Hence, I cover the whole spectrum from theoretical concepts and methods to very applied subjects. As a result, this work addresses both communities. Throughout this work I attempted to incorporate the conceptual modelers approach according to the principle "as simple as possible, as complex as necessary". I sincerely hope, that the analysis methods and modeling approaches, I developed within my dissertation contribute to establishing the complex systems' view on power grid stability assessment.

9.1 Resilience Analysis

How can the resilience of power grids towards extreme events be measured and improved?

The first question relates to how resilient power grids are in the case of natural or human-made extreme events. Here, Chapter 4 gave important insights to conceptual modelers by providing information on the necessary model detail for measures of transient stability assessments. For different grid topologies I compared the second- and fourth-order model of synchronous generators and motors with respect to their frequency response towards large perturbations. The voltage dynamics constitute the difference in model detail. I found evidence that some stable fixed points of the swing equation become unstable when voltage dynamics are added. Then the asymptotic behavior of the system can be significantly altered, and basin

stability estimates obtained with the swing equation can be dramatically wrong. In contrast, survivability does not change significantly when taking the voltage dynamics into account. This holds because transient voltage bounds are dominated by transient frequency bounds and play no large role for the assessment of survivability.

Related publication: S. Auer, K. Kleis, P. Schultz, J. Kurths, and F. Hellmann. "The impact of model detail on power grid resilience measures". In: The European Physical Journal Special Topics 225.3 225.3 (2016), pp. 609–625. doi: 10.1140/epjst/e2015-50265-9.

9.2 Static Voltage Stability

How can static voltage stability be ensured and grid congestions be avoided?

The second and most recognized challenge is how to ensure static voltage stability and avoid line capacity overloading while the deployment of RES in the distribution grid layers is massively increasing. As a possible solution to this problem, Chapter 5 analyzed the future technical potential of reactive power provision from decentral resources for the whole of Germany. For a 100% renewable electricity scenario, I set the possible reactive power supply in comparison with the reactive power requirements that are needed to realize the simulated future transmission grid power flows. Since an exact calculation of distribution grids' reactive power potential is difficult due to the lack of detailed grid models on such a scale, I estimated the potential by assuming a fully symmetrical, scaled and averaged distribution grid model connected to each of the transmission grid nodes. I find that for all, except a few transmission grid nodes, the required reactive power can be fully supplied from the modeled distribution grids. In future work, this study should be continued with more realistic hierarchical distribution grid models and incorporate an economic evaluation that compares decentral reactive power provision with the known alternatives.

Related publication: S. Auer, F. Steinke, W. Chunsen, A. Szabo, and R. Sollacher. "Can distribution grids significantly contribute to transmission grids' voltage management?" In: PES Innovative Smart Grid Technologies Conference Europe (ISGT-Europe), 2016 IEEE. IEEE. 2016, pp. 1-6.

9.3 Dynamical Stability

How can renewable energies be integrated in a dynamically stable way?

This question constitutes the main part of this work. Chapter 6 starts with studying the influence of local intermittent fluctuations on the stability and power quality of lossy distribution grids. For different model cases, I showed the importance of the network position for single-node fluctuations and their influence on the overall stochastic grid stability. There is a remarkable and subtle but robust interplay of dynamical and topological properties, even in the case of a homogeneous microgrid, where same-sized net consumers and producers are randomly distributed among the network nodes. This interplay is largely absent for lossless grids and would have stayed undiscovered without including this important characteristic of distribution grids.

I showed the appearance of branches with troublemakers or excitable nodes. Troublemakers or drivers of instability tend to pass on the temporal correlation of the intermittent power time series to the other grid nodes. At the same time, generally fluctuation sensitive nodes emerge. Such nodes of high excitability themselves have little capability to act as troublemakers. Instead they cause large frequency incoherencies. I could show that the left eigenvectors of the Laplacian determine which modes are excited by how much and thus, are able to predict troublemakers. Whereas the right eigenvectors says what the modes look like and serve as excitability predictor. These findings are not restricted to tree-like networks but also hold for meshed grids. Here, the addition of new links to distribution grid trees significantly reduces the risks of troublemakers occurring and the possibility of eigenmode excitation at the same time. Despite the conceptual modeling approach, I would like to make some careful distribution grid design recommendations. Long lines and cables are to be avoided in distribution grids since the occurrence of excitable nodes increases with reduced coupling strength. Also, the issue of troublemakers could be overcome with low resistance lines or the smart placement of few additional lines. However, the positioning of RES at nodes that are no troublemakers would be the cheapest solution if possible.

The simple form of the predictors found in this work, strongly suggests that future analytic work will be able to actually derive these predictors precisely. A related publication is in preparation and to be published after the submission of this thesis. Also, a study on multiple node fluctuations shall follow, which asks for a better understanding of the spatial correlation between fluctuations in renewable energy production. To capture the effect of future voltage issues, as a next step, the voltage dynamics shall be

introduced in the current model setup.

Related publication: S. Auer, F. Hellmann, M. Krause, and J. Kurths. "Stability of Synchrony against Local Intermittent Fluctuations in Tree-like Power Grids". In: Chaos 27 (12 2017). doi: 10.1063/1.5001818.

Second, the stability influence of delays from Decentral Smart Grid Control (DSGC) or power electronic resources, that connect RES to the grid, has been investigated in Chapter 7. Linear stability analysis reveals two destabilizing effects for the power grid. First, resonance catastrophes destabilize the system periodically. This instability can be cured by applying sufficient averaging. Second, a rebound effect emerges for large delays and destabilizes the system regardless of averaging which sets an upper limit for the delay $\tau = \tau_c$. I further investigated whether DSGC supports centralized or decentralized power production for different grid topologies and found it to be applicable to both. However, the results on cycle-like systems suggest that DSGC favors systems with decentralized production. Here, lower line capacities and lower averaging times are required compared to those with centralized production.

Related publication: B. Schäfer, C. Grabow, **S. Auer**, J. Kurths, D. Witthaut, and M. Timme. "Taming instabilities in power grid networks by decentralized control". In: The European Physical Journal Special Topics 225.3 (2016), pp. 569–582.

Finally, the potential of electric vehicles to balance grid frequency fluctuations was demonstrated in Chapter 8. For the first time in such a study, I explicitly modeled the network structure and incorporated non-Gaussian, strongly intermittent fluctuations typical for RES. I showed that EVs can completely eliminate frequency peaks. Using threshold randomization I further demonstrated that demand synchronization effects and battery stresses can be greatly reduced. In contrast, explicit frequency averaging has a strong destabilizing effect, suggesting that the role of delays in distributed control schemes requires further studies. In addition I find that distributed control outperforms central one. The results are robust against a further increase in renewable power production and fluctuations.

Related publication: S. Auer, C. Roos, J. Heitzig, F. Hellmann, and J. Kurths. "The Contribution of Different Electric Vehicle Control Strategies to Dynamical Grid Stability". In: arXiv preprint arXiv:1708.03531 (2017).

9.4 Personal Comment

All in all, through conceptual modeling this thesis has investigated several aspects of future power grids, starting from static stability assessment and moving towards integrating more aspects of future power grid dynamics. However, there are still many open questions and potential research subjects, of which I addressed some in this thesis. In this regard, I want to encourage further work in this exciting transdisciplinary field to prevent power grid stability to become a major bottle neck for the energy transition.

Appendix A

Parameterization of Multi-layer Power Grid Model

The parameterization of the multilayer power grid in Chapter 5 was derived as follows. For the power lines the standard overhead and cable line values for the different voltage levels are taken, see Tab. A.1. UHV/HV transformers have an overall capacity of 148 GVA and are 606 in number (Medjroubi et al. 2015). This results in an average capacity of 244 MVA. With 76,000 km HV lines (Deutsche Energie-Agentur 2012) that are ca. 94% overhead lines and a typical HV overhead line transmission capacity of 130 MVA on average there are $244/130 \approx 2$ overhead lines per UHV/HV transformer. Then, the average line length is $l_{HV} = 76,000/(606 \cdot 2)) = 62.7$ km. Similarly, I proceed with the lower grid levels with 4080 HV/MV transformers (Deutsche Energie-Agentur 2012), 523, 468km of MV lines of which ca. 64% are overhead lines (BNetzA 2013). The average line lengths are thus $l_{MV} = 9.43$ km ($\tilde{l}_{MV} = 0.5 \cdot 9.43 = 4.72$ km as consumer loads are connected to the middle of the line). Also, there are 460, 321 MV/LV transformers (Deutsche Energie-Agentur 2012) and LV lines add up to 1, 067, 100 km (BNetzA 2013).

Hence, the approximate proportionality ratios, corresponding to the tree graphs branching b_i for each node i in the chain network, are

$$b_i = \{1, 2, 3, 14, 9, 8\}. \tag{A.1}$$

That is, for each UHV/HV transformer there exist 2 HV lines, 6 HV/MV transformers etc.

Since Germany's peak load is about 80 GW and there are 606 UHV grid nodes (Medjroubi et al. 2015), each average distribution grid has a peak load of 132 MW. The real UHV nodes, however, have different peak consumer loads connected to them. Some nodes support large loads in big cities, other

rather supply load-poor rural areas. I thus rescale each node's generation capacities and loads to match one copy of the average grid model, perform the distribution grid power flow calculations, and then rescale its results to the original node size. Specifically, I introduce the norm factor $n_{load,i}$ for each UHV node i as

$$n_{load,i} = \max_t(D_{i,t})/132MW, \forall i \tag{A.2}$$

where $D_{i,t}$ is the consumer load at node i at time t. I then normalize the installed distribution power generation capacities C_i at node i with current actual power generation $P_{i,t}$ at time t to the average grid model as

$$D'_{i,t} = D_{i,t}/n_{load,i}, \tag{A.3}$$
$$C'_i = C_i/n_{load,i}, \tag{A.4}$$
$$P'_{i,t} = P_{i,t}/n_{load,i}. \tag{A.5}$$

Moreover, if the distributed power generation capacity C'_i exceeds the 1.5fold of the peak load of $132MW$ of the modeled distribution grid structure, it is unlikely that such generation capacity could be integrated into the existing grid without massive grid extensions. I thus only considered the plausibly integrateable part below such thresholds and normalize the generation capacities a second time with factor $n_{cap,i}$ defined as

$$n_{cap,i} = \begin{cases} C'/(1.5 \cdot 132) & C'_i > 1.5 \cdot 132 \\ 1 & C'_i \leq 1.5 \cdot 132 \end{cases}, \tag{A.6}$$

yielding

$$C''_i = C'_i/n_{cap,i}, \tag{A.7}$$
$$P''_{i,t} = P'_i/n_{cap,i}. \tag{A.8}$$

After the power flow simulation described in the following sections, the computed reactive power exchanges at the UHV level $Q''_{UHV,i}$, for C''_i and $P''_{i,t}$ are scaled back by

$$Q_{i,t} = Q''_{i,t} \cdot n_{cap,i} \cdot n_{load,i}. \tag{A.9}$$

Transformers	UHV/HV	HV/MV	MV/LV
C_j [MVA]	244	26	1
U_j [kV]	110	30	0.4
U_k [pu]	0.14	0.1	0.14
U_r [pu]	0.005	0.005	0.005
R [Ω/km]	0.2459	0.1731	8e-4
X [Ω/km]	6.8818	4.8431	2.24e-2
Y_{cr} [km/Ω]	0	0	0

Table A.1: Parameterization of nodes in the conceptual power chain network where C is the average transformer capacity, U_j the lower voltage side, U_r the ohmic voltage drop, U_k the short-circuit voltage, R the resistance, X the reactance and Y_{cr} the cross admittance. Parameters and transformer impedance calculation according to Oeding et al. 2004.

Lines	HV lines	MV lines	LV lines
C_j [MVA]	130	14	0.12
l_j [km]	62.7	4.72	0.17
L_j[1000 km]	76	523	1067.1
U_j [kV]	110	30	0.4
R [Ω/km]	0.1	0.4	0.5
X [Ω/km]	0.387	0.3	0.08
Y_{cr} [km/Ω]	2.983e-6	2.9202e-6	2.669e-6

Table A.2: Parameterization of links in the conceptual power chain network where C is the average transmission, U_j the lower voltage side, l the average power line length, R the resistance, X the reactance and Y_{cr} the cross admittance.

Appendix B

Derivation of Synchronous Machine Models

The Swing Equation is given by

$$\frac{\mathrm{d}\phi_i}{\mathrm{d}t} = \omega_i \ , \tag{B.1}$$

$$\frac{2H_i}{\omega_n}\frac{\mathrm{d}\omega_i}{\mathrm{d}t} = P_i - \sum_j U_i B_{ij} U_j \sin(\phi_i - \phi_j) - D_i\omega_i \ . \tag{B.2}$$

I work in the per unit (pu) system and thus the voltage is given in the node dependent unit pu that sets the nominal voltage to 1. Thus $U_i = 1\mathrm{pu}$ for the swing equation. The reduced parameters are obtained by absorbing $\frac{2H_i}{\omega_n}$ into D_i, B_{ij} and P_i:

$$P_i^r = \frac{P_i\omega_n}{2H_i},$$
$$D_i^r = \frac{D_i\omega_n}{2H_i},$$
$$B_{ij}^r = \frac{B_{ij}\omega_n}{2H_i}.$$

These reduced parameters have units s^{-2}, s^{-1} and $s^{-2}\mathrm{pu}^{-2}$ respectively. For performing simulations, time is often further re-parametrized to set $P = \pm 1$. I rescale by $\tau := \beta t$, and thus with $\mathrm{d}/\mathrm{d}t := \beta\mathrm{d}/\mathrm{d}\tau$. This leads to

the equations

$$\begin{aligned}\beta\frac{\mathrm{d}\phi_i}{\mathrm{d}\tau} &= \omega_i \ , \\ \beta^2\frac{\mathrm{d}\omega_i}{\mathrm{d}\tau} &= P_i^r - \sum_j U_i B_{ij}^r U_j \sin(\phi_i - \phi_j) - D_i^r \omega_i \ .\end{aligned}$$

With $\omega^s = \frac{\omega}{\beta}$, $P_i^s = \frac{P_i^r}{\beta^2} = \pm 1$, $K_{ij} = \frac{B_{ij}^r}{\beta^2}$ and $\alpha_i = \frac{D_i^r}{\beta}$ I obtain

$$\begin{aligned}\frac{\mathrm{d}\phi_i}{\mathrm{d}\tau} &= \omega_i^s \ , \\ \frac{\mathrm{d}\omega_i}{\mathrm{d}\tau} &= P_i^s - \sum_j U_i K_{ij} U_j \sin(\phi_i - \phi_j) - \alpha_i \omega_i^s, \\ \frac{\mathrm{d}\omega_i}{\mathrm{d}\tau} &= \pm 1 - \sum_j K_{ij} \sin(\phi_i - \phi_j) 1 \text{ pu}^2 - \alpha_i \omega_i^s \ .\end{aligned}$$

The Fourth-Order Model was transformed analogously. The voltages are not re-parametrized.

$$\begin{aligned}\frac{\mathrm{d}\phi_i}{\mathrm{d}\tau} &= \omega_i^s, \\ \frac{\mathrm{d}^2\phi}{\mathrm{d}\tau^2} &= P_i^s - (E_{q,i} I_{q,i}^s - E_{d,i} I_{d,i}^s) - \alpha_i \omega_i^s,\end{aligned}$$

with the current given by

$$I_i^s = \sum_{j=1}^{N} K_{ij} U_j e^{i(\phi_j - \phi_i)}.$$

The voltage equations are then given in terms of $T^s = \beta T$ and $X^s = \beta^2 \frac{2H_i}{\omega_n} X$:

$$\begin{aligned}T_{d,i}^s \frac{\mathrm{d}E_{q,i}}{\mathrm{d}\tau} &= -E_{q,i} + X_{d,i}^s I_{d,i}^s + E_f, \\ T_{q,i}^s \frac{\mathrm{d}E_{d,i}}{\mathrm{d}\tau} &= -E_{d,i} + X_{q,i}^s I_{q,i}^s.\end{aligned}$$

To summarize all relationships here:

$$\begin{aligned}
\beta^2 &= |P_i|, \\
\omega_i &= \omega_i^s \beta, \\
\alpha_i &= \frac{D_i^r}{\beta} = \frac{\omega_n}{2H_i\beta} D_i, \\
K_{ij} &= \frac{B_{ij}^r}{\beta^2} = \frac{\omega_n}{2H_i\beta^2} B_{ij}, \\
P_i^s &= \frac{P_i^r}{\beta^2} = \frac{\omega_n}{2H_i\beta^2} P_i = \pm 1, \\
T^s &= \beta T, \\
X^s &= \beta^2 \frac{2H_i}{\omega_n} X.
\end{aligned}$$

In terms of the reactances found in the literature, the parameter X is defined as the difference between the transient reactance, $X_{d,q}^{'}$, and the static reactance, $X_{d,q}$, in d-/q-axis:

$$X_{d,q} \coloneqq X_{d,q} - X_{d,q}^{'}, \tag{B.3}$$

where $X_d^{'}$ and $X_q^{'}$ are assumed to be equal.

Bibliography

50Hertz, Amprion, T. TSO, and TransnetBW (2012). *Netzentwicklungplan Strom*. URL: http://www.netzentwicklungsplan.de (cit. on pp. 5, 85).

Acharyya, S. and R. E. Amritkar (2012). *Synchronization of coupled non-identical dynamical systems*. DOI: 10.1209/0295-5075/99/40005. eprint: 1111.5408 (cit. on p. 33).

Albadi, M. H. and E. F. El-Saadany (2008). "A Summary of Demand Response in Electricity Markets". In: *Electric Power Systems Research* 78.11, pp. 1989–1996 (cit. on p. 26).

Alessio, E., A. Carbone, G. Castelli, and V. Frappietro (2002). "Second-order moving average and scaling of stochastic time series". In: *The European Physical Journal B-Condensed Matter and Complex Systems* 27.2, pp. 197–200 (cit. on p. 23).

Almeida, P. R., J. P. Lopes, F. Soares, and L. Seca (2011). "Electric vehicles participating in frequency control: Operating islanded systems with large penetration of renewable power sources". In: *PowerTech, 2011 IEEE Trondheim*. IEEE, pp. 1–6 (cit. on pp. 96, 97).

Anderson, P. M. and A. A. Fouad (2003). *Power System Control and Stability*. Wiley-IEEE Press (cit. on pp. 15, 16).

Anvari, M., G. Lohmann, M. Wächter, P. Milan, E. Lorenz, D. Heinemann, M. R. R. Tabar, and J. Peinke (2016). "Short term fluctuations of wind and solar power systems". In: *New Journal of Physics* 18.6, p. 063027 (cit. on pp. 5, 19, 22–25, 63, 67, 68, 97).

Anvari, M., B. Werther, G. Lohmann, M. Wächter, J. Peinke, and H.-P. Beck (2017). "Suppressing power output fluctuations of photovoltaic power plants". In: *Solar Energy* 157, pp. 735–743 (cit. on pp. 5, 19, 22–26).

Appen, J. von, M. Braun, T. Stetz, K. Diwold, and D. Geibel (2013). "Time in the sun: the challenge of high PV penetration in the German electric grid". In: *IEEE Power and Energy magazine* 11.2, pp. 55–64 (cit. on p. 98).

Arenas, A., A. Díaz-Guilera, J. Kurths, Y. Moreno, and C. Zhou (2008). "Synchronization in complex networks". In: *Physics reports* 469.3, pp. 93–153 (cit. on p. 63).

Asmussen, S. (2008). *Applied probability and queues*. Vol. 51. Springer Science & Business Media (cit. on p. 22).

Auer, S., F. Hellmann, M. Krause, and J. Kurths (2017). "Stability of Synchrony against Local Intermittent Fluctuations in Tree-like Power Grids". In: *Chaos* 27 (12). DOI: 10.1063/1.5001818 (cit. on pp. 63, 66).

Auer, S., K. Kleis, P. Schultz, J. Kurths, and F. Hellmann (2016). "The impact of model detail on power grid resilience measures". In: *The European Physical Journal Special Topics* 225.3, pp. 609–625. ISSN: 1951-6401. DOI: 10.1140/epjst/e2015-50265-9. URL: http://dx.doi.org/10.1140/epjst/e2015-50265-9 (cit. on pp. 15, 32, 35, 39, 100).

Auer, S., C. Roos, J. Heitzig, F. Hellmann, and J. Kurths (2017). "The Contribution of Different Electric Vehicle Control Strategies to Dynamical Grid Stability". In: *arXiv preprint arXiv:1708.03531* (cit. on pp. 65, 95).

Auer, S., F. Steinke, W. Chunsen, A. Szabo, and R. Sollacher (2016). "Can distribution grids significantly contribute to transmission grids' voltage management?" In: *PES Innovative Smart Grid Technologies Conference Europe (ISGT-Europe), 2016 IEEE*. IEEE, pp. 1–6 (cit. on pp. 11, 13, 49, 50, 66).

Bayer, E. (2015). "Report on the German power system". In: *Agora EnergieWende* (cit. on p. 99).

Belykh, V. N., I. V. Belykh, and M. Hasler (2004). "Connection graph stability method for synchronized coupled chaotic systems". In: *Physica D: nonlinear phenomena* 195.1, pp. 159–187 (cit. on pp. 35, 100).

Bergen, A. R. and D. J. Hill (1981). "A structure preserving model for power system stability analysis". In: *Power Apparatus and Systems, IEEE Transactions on* 1, pp. 25–35 (cit. on p. 33).

BMWi) (2014). *Ein Strommarkt für die Energiewende* (cit. on p. 5).

BMWi (2014). *Moderne Verteilernetze für Deutschland (Verteilernetzstudie)*. https://www.bmwi.de/Redaktion/EN/Publikationen/verteilernetzstudie.pdf (cit. on pp. 1, 95).

BNetzA (2013). *Netzentwicklungsplan Strom 2013* (cit. on pp. 53, 115).

Boccaletti, S., V. Latora, Y. Moreno, M. Chavez, and D.-U. Hwang (2006). "Complex networks: Structure and dynamics". In: *Physics reports* 424.4, pp. 175–308 (cit. on p. 11).

Boßmann, T. and I. Staffell (2015). "The shape of future electricity demand: exploring load curves in 2050s Germany and Britain". In: *Energy* 90, pp. 1317–1333 (cit. on pp. 65, 99).

Boyle, G. (2004). *Renewable Energy*. Oxford University Press, Oxford (cit. on p. 5).

Brown, R. E. (2008). *Electric power distribution reliability*. CRC press (cit. on p. 1).

Butler, D. (2007). "Energy Efficiency: Super Savers: Meters to manage the Future". In: *Nature* 445.7128, pp. 586–588 (cit. on p. 26).

Carbone, A., G. Castelli, and H. Stanley (2004). "Analysis of clusters formed by the moving average of a long-range correlated time series". In: *Physical Review E* 69.2, p. 026105 (cit. on p. 23).

Carrasco, J. M., L. G. Franquelo, J. T. Bialasiewicz, E. Galván, R. C. PortilloGuisado, M. M. Prats, J. I. León, and N. Moreno-Alfonso (2006). "Power-electronic systems for the grid integration of renewable energy sources: A survey". In: *IEEE Transactions on industrial electronics* 53.4, pp. 1002–1016 (cit. on p. 49).

Carvalho, P., P. F. Correia, and L. A. Ferreira (2008). "Distributed reactive power generation control for voltage rise mitigation in distribution networks". In: *Power Systems, IEEE transactions on* 23.2, pp. 766–772 (cit. on p. 50).

Chandler, D. (1987). "Introduction to modern statistical mechanics". In: *Introduction to Modern Statistical Mechanics, by David Chandler, pp. 288. Foreword by David Chandler. Oxford University Press, Sep 1987. ISBN-10: 0195042778. ISBN-13: 9780195042771*, p. 288 (cit. on p. 24).

Chatfield, C. (2016). *The analysis of time series: an introduction*. CRC press (cit. on p. 23).

Coelho, E. A. A., P. C. Cortizo, and P. F. D. Garcia (2002). "Small-signal stability for parallel-connected inverters in stand-alone AC supply systems". In: *IEEE Transactions on Industry Applications* 38.2, pp. 533–542 (cit. on p. 67).

Coumou, D. and S. Rahmstorf (2012). "A decade of weather extremes". In: *Nature climate change* 2.7, pp. 491–496 (cit. on pp. 1, 3).

De Brabandere, K., B. Bolsens, J. Van den Keybus, A. Woyte, J. Driesen, and R. Belmans (2007). "A voltage and frequency droop control method for parallel inverters". In: *IEEE Transactions on power electronics* 22.4, pp. 1107–1115 (cit. on p. 20).

Demirok, E., P. Casado Gonzalez, K. H. Frederiksen, D. Sera, P. Rodriguez, and R. Teodorescu (2011). "Local reactive power control methods for overvoltage prevention of distributed solar inverters in low-voltage grids". In: *Photovoltaics, IEEE Journal of* 1.2, pp. 174–182 (cit. on p. 50).

Deutsche Energie-Agentur (2012). *dena-Verteilnetzstudie - Ausbau- und Innovationsbedarf der Stromverteiilnetze in Deutschland bis 2030* (cit. on p. 115).

Dierkes, S., F. Bennewitz, M. Maercks, L. Verheggen, and A. Moser (2014). "Impact of distributed reactive power control of renewable energy sources in smart grids on voltage stability of the power system". In: *Electric Power Quality and Supply Reliability Conference (PQ), 2014*. IEEE, pp. 119–126 (cit. on pp. 13, 50).

Dörfler, F. and F. Bullo (2014). "Synchronization in complex networks of phase oscillators: A survey". In: *Automatica* 50.6, pp. 1539–1564 (cit. on p. 63).

Dörfler, F., J. W. Simpson-Porco, and F. Bullo (2016). "Breaking the hierarchy: Distributed control and economic optimality in microgrids". In: *IEEE Transactions on Control of Network Systems* 3.3, pp. 241–253 (cit. on p. 20).

Elgerd, O. I. (1982). "Electric energy systems theory: an introduction". In: (cit. on p. 13).

Elisabeth Ilskog (2011). *The Zanzibar Blackout – a case study on consequences from an electricity power crisis*. Haninge, Sweden. URL: `https://www.diva-portal.org/smash/get/diva2:450394/FULLTEXT01.pdf` (cit. on p. 3).

Eminoglu, U. and M. H. Hocaoglu (2008). "Distribution systems forward/backward sweep-based power flow algorithms: a review and comparison study". In: *Electric Power Components and Systems* 37.1, pp. 91–110 (cit. on p. 52).

ENTSO-E (2016). *Network code on requirements for grid connection applicable to all generators (rfg)*. URL: `https://electricity.network-codes.eu/network_codes/rfg/` (cit. on pp. 35, 84).

— (2017). *High Penetration of Power Electronic Interfaced Power Sources (HPoPEIPS) – ENTSO-E Guidance document for national implementation for network codes on grid connection*. URL: `https://consultations.entsoe.eu/system-development/entso-e-connection-codes-implementation-guidance-d-3/user_uploads/igd-high-penetration-of-power-electronic-interfaced-power-sources.pdf` (cit. on pp. 5, 6, 21, 29).

Ericsson, G. N. (2010). "Cyber Security and Power System Communication - Essential Parts of a Smart Grid Infrastructure". In: *Power Delivery, IEEE Transactions on* 25.3, pp. 1501–1507 (cit. on p. 26).

EY GmbH (2013). *Cost-benefit Analysis for the Comprehensive Use of Smart Metering Systems - Final Report - Summary* (cit. on p. 26).

Faiz, J. and B. Siahkolah (2011). *Electronic tap-changer for distribution transformers*. Vol. 2. Springer Science & Business Media (cit. on p. 51).

Fang, X., S. Misra, G. Xue, and D. Yang (2012). "Smart Grids - The new and improved Power Grid: A Survey". In: *Communications Surveys & Tutorials, IEEE* 14.4, pp. 944–980 (cit. on p. 26).

Feller, W. (1967). *An introduction to probability theory and its applications*. Vol. 1. Wiley, New York (cit. on p. 36).

Filatrella, G., A. H. Nielsen, and N. F. Pedersen (2008). "Analysis of a Power Grid using a Kuramoto-like Model". In: *The European Physical Journal B-Condensed Matter and Complex Systems* 61.4, pp. 485–491 (cit. on p. 15).

Fraunhofer IWES, Siemens AG, IEH Uni Hannover, and CUBE Engineering GmbH (2014). "Abschlussbericht des Forschungsprojektes Kombikraftwerk 2". In: (cit. on pp. 50, 53, 56, 59).

Groß, D., S. Bolognani, B. K. Poolla, and F. Dörfler (2017). "Increasing the Resilience of Low-inertia Power Systems by Virtual Inertia and Damping". In: *Bulk Power Systems Dynamics and Control Symposium (IREP)* (cit. on p. 21).

Hammersley, J. (2013). *Monte carlo methods*. Springer Science & Business Media (cit. on p. 13).

Heide, D., L. V. Bremen, M. Greiner, C. Hoffmann, M. Speckmann, and S. Bofinger (2010). "Seasonal Optimal Mix of Wind and Solar Power in a Future, Highly Renewable Europe". In: *Renewable Energy* 35.11, pp. 2483–2489 (cit. on p. 5).

Hellmann, F., P. Schultz, C. Grabow, J. Heitzig, and J. Kurths (2016). "Survivability of deterministic dynamical systems". In: *Scientific reports* 6, p. 29654 (cit. on pp. 34, 35, 39, 47, 100).

Hertem, D. V., J. Verboomen, K. Purchala, R. Belmans, and W. L. Kling (2006). "Usefulness of DC Power Flow for Active Power Flow Analysis with Flow Controlling Devices". In: *AC and DC Power Transmission, 2006. ACDC 2006. The 8th IEE International Conference on*. IET, pp. 58–62 (cit. on p. 84).

Hilborn, R. C. (2000). *Chaos and nonlinear dynamics: an introduction for scientists and engineers*. Oxford University Press on Demand (cit. on pp. 14, 15, 34).

Hofmann, L. and M. Sonnenschein (2015). *Smart Nord Final Report*. URL: `http://smartnord.de/downloads/SmartNordFinalReport.pdf` (cit. on p. 26).

Hurst, H. (1956). "The problem of long-term storage in reservoirs". In: *Hydrological Sciences Journal* 1.3, pp. 13–27 (cit. on p. 23).

Ian, W., K. Ruth, T. Philip, R. David, T. Stathis, and N. Aristomenis (2003). "Intelligent load control strategies utilising communication capabilities to improve the power quality of inverter based renewable island power systems". In: *International Conference RES for Island, Tourism & Water* (cit. on p. 96).

Jansen, M., C. Richts, and N. Gerhardt (2015). *Strommarkt-Flexibilisierung - Hemmnisse und Lösungskonzepte* (cit. on p. 5).

K. Schmietendorf, J. P. and O. Kamps (2016). "On the stability and quality of power grids subjected to intermittent feed-in". In: *arXiv:1611.08235 [nlin.AO], submitted* (cit. on pp. 5, 19, 23–25, 63, 64, 67, 68).

Karki, R., R. Billinton, and A. K. Verma (2014). *Reliability Modeling and Analysis of Smart Power Systems*. Springer (cit. on pp. 96, 97).

Kok, J. K., C. J. Warmer, and I. Kamphuis (2005). "PowerMatcher: Multiagent Control in the Electricity Infrastructure". In: *Proceedings of the Fourth International joint Conference on Autonomous Agents and Multiagent Systems*. ACM, pp. 75–82 (cit. on p. 26).

Kotler, P. (1986). "The Prosumer Movement: A new Challenge for Marketers". In: *Advances in Consumer Research* 13.1, pp. 510–513 (cit. on p. 83).

Kraiczy, M., G. Lammert, T. Stetz, S. Gehler, G. Arnold, M. Braun, M. Braun, S. Schmidt, H. Homeyer, U. Zickler, et al. (2015). "Parameterization of Reactive Power Characteristics for Distributed Generators: Field Experience and Recommendations". In: *ETG-Fachbericht-International ETG Congress 2015*. VDE VERLAG GmbH (cit. on p. 51).

Krause, S. M., S. Börries, and S. Bornholdt (2015). "Econophysics of adaptive power markets: When a market does not dampen fluctuations but amplifies them". In: *Physical Review E* 92.1, p. 012815 (cit. on p. 95).

Kundur, P., N. J. Balu, and M. G. Lauby (1994). *Power system stability and control*. Vol. 7. McGraw-hill New York (cit. on pp. 1, 31, 33).

Liu, H., Z. Hu, Y. Song, and J. Lin (2013). "Decentralized vehicle-to-grid control for primary frequency regulation considering charging demands". In: *IEEE Transactions on Power Systems* 28.3, pp. 3480–3489 (cit. on pp. 96, 97).

Lödl, M., R. Witzmann, and M. Metzger (2011). "Operation strategies of energy storages with forecast methods in low-voltage grids with a high degree of decentralized generation". In: *Electrical Power and Energy Conference (EPEC), 2011 IEEE*. IEEE, pp. 52–56 (cit. on p. 52).

Machowski, J., J. Bialek, and J. Bumby (2011). *Power System Dynamics: Stability and Control*. John Wiley & Sons (cit. on p. 84).

Madina, C., I. Zamora, and E. Zabala (2016). "Methodology for assessing electric vehicle charging infrastructure business models". In: *Energy Policy* 89, pp. 284–293 (cit. on p. 99).

Mamandur, K. and R. Chenoweth (1981). "Optimal control of reactive power flow for improvements in voltage profiles and for real power loss minimization". In: *Power Apparatus and Systems, IEEE Transactions on* 7, pp. 3185–3194 (cit. on p. 51).

MATLAB (2014). *version 7.10.0 (R2014b)*. Natick, Massachusetts: The MathWorks Inc. (cit. on p. 53).

Medjroubi, W., C. Matke, and D. Kleinhans (2015). *SciGRID - An Open Source Reference Model for the European Transmission Network (v0.1)*. URL: `http://www.scigrid.de` (cit. on p. 115).

Menck, P. J., J. Heitzig, J. Kurths, and H. J. Schellnhuber (2014). "How dead ends undermine power grid stability". In: *Nature communications* 5 (cit. on p. 44).

Menck, P. J., J. Heitzig, N. Marwan, and J. Kurths (2013). "How basin stability complements the linear-stability paradigm". In: *Nature Physics* 9.2, pp. 89–92 (cit. on pp. 34, 35, 39, 100).

Metz, M. and C. Doetsch (2012). "Electric vehicles as flexible loads–A simulation approach using empirical mobility data". In: *Energy* 48.1, pp. 369–374 (cit. on p. 99).

Milan, P., M. Wächter, and J. Peinke (2013). "Turbulent character of wind energy". In: *Physical review letters* 110.13, p. 138701 (cit. on pp. 5, 23–25, 63).

Moghadam, M. R. V., R. Zhang, and R. T. Ma (2016). "Distributed Frequency Control via Randomized Response of Electric Vehicles in Power Grid". In: *IEEE Transactions on Sustainable Energy* 7.1, pp. 312–324 (cit. on pp. 95, 103).

Mohsenian-Rad, A.-H., V. W. Wong, J. Jatskevich, R. Schober, and A. Leon-Garcia (2010). "Autonomous demand-side management based on game-theoretic energy consumption scheduling for the future smart grid". In: *IEEE transactions on Smart Grid* 1.3, pp. 320–331 (cit. on pp. 95, 103).

Naduvathuparambil, B., M. C. Valenti, and A. Feliachi (2002). "Communication delays in wide area measurement systems". In: *System Theory, 2002. Proceedings of the Thirty-Fourth Southeastern Symposium on*. IEEE, pp. 118–122 (cit. on p. 84).

Newman, M. E. (2003). "The structure and function of complex networks". In: *SIAM review* 45.2, pp. 167–256 (cit. on pp. 11, 73).

Nick Harmsen (2016). *South Australian blackout costs business $367m, fears summer outages on way, lobby group says*. URL: `http://www.abc.net.`

au/news/2016-12-09/sa-blackout-costs-could-have-been-worse-business-sa-says/8106600 (cit. on p. 4).

Nishikawa, T. and A. E. Motter (2006). "Synchronization is optimal in nondiagonalizable networks". In: *Physical Review E* 73.6, p. 065106 (cit. on pp. 35, 100).

— (2015). "Comparative analysis of existing models for power-grid synchronization". In: *New Journal of Physics* 17 (cit. on pp. 15, 33).

Oeding, D. and B. R. Oswald (2004). *Elektrische Kraftwerke Und Netze*. Springer (cit. on p. 117).

Pai, M., K. Padiyar, and C. Radhakrishna (1981). "Transient stability analysis of multi-machine AC/DC power systems via energy-function method". In: *Power Apparatus and Systems, IEEE Transactions on* 12, pp. 5027–5035 (cit. on p. 33).

Palensky, P. and D. Dietrich (2011). "Demand Side Management: Demand Response, Intelligent Energy Systems, and Smart Loads". In: *Industrial Informatics, IEEE Transactions on* 7.3, pp. 381–388 (cit. on p. 26).

Pasaoglu, G., C. Thiel, A. Martino, A. Zubaryeva, D. Fiorello, and L. Zani (2013). "Projections for Electric Vehicle Load Profiles in Europe Based on Travel Survey Data". In: *Joint Research Centre of the European Commission: Petten, The Netherlands* (cit. on p. 96).

Pavella, M., D. Ernst, and D. Ruiz-Vega (2000). *Transient stability of power systems: a unified approach to assessment and control*. Vol. 581. Springer Science & Business Media (cit. on pp. 31–33).

Pecora, L. M. and T. L. Carroll (1998). "Master stability functions for synchronized coupled systems". In: *Physical review letters* 80.10, p. 2109 (cit. on pp. 33, 35, 100).

Pikovsky, A., M. Rosenblum, and J. Kurths (2003). *Synchronization: a universal concept in nonlinear sciences*. Vol. 12. Cambridge university press (cit. on pp. 31, 33).

Pillai, J. R. and B. Bak-Jensen (2010). "Vehicle-to-grid systems for frequency regulation in an Islanded Danish distribution network". In: *2010 IEEE Vehicle Power and Propulsion Conference*. IEEE, pp. 1–6 (cit. on pp. 96, 97).

Preis, T., P. Virnau, W. Paul, and J. J. Schneider (2009). "Accelerated fluctuation analysis by graphic cards and complex pattern formation in financial markets". In: *New Journal of Physics* 11.9, p. 093024 (cit. on p. 23).

Richter, J. and D. Lindenberger (2010). "Potenziale der Elektromobilität bis 2050–Eine szenarienbasierte Analyse der Wirtschaftlichkeit". In: *Umweltauswirkungen und Systemintegration. ewi, Köln* (cit. on p. 99).

Rodrigues, F. A., T. K. D. Peron, P. Ji, and J. Kurths (2016). "The Kuramoto model in complex networks". In: *Physics Reports* 610, pp. 1–98 (cit. on p. 15).

Rogelj, J., M. Den Elzen, N. Höhne, T. Fransen, H. Fekete, H. Winkler, R. Schaeffer, F. Sha, K. Riahi, and M. Meinshausen (2016). "Paris Agreement climate proposals need a boost to keep warming well below 2 C". In: *Nature* 534.7609, pp. 631–639 (cit. on p. 1).

Rohden, M., A. Sorge, D. Witthaut, and M. Timme (2014). "Impact of Network Topology on Synchrony of Oscillatory Power Grids". In: *Chaos: An Interdisciplinary Journal of Nonlinear Science* 24.1, p. 013123 (cit. on pp. 85, 91).

Rohden, M. (2015). "Synchronization and Stability in Dynamical Models of Power Supply Networks". PhD thesis (cit. on p. 95).

Roos, C. (2016). *How different EV control strategies affect the dynamical grid stability* (cit. on p. 95).

Roussel, M. R. (2005). *Delay-differential equations*. URL: `http://people.uleth.ca/~roussel/nld/delay.pdf` (cit. on p. 85).

Sauer, P. and A. Pai (2006). *Power System Dynamics and Stability*. Stipes Publishing L.L.C. ISBN: 9781588746733. URL: `https://books.google.co.in/books?id=yWi9PAAACAAJ` (cit. on pp. 15, 31, 33, 51).

Schäfer, B., M. Matthiae, M. Timme, and D. Witthaut (2015). "Decentral Smart Grid Control". In: *New Journal of Physics* 17.1, p. 015002 (cit. on pp. 6, 26, 27, 84–87, 89–92, 96, 105).

Schäfer, B., C. Grabow, S. Auer, J. Kurths, D. Witthaut, and M. Timme (2016). "Taming instabilities in power grid networks by decentralized control". In: *The European Physical Journal Special Topics* 225.3, pp. 569–582 (cit. on pp. 95, 105).

Schäfer, B., M. Matthiae, X. Zhang, M. Rohden, M. Timme, and D. Witthaut (2017). "Escape routes, weak links, and desynchronization in fluctuation-driven networks". In: *Phys. Rev. E* 95 (6), p. 060203. DOI: `10.1103/PhysRevE.95.060203`. URL: `https://link.aps.org/doi/10.1103/PhysRevE.95.060203` (cit. on p. 64).

Scherer, M. (2016). "Spannungshaltung im Schweizer Übertragungsnetz - Finanzieller Anreiz für Kraftwerks- und Verteilungsnetzbetreiber". In: *ew Magazin für die Energieewritschaft* (cit. on p. 60).

Schiffer, J., F. Dörfler, and E. Fridman (2017). "Robustness of distributed averaging control in power systems: Time delays & dynamic communication topology". In: *Automatica* 80, pp. 261–271 (cit. on p. 6).

Schiffer, J., D. Goldin, J. Raisch, and T. Sezi (2013). "Synchronization of droop-controlled microgrids with distributed rotational and electronic

generation". In: *Decision and Control (CDC), 2013 IEEE 52nd Annual Conference on*. IEEE, pp. 2334–2339 (cit. on pp. 22, 67, 97).

Schiffer, J., D. Zonetti, R. Ortega, A. M. Stanković, T. Sezi, and J. Raisch (2016). "A survey on modeling of microgrids –From fundamental physics to phasors and voltage sources". In: *Automatica* 74, pp. 135–150 (cit. on pp. 21, 66, 67, 97).

Schmietendorf, K., J. Peinke, R. Friedrich, and O. Kamps (2014). "Self-organized synchronization and voltage stability in networks of synchronous machines". English. In: *The European Physical Journal Special Topics* 223.12, pp. 2577–2592. ISSN: 1951-6355. DOI: 10.1140/epjst/e2014-02209-8. URL: http://dx.doi.org/10.1140/epjst/e2014-02209-8 (cit. on p. 15).

Schultz, P., J. Heitzig, and J. Kurths (2014a). "Detours around Basin Stability in Power Networks". In: *New Journal of Physics* 16.12, p. 125001 (cit. on p. 84).

Schultz, P., J. Heitzig, and J. Kurths (2014b). "A random growth model for power grids and other spatially embedded infrastructure networks". In: *The European Physical Journal Special Topics* 223.12, pp. 2593–2610 (cit. on pp. 11, 13, 14, 97).

Schultz, P., F. Hellmann, J. Heitzig, and J. Kurths (2016). "A Network of Networks Approach to Interconnected Power Grids". In: (cit. on pp. 2, 11).

Schweppe, F. C. (1982). *Frequency Adaptive, Power-Energy Re-scheduler*. US Patent 4,317,049 (cit. on p. 26).

Sen, P. C. (2007). *Principles of electric machines and power electronics*. John Wiley & Sons (cit. on p. 66).

Serdukova, L., Y. Zheng, J. Duan, and J. Kurths (2016). "Stochastic basins of attraction for metastable states". In: *Chaos: An Interdisciplinary Journal of Nonlinear Science* 26.7, p. 073117 (cit. on p. 35).

Short, J. A., D. G. Infield, and L. L. Freris (2007). "Stabilization of Grid Frequency through Dynamic Demand Control". In: *Power Systems, IEEE Transactions on* 22.3, pp. 1284–1293 (cit. on pp. 26, 95, 96, 103).

Silva, C., M. Ross, and T. Farias (2009). "Analysis and simulation of "low-cost" strategies to reduce fuel consumption and emissions in conventional gasoline light-duty vehicles". In: *Energy Conversion and Management* 50.2, pp. 215–222 (cit. on p. 99).

Sowa, T., P. Goergens, A. Schnettler, R. Koeberle, and M. Metzger (2015). "Potential of the AUEW Network Area to Provide Reactive Power to Transmission Network Level". In: *ETG-Fachbericht-International ETG Congress 2015*. VDE VERLAG GmbH (cit. on pp. 50, 51).

Talavera, I., S. Stepanescu, F. Bennewitz, J. Hanson, R. Huber, F. Oechsle, and H. Abele (2015). "Vertical Reactive Power Flexibility based on Different Reactive Power Characteristics for Distributed Energy Resources". In: *ETG-Fachbericht-International ETG Congress 2015*. VDE VERLAG GmbH (cit. on pp. 50, 51, 61).

Tchuisseu, E. T., D. Gomila, D. Brunner, and P. Colet (2017). "Effects of dynamic-demand-control appliances on the power grid frequency". In: (cit. on pp. 102, 107).

Tesla Motors (2016). *Model S Specifications*. `https://www.teslamotors.com/support/model-s-specifications`, accessed at 02-05-2016 (cit. on p. 99).

Troester, E. (2009). "New German grid codes for connecting PV systems to the medium voltage power grid". In: *2nd International workshop on concentrating photovoltaic power plants: optical design, production, grid connection*, pp. 9–10 (cit. on p. 95).

Turitsyn, K., S. Backhaus, M. Chertkov, et al. (2011). "Options for control of reactive power by distributed photovoltaic generators". In: *Proceedings of the IEEE* 99.6, pp. 1063–1073 (cit. on p. 51).

Turner, J. A. (1999). "A Realizable Renewable Energy Future". In: *Science* 285.5428, pp. 687–689 (cit. on p. 5).

Van Haaren, R. (2011). "Assessment of electric cars' range requirements and usage patterns based on driving behavior recorded in the National Household Travel Survey of 2009". In: *Earth and Environmental Engineering Department, Columbia University, Fu Foundation School of Engineering and Applied Science, New York* 51, p. 53 (cit. on pp. 96, 99).

Vasconcelos, J. (2008). "Survey of regulatory and technological developments concerning smart metering in the European Union electricity market". In: (cit. on p. 6).

Verband der Netzbetreiber e.V. (2007). *Transmission Code – Netz- und Systemregeln der deutschen Übertragungsnetzbetreiber*. `https://www.bdew.de/internet.nsf/id//$file/TransmissionCode2007.pdf` (cit. on pp. 31, 36, 100, 102).

Viawan, F., D. Karlsson, et al. (2008). "Voltage and reactive power control in systems with synchronous machine-based distributed generation". In: *Power Delivery, IEEE Transactions on* 23.2, pp. 1079–1087 (cit. on p. 51).

Von Meier, A. (2006). *Electric power systems: a conceptual introduction*. John Wiley & Sons (cit. on p. 30).

Walter, T. (2014). *Smart Grid neu gedacht: Ein Lösungsvorschlag zur Diskussion in VDE/ETG*. URL: http://www.vde.com/de/fg/ETG/Pbl/MI/2014-01/Seiten/Homepage.aspx (cit. on p. 26).

Wang, H., T. Stetz, F. Marten, M. Kraiczy, S. Schmidt, C. Bock, M. Braun, and M. Braun (2015). "Controlled Reactive Power Provision at the Interface of Medium-and High Voltage Level: First Laboratory Experiences for a Bayernwerk Distribution Grid using Real-Time-Hardware-in-the-Loop-Simulation". In: *ETG-Fachbericht-International ETG Congress 2015*. VDE VERLAG GmbH (cit. on p. 51).

Wang, J., C. Liu, D. Ton, Y. Zhou, J. Kim, and A. Vyas (2011). "Impact of plug-in hybrid electric vehicles on power systems with demand response and wind power". In: *Energy Policy* 39.7, pp. 4016–4021 (cit. on p. 96).

Watts, D. J. and S. H. Strogatz (1998). "Collective dynamics of 'small-world' networks". In: *nature* 393.6684, pp. 440–442 (cit. on pp. 14, 15, 34).

Weckesser, T., H. Jóhannsson, and J. Ostergaard (2013). "Impact of model detail of synchronous machines on real-time transient stability assessment". In: *Bulk Power System Dynamics and Control-IX Optimization, Security and Control of the Emerging Power Grid (IREP), 2013 IREP Symposium*. IEEE, pp. 1–9 (cit. on pp. 15, 33, 39).

Wikipedia, M. (2010). *Electricity Grid Schematic English*. URL: https://en.wikipedia.org/wiki/File:Electricity_Grid_Schematic_English.svg (cit. on p. 2).

Willems, J. L. and J. C. Willems (1970). "The application of Lyapunov methods to the computation of transient stability regions for multimachine power systems". In: *Power Apparatus and Systems, IEEE Transactions on* 5, pp. 795–801 (cit. on p. 33).

Woyte, A., R. Belmans, and J. Nijs (2007). "Fluctuations in instantaneous clearness index: Analysis and statistics". In: *Solar Energy* 81.2, pp. 195–206 (cit. on p. 63).

Yu, M., A. J. Roscoe, C. D. Booth, A. Dysko, R. Ierna, J. Zhu, and H. Urdal (2016). "Use of an inertia-less virtual synchronous machine within future power networks with high penetrations of converters". In: *Power Systems Computation Conference (PSCC), 2016*. IEEE, pp. 1–7 (cit. on p. 105).

Zhang, X., S. Hallerberg, M. Matthiae, D. Witthaut, and M. Timme (2017). "Dynamic Network Response Patterns". In: *in prep.* (Cit. on pp. 63, 64, 70, 74).

Zheng, Y., L. Serdukova, J. Duan, and J. Kurths (2016). "Transitions in a genetic transcriptional regulatory system under Lévy motion". In: *Scientific reports* 6, p. 29274 (cit. on p. 35).

Selbstständigkeitserklärung

Ich erkläre, dass ich die Dissertation selbständig und nur unter Verwendung der von mir gemäß § 7 Abs. 3 der Promotionsordnung der Mathematisch-Naturwissenschaftlichen Fakultät, veröffentlicht im Amtlichen Mitteilungsblatt der Humboldt-Universität zu Berlin Nr. 126/2014 am 18.11.2014 angegebenen Hilfsmittel angefertigt habe und alle Quellen angegeben habe.

_____ _____

Place, Date Signature